Abstract. Using fast pulse techniques the resistivity, Hall effect and magnetoresistance of PbS have been measured in electric fields up to 10^3 volt cm^{-1} and in magnetic fields up to 37 K-gauss with a view to determining the main scattering mechanisms at 77 K and in the helium temperature range. At 77 K, apart from a shallow minimum at low fields, the resistivity increases with electric field confirming phonon scattering at this temperature. The comparison of experiment with theory provides strong evidence of a substantial contribution from polar optical phonons. This evidence, produced at a fixed lattice temperature, cannot be explained in terms of a temperature dependent effective mass which has been used by some authors to explain the temperature dependence of mobility without considering optical phonons. It can therefore be claimed beyond any reasonable doubt that optical phonons play a substantial part in scattering electrons at 77 K and thus presumably at higher temperatures.

In contrast to the increase in resistance with electric field at 77 K a decrease is found at low temperatures so it is at once clear that phonon scattering is no longer dominant. Neutral impurity scattering can be ruled out since it is independent of electron energy. Ionised impurity scattering should give a decrease in resistance as the electric field increases but we would expect the effect to increase with the electron density. In fact the change in resistivity decreases with the increase of electron density, the resistivity becoming virtually constant with electric field for a concentration of 5×10^{17} cm^{-3}. Ionised impurity scattering can therefore also be ruled out in agreement with several other kinds of evidence.

However, over the same concentration range from about 5×10^{17} to less than 10^{16} cm^{-3} it has been found that both a negative magnetoresistance and a resistance minimum increase in value. To explain this, scattering by localised spins has been suggested and a tentative theory by Toyozawa predicts just such a change in effect with impurity concentration. The application of the theory to negative magnetoresistance and resistance minimum is similar to that used by Kondo for dilute alloys. It has been adapted by Tanaka for semiconductors and following his method of calculation we do indeed find a decrease in localised spin concentration as the electron density increases.

We suggest therefore that, for samples of PbS in the $10^{16} - 10^{17}$ cm^{-3} range, scattering by localised spins is responsible for the observed behaviour at liquid helium temperatures.

At low electric fields the resistance is independent of field as is to be expected since the electrons remain at the lattice temperature. At very high fields the resistance is again approximately independent of field since by then the degeneracy which is essential for Kondo type behaviour has been largely removed. In the intermediate range the experimental results when plotted on a ρ - ln E graph, give straight line portions similar to those obtained from ρ - ln T graphs obtained at constant field.

The change in resistivity with electric field is found to increase with magnetic field, rather slowly at first but much more rapidly for fields greater than 10^4 gauss. The magnetoresistance anisotropy decreases as the electric field increases and effectively vanishes at high electric field.

Thesis entitled "High Field Effects in Lead Sulphide at Low Temperatures" presented by Kin Lun Yau in application for the degree of PhD, 1971.

HIGH FIELD EFFECTS IN LEAD SULPHIDE AT LOW TEMPERATURES

A Thesis presented by

Kin Lun Yau, M.Sc.

to the

University of St Andrews

in application for

The Degree of Doctor of Philosophy

1971

DECLARATION

I hereby certify that this thesis has been composed by me, that it is a record of my work and that it has not previously been presented for a higher degree.

The research was carried out in the School of Physical Sciences in the University of St. Andrews, under the supervision of Dr. D.M. Finlayson.

(Kin Lun Yau)

CERTIFICATE

I certify that Kin Lun Yau, M.Sc., has spent nine terms at research work in the School of Sciences in the University of St. Andrews under my direction, that he has fulfilled the conditions of the Resolution of the University Court, 1967, No. 1, and that he is qualified to submit the accompanying thesis in application for the Degree of Doctor of Philosophy.

_____

Research Supervisor

CAREER

I first matriculated in the University of St. Andrews in October 1968 after I obtained my B.Sc. Degree (special honours, 1965) and M.Sc. Degree (1968) in the University of Hong Kong, Hong Kong.

I was enrolled as a research student in the Department of Physics with an award of a University Research Scholarship leading to the Degree of Doctor of Philosophy under the Resolution of the University Court, 1967, No.1.

ACKNOWLEDGEMENTS

I wish to express my sincere gratitude to my supervisor, D. M. Finlayson for his guidance and supervison without which the completion of this work would not have been possible. I would also like to thank Professor J. F. Allen for his constant encouragement and providing research facilities during my years in St. Andrews. I am grateful to D. M. McCall, K. Turvey and T. Y. Stokoe for their valuable discussions.

My thanks are also due to the technical staff of the Physics Department for their technical asistance.

A University Research Scholarship from the University of St. Andrews is also gratefully acknowledged.

ABSTRACT

This thesis reports a study of electron scattering mechanisms by means of high field measurements in lead sulphide at cryogenic temperatures.

High field resistivity, magnetoresistivity and Hall effect measurements are obtained for samples of electron concentration ranging from 7.49×10^{15} cm^{-3} to 5×10^{17} cm^{-3}. The measurements are made at nitrogen temperature and helium temperatures with steady magnetic fields up to 3×10^{4} gauss in both transverse and longitudinal configurations. The external electric field is applied in the form of pulses ranging in pulse height from 10^{-2} volt/cm to 10^{3} volt/cm with repetition frequencies of the order of 100 cps and rise-time, 4×10^{-9} sec. Correspondingly, fast pulse techniques including fast pulse generation, a pulse bridge and a pulse detection system are used.

It has been found that at nitrogen temperature polar optical phonon scattering plays an important role in PbS in the warm electron region and that at helium temperatures Kondo type spin flip scattering is responsible for the resistivity drop in the range of 5--50 volt/cm. The idea of a hot electron temperature is introduced in both cases. An anisotropy of magnetoresistance is also studied at helium temperature and interpretations are given. A discussion is given on the effect of magnetic field on the measurements.

CONTENTS

CHAPTER 1
INTRODUCTION

1.1 The hot electron

Like Hooke's law, Newton's second law of motion and Ohm's law, the starting point of many branches of physics is a linear relation. In most of these cases, the linear relation is only an approximation showing the functional relationship between two variables. Important physical principles are brought to attention when the nonlinear range is reached.

In semiconductors at ordinary temperatures and at low field, Ohm's law holds quite well. However, for semiconductors and semimetals at low temperatures and at higher fields significant deviations from Ohm's law are observed. This is due to the fact that the electrons are heated to a temperature above that of their host crystal lattice. Electrons in a crystal can exchange energy with the crystal lattice by certain scattering processes. This energy exchange maintains the electron distribution in equilibrium at the temperature of the lattice. However if the electrons are supplied with additional energy at a rate comparable to the electron lattice exchange rate, then the electron distribution is altered significantly from the equilibrium state and hence is no longer strictly Maxwellian. "Hot electrons" is the term used for nonequilibrium electrons whose average energy $\langle \mathcal{E} \rangle$ exceeds the equilibrium temperature $3/2kT$ where T is the lattice temperature.

1.2 High field effects

High field effects are studied for the following reasons.

The heating of carriers alters the energy distribution function and this affects the well known transport phenomena, for example, the electrical resistivity. From the experimental deviation from Ohm's law one can obtain information on the carrier scattering mechanisms.(1)--(7)

Moreover, when carriers are hotter than the lattice one can investigate the kinetics of the energy dissipation by electrons which cannot be done in the equilibrium state.

The heating of carriers also gives rise to new effects in semiconductors which are observed only when the carrier gas is hot. For instances, these are anisotropy of resistivity, hot electron emission and the Gunn effect etc..

The anisotropy of electrical conductivity in cubic crystals can be interpreted as the differential heating of the carrier in the k-space valleys which are oriented in different ways with respect to the field and the associated redistribution of electrons between valleys.(8)--(13)

The observation of the emission of hot electrons from a crystal with a cold lattice is of practical importance in electronics(14) (15) although the physical nature of this effect is not yet clear at present.

The various instabilities accompanying the heating of carriers is well known e.g. the Gunn effect(16)--(20) which gives further information about the nature of electrons in solids.

Recently, hot electron effects have been increasingly used in radio and electronics; semiconductor light sources and

Gunn effect devices are some of the outstanding examples.

1.3 Theoretical approaches

The available theories describing the behavior of hot carriers are based on some important approximations.

1.3.1 Electron Temperature Model

The central theoretical problem in examination of hot electron effects lies in the determination of the disturbed distribution function. Generally, this seems extremely difficult, but the problem is eased by applying the electron temperature approximation. This model, ETM, was originally proposed by Frohlich.[21] It is assumed that the energy distribution function of electrons is of the Maxwellian type with a temperature $T_e > T$. The electron temperature T_e is derived from the condition of conservation of energy and momentum. The electron temperature approximation applies at sufficiently high electron density[22] so that the exchange of energy between electrons is considerably greater than the exchange of energy between electrons and the lattice. In 1958 Stratton[23] extended the previous ideas to include a variety of scattering mechanisms and lattice temperatures.

The ETM simplification based on the fact that the Boltzmann transport equation need not be solved, allows many problems that would otherwise be avoided because of their complexity, to be at least investigated for their physical content. The ETM is extensively applied and mostly agrees quite well with

experiments.[24] However the assumption of maintaining a Maxwellian distribution by strong electron-electron scattering is not necessarily always valid.

1.3.2 Direct solution of the Boltzmann equation

A more rigorous and general approach is to find the distribution function starting from the steady state transport equation,

$$\left(\frac{df}{dt}\right)_E + \left(\frac{df}{dt}\right)_C = 0$$

where the first term represents the change in the distribution function f due to the presence of external fields and the second due to scattering.

The approximate solution of the equation has so far been found only for special cases.

Assuming that the drift velocity is very much less than the thermal velocity in weak fields, Yamashita and Watanabe [25] were able to give the solution for the acoustic scattering case,

$$f_o(x) \sim \left(\frac{\mathcal{E}}{kT_o} + \beta_{ac} E^2\right)^{\beta_{ac} E^2} e^{-\frac{\mathcal{E}}{kT_o}}$$

where β_{ac} is a constant.

For the case of scattering by acoustic phonons and ionized impurities, Adawi gave an expression in 1958, [26]

$$f_o(x) \sim e^{-\int_0^{\mathcal{E}/kT} \left(\frac{d\mathcal{E}}{kT_o + \beta_I E^2 \mathcal{E}(\mathcal{E}^2/k^2T_o^2 + \beta_I)^{-1}}\right)}$$

where β_I is a quantity proportional to the ratio of acoustical momentum relaxation time to impurity momentum relaxation time.

In the presence of acoustical and optical scattering with low optical phonon energy Inone[27] found

$$f_o(x) \sim C(\mathcal{E}/kT_o + AE^2 + B)^{AE^2+D} \, e^{-\frac{\mathcal{E}}{kT_o}}$$

where A,B,C and D are constants representing the scattering parameters.

The other approaches like diffusion approximation [28],[29] and numerical method , for example, the Monte Carlo method[30],—[32] are also used.

1.3.3 Theory for many valley semiconductors

It is sometimes useful to sub-classify the various types of electron scattering process into intra-valley and inter-valley transition. In a semiconductor like indium antimonide which has a single valley near $\underline{k}=0$ one is usually only interested in electron transitions within this valley. Such transitions are called intra-valley transitions. However in a many-valley-semiconductor such as germanium,lead sulphide transitions within each valley and transitions between valleys are of interest. The latter are called inter-valley transitions.

The theory becomes much more complicated for many-valley semiconductors due to the orientation of each individual valley and the inter-valley transitions, and therefore it is not surprising that there have been only a few calculations for the hot electron effects.[33],[34] So far qualitative interpretations can only be given.

1.4 Previous work and the present investigation

The early work on lead salts tended to explain the experimental data at moderately low temperatures by acoustic scattering.[96] An empirical equation was deduced to show that the mobility is proportional to $T^{-5/2}$ but no theoretical basis for such a variation has been given.

Scattering by optical phonons in polar crystals was discussed at length by Howarth and Soudheimier[63]. Petritz and Scanlon suggested that this theory may be valid for lead salts down to liquid nitrogen temperature when acoustical scattering is also taken into account.[97]

Later Finlayson and Greig extended the experiment to the temperature below 77^{0}K and pointed out that the mobility varies with the impurity concentration and that at low temperature, lattice scattering, both acoustical and optical, is completely masked.[98] An attempt has also been made by them[99] by measuring the thermoelectric properties of PbS to show the relative importance of optical modes in the carrier scattering processes at intermediate temperatures.

In the early 1960's work in the Leningrad Semiconductor Institute cast doubt on the earlier interpretations since they were able to explain their experimental measurements in terms of a temperature dependent effective mass, see for example Smirnova et al. in 1960.[100] The same Institute produced substantial theoretical backing for this idea.

More recently, Russian papers seemed to show that these ideas were also inadequate.[35]--[37] In particular, Muzhdaba[101] indicated that at temperatures of the order of 80^{0}K the scattering of carriers in lead salts is essentially inelastic and Kaidanov et al[102] by measuring the Nernst-Ettingshausen effect obtained a value closer to the predicted value for the optical scattering rather than to that for the acoustic scattering. In 1970 Yu. Ravich[38] et al tried to show that at high concentrations of the order of 10^{20} cm^{-3} scattering by acoustic phonons predominates; while at concentrations of the order of 10^{19} cm^{-3} and below polar phonons scattering plays a significant role.

Writing in 1968, when this work was begun, Ravich[38] noted that " At present, there is no agreement about the dominant scattering mechanism in lead chalcogenides."

Besides the uncertainty in scattering mechanisms existing experimental work has not covered a wide range of temperature and concentrations. Most previous work was carried out at liquid nitrogen temperatures. This narrow range of temperature apparently is not able to provide a full story of the behaviour of electrons in the lead salts. It seems, therefore, worthwhile to extend the measurements down to liquid helium temperatures.

In the helium temperature range early measurements (summarised by Scanlon in Solid State Physics,9) indicated the

absence of ionised impurity scattering. This was explained by the very high values of the dielectric constant and this has since been confirmed experimentally.

Measurements by Finlayson and Mathewson[70] showed that the magnetoresistance was negative for fairly low magnetic fields and for electron concentrations up to 5×10^{17} cm^{-3}. Later measurements by Chan et al[81] showed that there is a close correlation between a minimum in the resistance temperature curve and the negative magnetoresistance. Such effects have been observed in a number of semiconductors and interpreted in terms of scattering by localised spins.

In the present investigation we aim at remedying the relative lack of information in PbS by measuring the resistivity, Hall effect and magnetoresistance at high electric fields at nitrogen and helium temperatures for electron concentrations raging from 7.5×10^{15} to 5×10^{17} cm^{-3} with the aim of clarifying the scattering mechanisms at $77^{0}K$ and in the very low temperature region.

The electric field has been applied in the form of pulses ranging in pulse height from 10^{-2} to 10^{3} volt/cm with repetition frequencies of the order of 100 cps. Steady magnetic fields up to 37 K-gauss have been obtained from a superconducting magnet and applied to the crystals in both transverse and longitudinal configurations.

CHAPTER 2

THE SAMPLE —— PHYSICAL PROPERTIES, PREPARATION AND MOUNTING

2.1 Introduction

Lead sulphide occurs in nature as the mineral galena and is one of the commonest ores of lead. For semiconductor work large single crystals of natural galena are comparable in quality with the best material prepared in the laboratory. It is not surprising that lead sulphide was one of the first semiconductors to be studied, and was one of the first materials to be used as a contact rectifier in the early days of radio.

An important application of these materials is in the manufacture of photoconductive infra-red detectors. These devices were exploited during and shortly after the Second World War. Recently, Lovell[39] gave a very detailed survey of this topic.

We will see that the interest in the lead sulphide type semiconductor is due to their unusual properties which ensure their use as detectors of infra-red radiation. However, in addition, these crystals in themselves provide an interesting study. This is why nowadays investigations of this material continue; these not only provide infra-red sensitive detectors useful in a broad variety of application, but also the studies of their electrical and optical properties are responsible for an improved understanding of matter.

2.2 IV - VI compound

2.2.1 Pb --- a group IV element

The electronic structure of lead is $6s^2$, $4f^{14}$, $5d^{10}$, $6p^2$. It shows a covalency of four, which necessitates promotion of electrons from the ground state to an excited state, and so sp^3 hybridization of the orbits results in a tetrahedral structure $4f^{14}$, $5d^{10}$, $6s^2$, $6p^2$.

2.2.2 S --- a group VI element

The electronic structure is $3s^2$, $3p^4$ since sulphur has d orbitals available for bonding, it forms four bonds --- $s^2p^3d^1$ hybridization or six bonds --- $s^1p^3d^2$ hybridization in the excited state which has 2 unpaired electrons in ground state.

2.2.3 PbS --- a polar compound semiconductor

Recalling that the fundamental idea connected both with atomic structure and chemical binding is the formation of closed shells of electrons, when Pb and S react together the outer electrons of lead, $6p^2$ is transferred to the sulphur's $3s^2$, $3p^4$ electrons. This produces ions Pb^{++} and S^{--} held together by the electrostatic attraction of their opposite charges at a certain distance, the lattice constant, which is analogous to a dipole and is therefore called a polar compound. The crystal structure is a simple rock-salt type (Figure 2.2). Deviations from perfect stoichiometric composition may take place and give rise to imperfection in the crystal lattice.

In a perfect crystal of PbS there are exactly the same number of Pb atoms and S atoms. It is well known, however that an excess of Pb gives an n-type sample. More accurately, PbS may exist as a homogeneous crystalline phase with composition $Pb_{1+\delta}S$, δ being a fraction having a value up to about 10^{-3}. Each excess Pb atom acts as a donor impurity giving an energy level very close to the conduction band. In practice, sometimes they may be considered as overlapping. A value of δ of 10^{-3} would correspond to over 10^{19} donors per cm^3.

2.3 General Properties of PbS

The general properties of PbS are summarised in the Tables 2.1 and 2.2 [40] [41] and the diagrams in Figure 2.1 and Figure 2.2 show its simple cubic, rock-salt structure and the energy bands[42] respectively.

The characteristics such as small energy gap, low resistivity large carrier mobility and unusually high dielectric constant (static), which do not usually appear in polar crystals will have a profound effect on the electrical and optical measurements.

2.3.1 Energy bands

Cuff et al[43] indicated that the valence and conduction band extrema are located at the L points on the Brillouin-zone face (see Figure 2.1). We can also point out that the gap must lie between an adjacent pair of L_1 and L_2', L_3 and L_3' levels which are degenerate in normal conditions.

This is due to the following facts:

(a) The band edges at L belong to states with opposite parity; and we know by symmetry arguments that all allowed direct transitions taking place at L can happen only between states with opposite parity under inversion.

(b) The effective mass of PbS is positive as shown in the Tables 2.1 and 2.2. Hence we know that if L_3' and L_2' belong to the conduction band then L_1, L_3 belong to the valence band.

(c) Furthermore, the extrema of both the conduction and valence bands are located at the zone edge so that there are equivalent ellipsoids. Thus, intervalley transition is sometimes possible.

One more important characteristic for PbS shown in Figure 2.1 is the strong non-parabolicity of conduction and valence band. This complicates the discussion of Phonon interaction. (see Chapter 4)

2.3.2 Extrinsic carriers

As we know that n-type samples are given by excess of Pb atoms, one free electron to the conduction band is contributed by each excess Pb. In our case, samples with free electron concentrations of $10^{16} cm^{-3}$ requires a departure from stoichiometry of less than 1 part of 10^6. The impurity levels associated with these extrinsic carriers lie very close to or within the conduction band.

2.4 Preparation of the sample

2.4.1 Selection of samples

The samples of lead sulphide used in this experiment were

Property	PbS
Crystal structure	Rock-salt
Lattice constant A	5·94
Linear expansion coefficient	$2{\cdot}6 \times 10^{-5}$
Density (g cm^{-3})	7·60
Elastic constants (dyn cm^{-2})[87, 88]	
C_{11}	$12{\cdot}7 \times 10^{11}$
C_{44}	$2{\cdot}48 \times 10^{11}$
C_{12}	$2{\cdot}98 \times 10^{11}$
Melting point (°C)[89]	1114
Heat of formation (kcal mole^{-1})	−22·54
Molar heat at 200°K (cal mole^{-1} deg^{-1})[62]	11·4
Effective Debye temperature at 200°K (°K)[62]	227
Thermal conductivity at 300°K (w cm^{-1} deg^{-1})[7, 90, 91]	0·03
Refractive index at 6 μm[32]	4·19
* Dielectric constant[70] ε_o, ε_∞	190, 18
Piezoresistance constants at 300°K (cm^2 dyn^{-1})	
π_{11}	
π_{44}	
π_{12}	
Magnetic susceptibility (c.g.s. units)[92]	$-0{\cdot}37 \times 10^{-6}$
* Energy gap at 300°K (ev)[40]	
Direct transitions	0·41
Indirect transitions	0·37
Temperature coefficient of energy gap (ev deg^{-1}) (20–400°K)[31]	$+4 \times 10^{-4}$
Intrinsic carrier concentration at 300°K (cm^{-3})	2×10^{15}
Lattice mobility at 300°K (cm^2 v^{-1} s^{-1})	600 (n)† 700 (p)
Temperature dependence of lattice mobility in pure samples	$T^{-5/2}$
Typical values of observed mobility at 77°K	5×10^3–10^4
Typical values at 4°K	10^4–10^5

TABLE 2.1

Crystal structure	Crystal type	cubic
Melting point	T_S (°C)	1,114
Lattice constant	a (Å)	5·91
Thermoelectric power	α (μV/°)	400
Refractive index	n_{opt}	3·91
Optical absorption	λ_0 (mμ)	3,000
Effective mass	$\left(\frac{m_{eff}}{m_e}\right)$ % n / p	— / 0.1
Diffusion coefficient (300°K)	D_n (cm^2 s^{-1})	16*
Life time of electron	τ_n (s)	$2{\cdot}5 \cdot 10^{-7}$*
Electron diffusion mean free path	L_n (cm)	$2 \cdot 10^{-3}$
Hall coefficient	R_H (cm^3/A s)	-10^2
Magnetoresistivity	$\left(\frac{\Delta\rho}{\rho}\right)_{H=10^4 G\beta}$ %	—
Resistivity	ρ (Ωcm)	50
Impurity level	ΔE_{St} (eV)	—
Temperature coefficient of energy gap	$\frac{d\Delta E}{dT}$ (eV/°)	$-2{\cdot}5 \cdot 10^{-4}$
Energy gap	ΔE (eV)	0·37
Mobility	μ_p (cm^2/V s)	350
Mobility	μ_n (cm^2/V s)	640
		PbS

TABLE 2.2

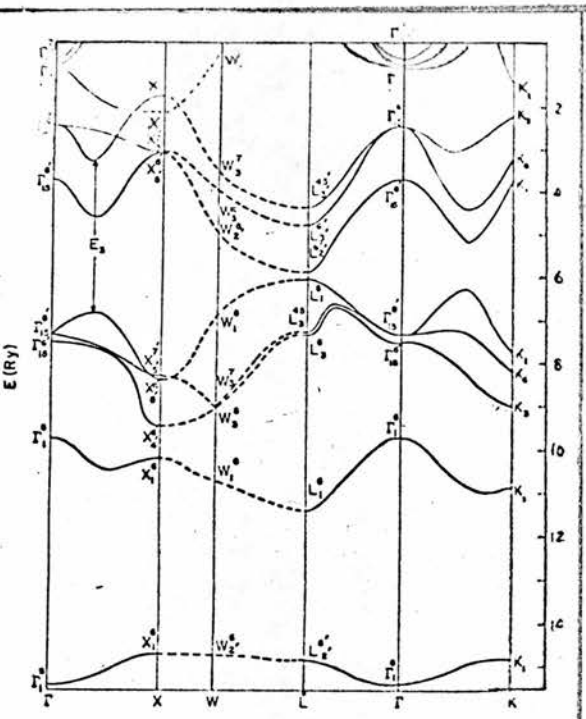

Energy bands of PbS. The solid lines were calculated at several points. The dashed lines are merely sketched in between symmetry points.

FIG. 2.1

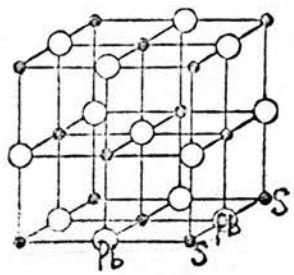

FIG. 2.2

selected from blocks of natural galena. Because of the cubic crystallographic structure, samples could be eleaved easily with a sharp razor blade in the directions parallel to their cubic axes. Bright metallic lustre and smooth and flat surfaces were checked for every sample.

The electron concentration for n-type PbS sample were determined by room temperature Hall effect measurements. Samples of concentrations from $7.49 \times 10^{15}/cm^3$ to 5×10^{17} were selected.

The existence of very few Mn impurities in some of PbS samples was found by a neutron activation experiment done in the Reactor Centre in East Kilbride.

The homogeneity of the sample had to be tested by measuring the resistivity of the bulk sample at short intervals along its dimensions. Fairly homogeneous samples with tolerance less than 10% were selected.

2.4.2 The cutting and etching

Samples were eleaved roughly in rectangular shape by using razor blade and cut accurately to required dimensions by spark machine.

The machine used was a Servomet typeSMD spark machine which was specifically designed for cutting hard brittle or delicate crystals. The machine removes the material from the surface of sample in the immediate vicinity of the cutting tool without mechanical contact with the sample by generating a series of controlled spark

discharges between the cutting tool and the sample. The removal of small crater of material by each spark is finished by melting and vaporisation. Fine surfaces without mechanical distortions or dislocations caused by the cutting are supposed to be obtained.

The typical sample dimensions were 5 x 0.5 x 0.3 mm. measured by a travelling microscope; hence size effects in the Hall measurements can be neglected.

After cutting by the spark machine or lengthy exposure to the atmosphere the sample became oxidised and it could be etched in a warm solution of thioureaic acid for about 30 seconds; the solution was prepared from 30 gm Thiourea + 100 c.c. H_2O + 30 c.c. concentrated HCl. The sample was finally cleaned by running warm water.

2.5 Sample holders and probes

2.5.1 Holder I

For transverse measurements the sample was mounted onto the sample holder I shown in Figure 23. The current-pulse leads were soldered to a pair of copper-block electrodes which could be moved to press on to the two ends of the sample. Two resistivity probes and two Hall probes were press-contacted to the sample. The contact-pressure at the electrodes or probes was adjustable by means of the screws F acting on small phosphor bronze strips. A force of about 50 gm-wt/mm^2 was found to give a contact resistance of less than 1 - 0.5 percent of the total resistance and appeared to cause

(A)

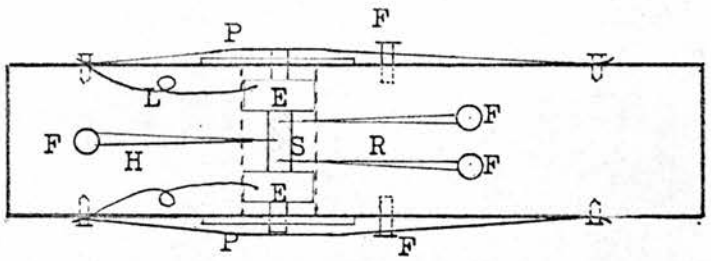

L: pulsed current leads
E: copper-block electrode
S: sample
H: hall probe
R: resistivity probe
F: adjustable screw
P: spring

(B)

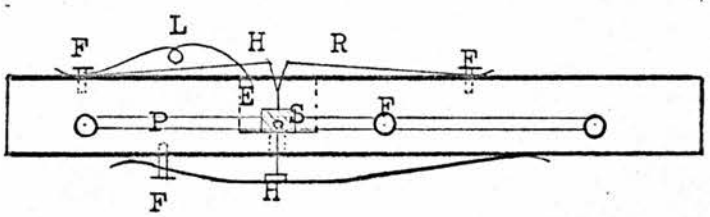

(A) Front-view

(B) Side-view

FIG. 2.3

no damage to the surface of the crystal.

The photograph of the holder is shown in Figure 2.4.

2.5.2 Holder II

For longitudinal resistivity measurements the sample was mounted on to the sample holder II which was specially designed for the small experimental space in the 77°K cryostat II (see next chapter). Similar electrodes and probes were constructed. The diagram and photograph are shown in Figure 2.5 and Figure 2.6 respectively. Similarly the contact force at the upper electrode can be adjusted by screw F acting on a small spring.

For both holders, the probes were required to be as small as possible in order to avoid introducing errors in the measurement. The contact area of the probe was about 0.3 mm^2.

2.5.3 Special precautions

Before mounting the sample on the holder, each end of the sample was coated with a soft and thick copper layer; this is done for press-contacts to ensure better electrical conduction.

One of the serious difficulties in the use of this fast pulse method (see next chapter) was the presence of spurious voltages due to the vibrations of leads and the sample itself. Therefore, the electrodes and probes were fixed firmly to the holder. The leads were fastened solidly to the head of the holder to prevent any relative motion. Shielding and good earthing were also used to

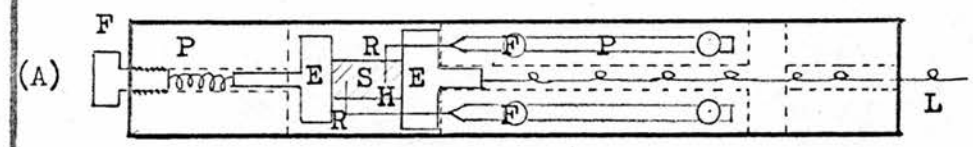

L:pulsed current leads
E: copper-block electrode
S: sample
H: thermal couple
R: resistivity probe
F: adjustable screw
P: spring

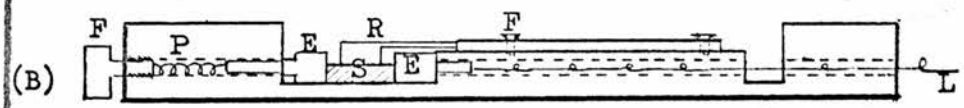

(A) FRONT-VIEW

(B) SIDE-VIEW

FIG. 2.5

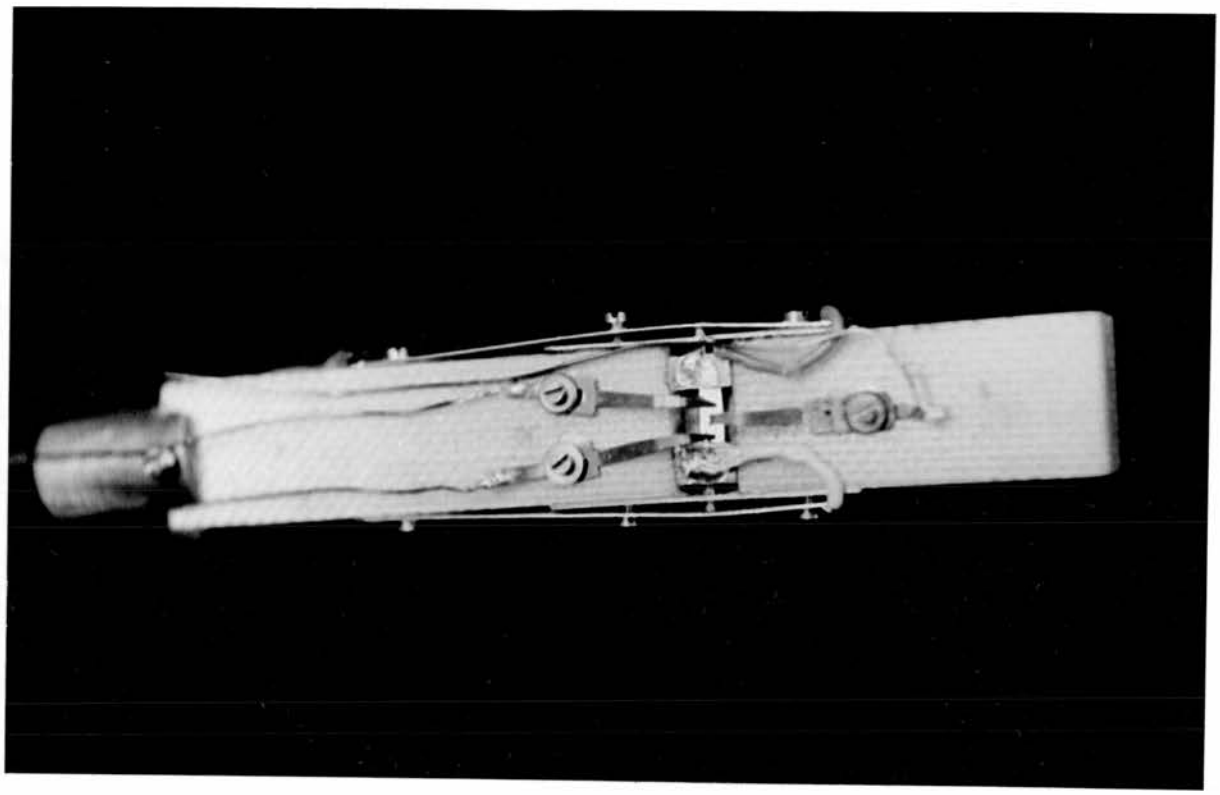

FIG. 2.4

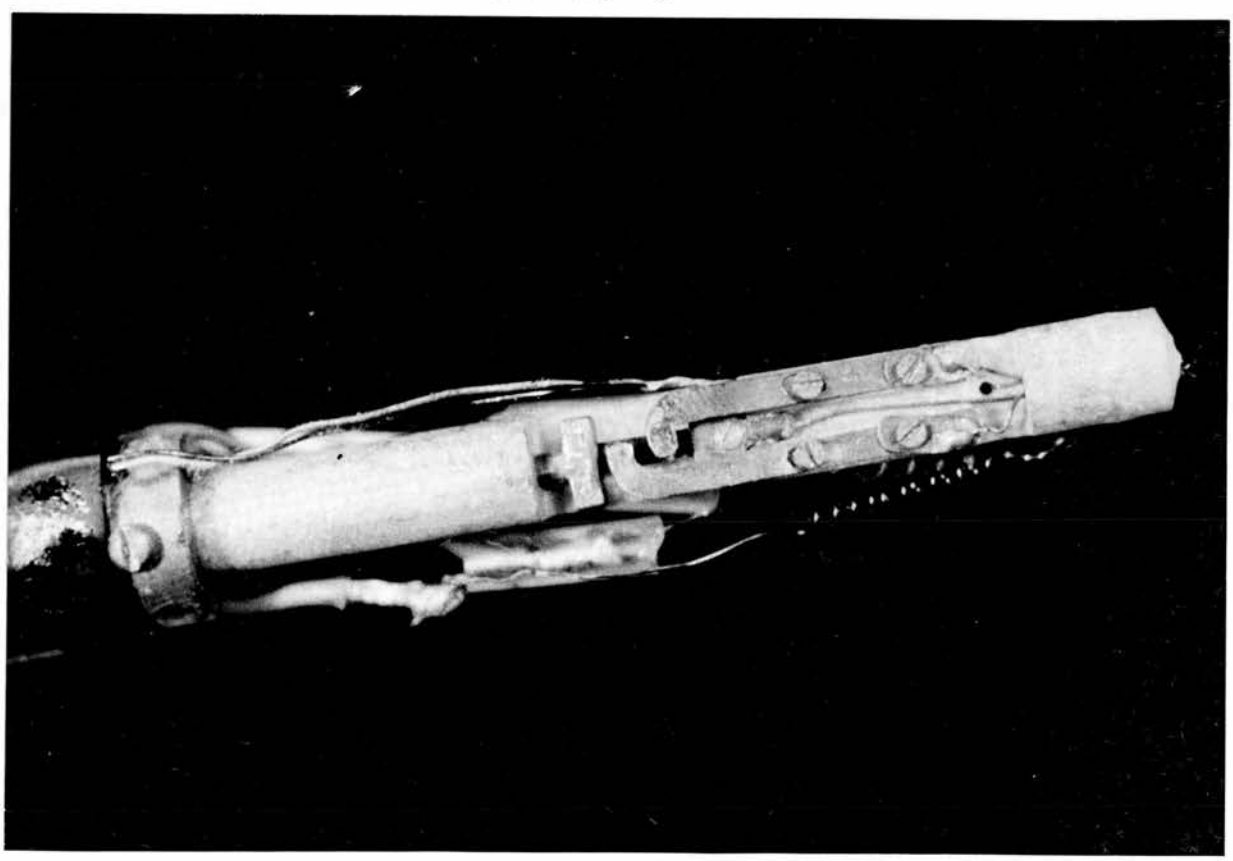

FIG. 2.6

reduce circuit noise and stray voltages; while well-matched cables, sockets and plugs were used to eliminate unwanted reflections of pulses.

To reduce the geometrical effects that distort the magneto resistance measurement results, the resistivity probes made contact to the sample at a distance exceeding double the width of the sample away from the current electrodes and the current electrodes cover the entire end-surface area of the sample. It was also necessary to locate with great care the resistivity probes along the current lines on the sample; and to pay close attention to the correct placement of the sample in the magnetic field.

2.5.4 The problem of injection of carriers

Since this kind of sample holder involved contacts of metal and semiconductor, injection of minority carriers should be considered. The potential barrier existing at the semiconductor surface can be illustrated by the potential diagram of Figure 2.7.

The significant injection quantity for a contact is given by $r_c - r_o$, where r_c is the fraction of the total current at the contact due to minority carrier and r_o is a constant representing the minority carrier current fraction in the bulk material for equilibrium condition. For our n-type samples, fairly close to intrinsic material has been selected (see 2.4.1); so samples have large minority carrier density. $r_c - r_o$ will be slightly larger than zero and the contact will be very weakly injecting.

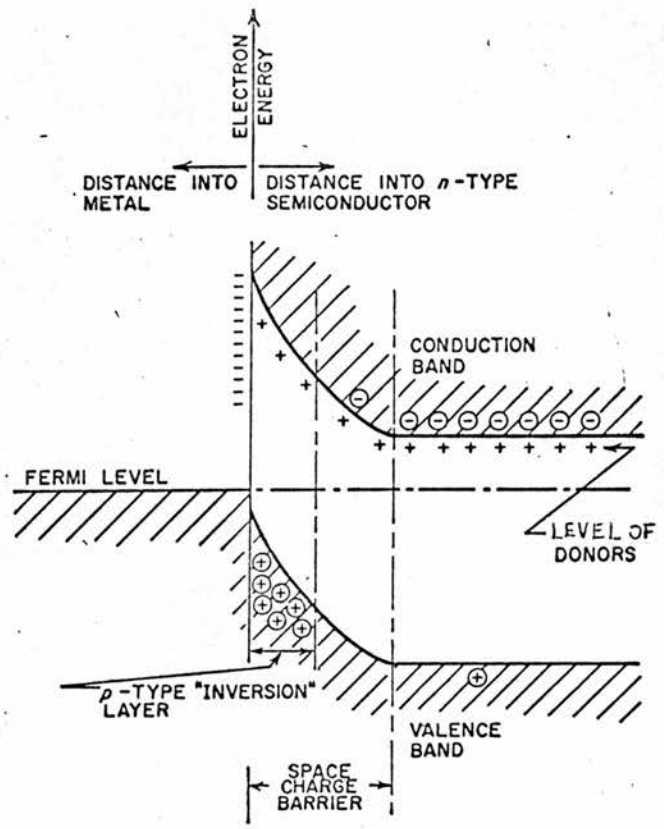

Equilibrium potential energy diagram for contact between a metal and an *n*-type semiconductor. The formation of a *p*-type "inversion" layer permits hole injection into the semiconductor when the metal is biased positively.

FIG. 2.7

Experimentally, the flatness of the current pulses checked by sampling oscilloscope gave evidence that there was no injection from the contacts.

Furthermore, probes are quite far away from the electrode contacts and no current is supposed to pass through them during the measurement in our pulse-bridge method (see next chapter). Therefore, the injection effect can be ignored.

CHAPTER 3

EXPERIMENTATION AND EQUIPMENT

3.1 Cryogenic temperature baths

It is easier to raise the electron temperature above that of the lattice if the lattice itself is cooled to low temperatures.

Since the transport behaviour of the conduction electrons is sensitive to the lattice temperature, different cryostats were designed for different investigations.

3.1.1 Cryostat I —— Liquid helium bath

Most of the experiments were done at the temperatures between $4.2^{\circ}K$ and $1.4^{\circ}K$. The sample was mounted on the sample holder immersed in liquid helium in a dewar vessel. Since all glass dewars are to some extent permeable to helium gas and hence lose their vacuum insulation rather easily, a metal dewar was therefore used in our experiment. A not-to-scale schematic diagram of this dewar is shown in Figure 3.1.

Based on the fact that the saturation vapour pressure of liquid helium is a function of its temperature, the bath temperature could be varied from $1.4^{\circ}K$ to $4.2^{\circ}K$ by changing the vapour pressure. The experimental arrangement is shown in Figure 3.2. The pump removes the vapour. V_a and V_b represent valves which present variable impedances in the line to allow the effective pumping rate to be set anywhere from zero to the full speed of the pump. V_a is a coarse control while V_b a fine one. They are adjusted to bring the manometer pressure

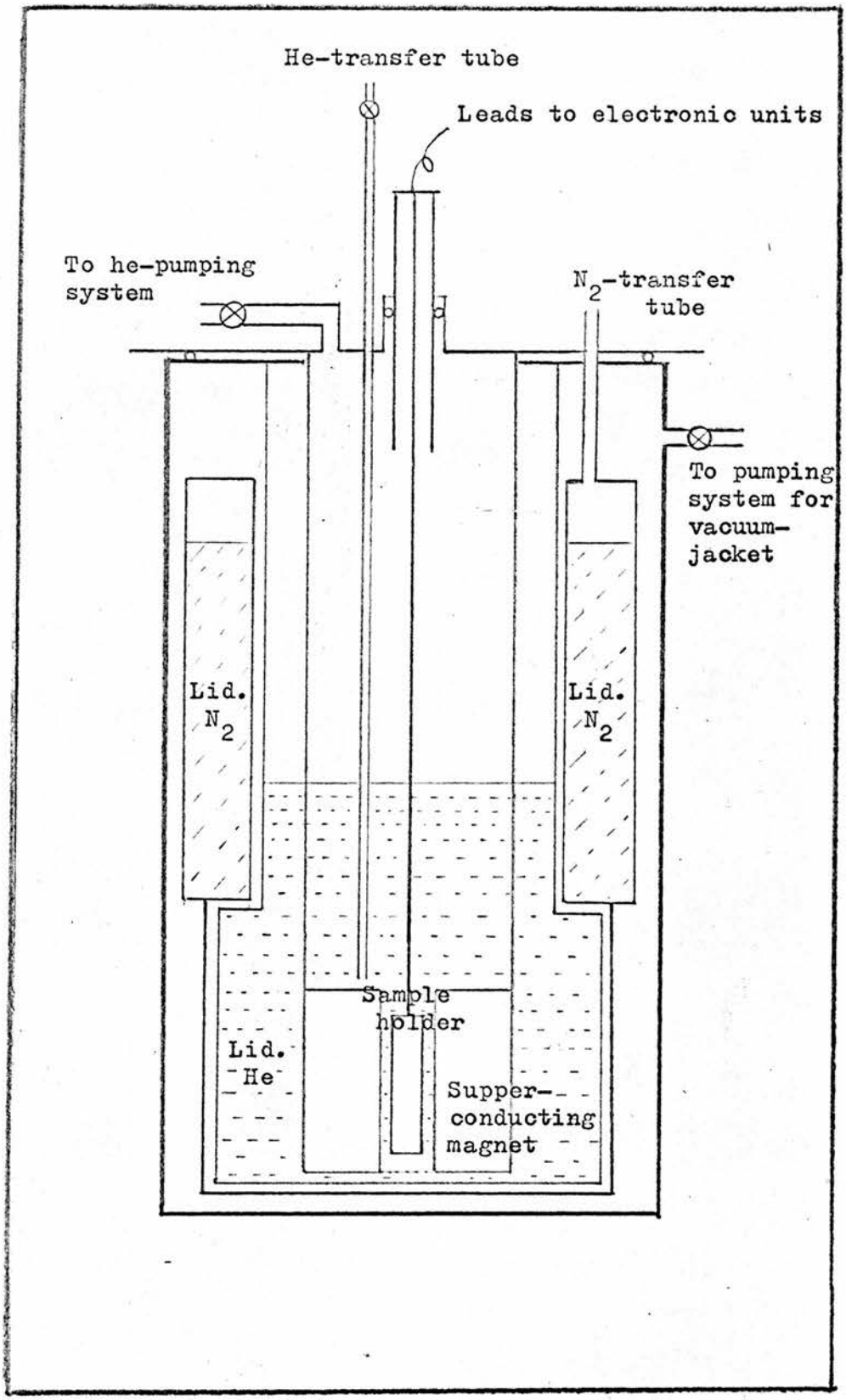
He-transfer tube
Leads to electronic units
To he-pumping system
N_2-transfer tube
To pumping system for vacuum-jacket
Lid. N_2
Lid. N_2
Sample holder
Lid. He
Supper-conducting magnet

FIG. 3.1

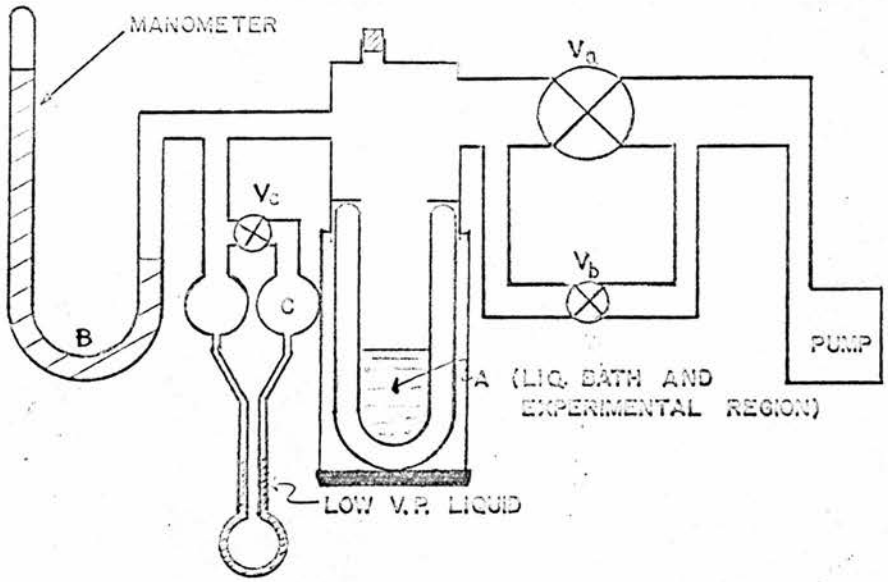

Arrangement of possible liquid helium cryostat. The manometer on the left-hand side becomes, in effect, the thermometer.

FIG. 3.2

to the desired value. The pressures shown on the manometers B and C which are filled with mercury and butyl phthalate respectively, can readily be converted to temperatures by standard tables.

The liquid levels could be detected by the change of resistance of a series of thermal-resistors which were located at different levels inside the dewar.

3.1.2 Cryostat II —— Liquid nitrogen bath

Some of the experiments in this work were carried out at liquid nitrogen temperature 77°K with high magnetic fields. Requiring some modification of a standard cryostat, we have constructed a simple device, cryostat II[44] which enables us to maintain a constant temperature, 77°K, for the sample in the core of a superconducting solenoid immersed in liquid helium.

The assembly is shown in Figure 3.3. The sample chamber consists of a vacuum-jacketed stainless steel tube which fits into the inner cylinder of the magnet. The outlet F is connected to a diffusion pump to obtain a vacuum of better than 10^{-4} torr and the surfaces E of the jacket are polished to reduce radiation.

A liquid nitrogen reservoir B of spiral exit type is connected to the sample chamber through a needle valve C which controls the nitrogen flow. Below the sample holder G and thermometer K is placed a small 30 ohm heater P connected to a power supply.

Imperfect thermal-isolation of the liquid nitrogen from the

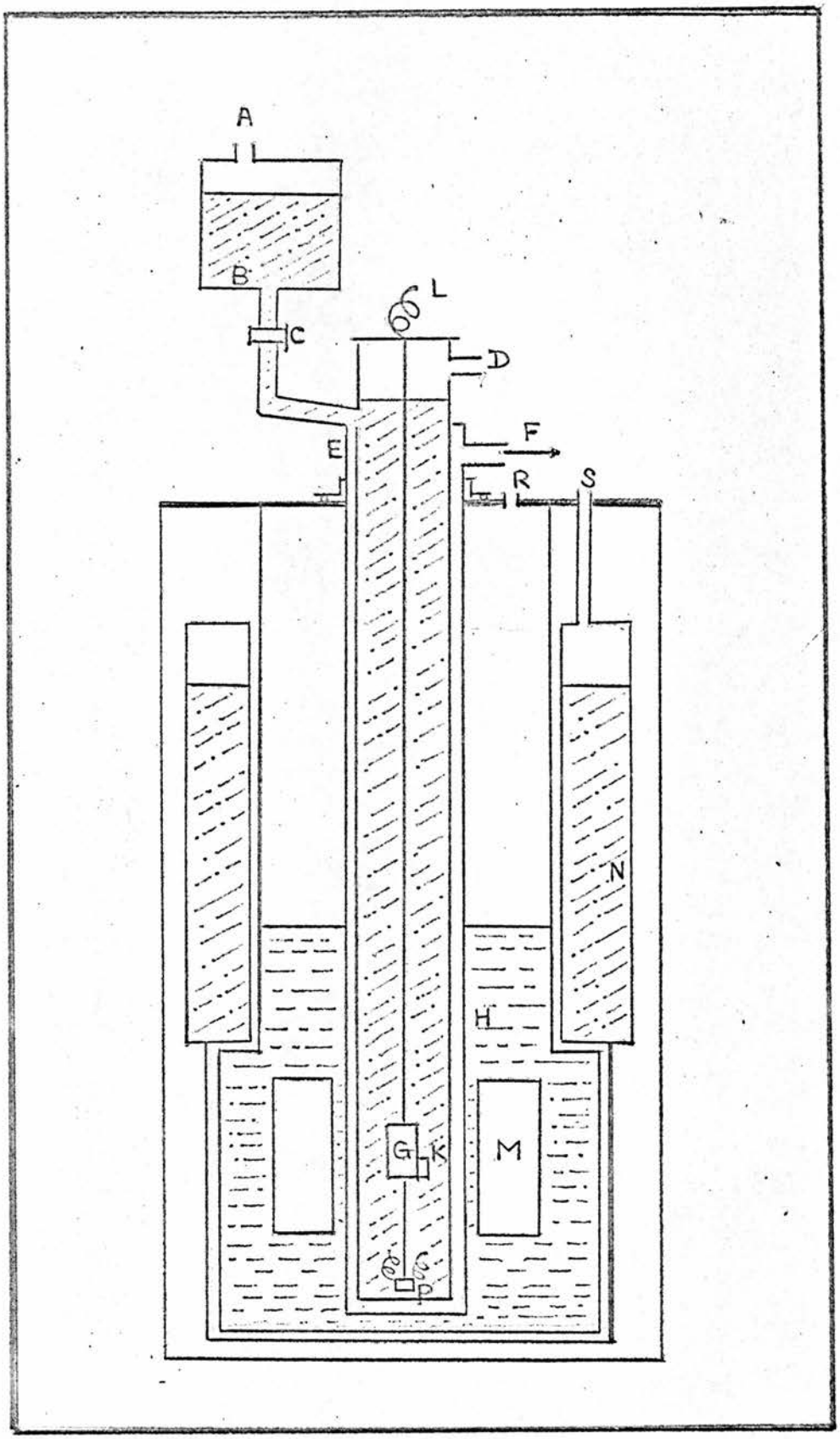

FIG. 3.3

helium bath tends to cool the nitrogen in the region of the sample holder below the temperature of the normal boiling point. This is balanced by applying about one watt from heater P situated at the bottom of the chamber. To maintain the liquid level constant the needle valve C is adjusted to give a flow of liquid of about 0.1 cc per second. In operation, once the current through P and the liquid flow through C has been set, no further attention is required.

Checks on thermometer K, adjacent to the sample holder, show that the temperature remains constant within 0.5°K for several hours.

3.2 Superconducting magnet

Magnetic fields used in our measurements were generated by a superconducting solenoid immersed in the liquid helium. It is a cold-drawn niobium-titanium coil made by Oxford Instr. Co. which provides magnetic fields up to 40 K-gauss.

The solenoid was driven by an Oxford Instrument 3 phase superconducting magnet power supply unit. A build-in automatic cut-out switch served as a safety device in case of the magnet going normal.

When running up the solenoid, care should be taken to avoid sharp current transitions and the magnet should not be run at currents in excess of the specified maximum value. A sweep unit was used which provided an automatic linear sweep of magnet current. The usual running-up time from zero to a desired value is of the order of 2 to 5 minutes.

3.3 The fast pulse technique

In order to heat the electron gas but avoid the Joule-heat generated in the sample, fast pulse techniques were employed in the present experiment. The pulse used was square in wave form, 5 to 10 μ-sec in width, 30 to 100 cycle per second in repetition and 2 to 4 n-sec in 5% to 95% rise-time.

3.3.1 The generation of fast pulse with high output power

(a) Advance Instrument PG 55 high power pulse generator:-

Pulses below 1 amp fed to the sample were obtained from the Advance Instrument PG 55 generator. It is basically a solid state electronic multivibrator system with a clock timing device. The output stage is fully protected against accidental short circuit or open circuit. Coaxial cable of 50 ohm was required to match the output impedance.

(b) Delay-line pulse generator

When the output power of a pulse is required to have more than 1 ampere to feed the sample, a generator of electronic type encounters considerable difficulties if a rapid rise-time is to be maintained. Therefore a special type, delay-line generator has to be designed to provide fast rise-time and high power. Furthermore these have the advantage over the multivibrator type of generator that the pulse length is determined solely by a static element, the delay-line and the rise-time by a mercury-wetted relay switch, and does not depend on the stability of transistor characteristics.

Figure 3.4 shows the circuit of the generator. The power supply provided stabilized high current to the mercury relay so that with the contact in one position the delay line was charged. When the contact moved to the other position the line was connected to the sample. A voltage step then moved down the line half discharging the distributed capacity as it went. On reflection from the far end of the line the step travelled back discharging the line completely and thus giving rise, at the input end, and hence across the sample, to a square pulse whose length depended on the length of the line.

The mercury-wetted relay used was a Elliott EB SC 65017/01 with switching time 2 to 4 n-sec; while the delay line is Radiospear uniradio 95 coaxial cable. The length of the cable was adjusted to have suitable pulse width.

The contact assembly of the mercury-wetted relay is sealed in a glass capsule filled with high pressure ultra dry hydrogen.

The platinum contact surfaces are wetted with mercury, which when switching action is taking place, is continuously renewed from the reservoir by capillary action.

A magnetic field in proximity to the capsule causes the armature to transfer from the normally closed contact to the normally open contact.

In Figure 3.5 the procedure of action during a switch cycle is shown as follows:-

1. Mercury (shown hatched) covers armature and contact faces.

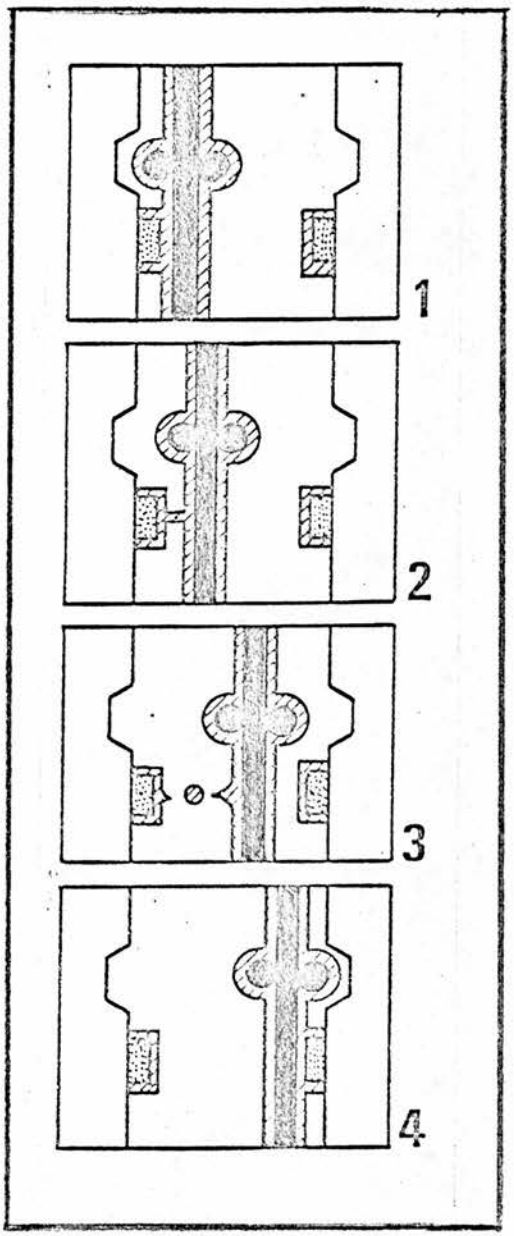

FIG. 3.5

2. & 3. As armature moves from open to closed position, mercury filament breaks before new contact is made in a "break before make" action. Ruptured mercury surfaces accelerate away from each other at a very high acceleration. This produces an extremely rapid make and break action.

4. Contact surfaces join. Mercury wetting dampens rebound, eliminates chatter, provides uninterrupted metallic contact, for the mercury on the contacts absorbs the mechanical energy during the "make" condition.

Similar action occurs on release.

3.3.2 The pulse bridge

To provide a null-detecting method in this experiment, a pulse-bridge was constructed. Figure 3.6 shows the bridge and the related schematic circuit. The bridge consists of four arms, namely a sample which has a resistance R_x between the two current electrodes, a standard resistance R_s, a variable resistance R_b with a precision scale to balance the whole bridge when R_x changes value and a potentiometer-resistance R_p with a dial scale precisely indicating the position of a sliding contact. Usually R_s was chosen to be about one tenth of R_x and R_b was one sixth of R_p. All resistances used were non-inductive.

3.3.3 Detecting system

The input pulse height and pulse form were measured by CRO 2 across the standard resistance R_s. This was a Tektronix's 502A high

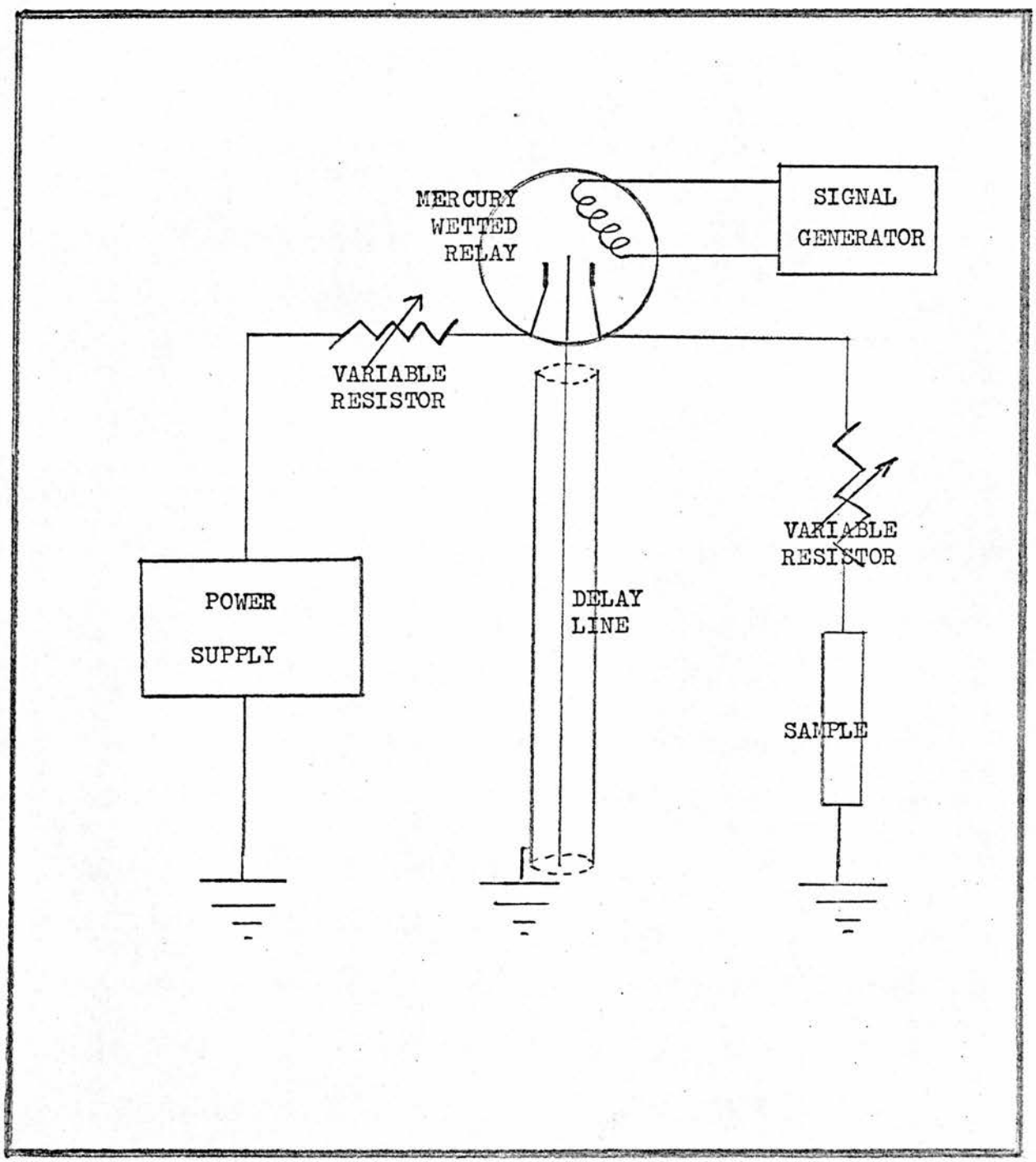
MERCURY
WETTED
RELAY
SIGNAL
GENERATOR
VARIABLE
RESISTOR
VARIABLE
RESISTOR
POWER
SUPPLY
DELAY
LINE
SAMPLE

FIG. 3.4

gain, fast oscilloscope. The Null-detecting system consists of two identical differential amplifiers and a fast oscilloscope as a balance detector. The oscilloscope was either the Tektronix's 502A or a Tektronix 3S76 sampling CRO which gave a clearer additional check of pulse form.

3.4 The measurements

3.4.1 The experimental set-up

The block diagram for apparatus used in this experiment is shown in Figure 3.7. It consists of the following main units.

(1) Cryostat: the sample mounted on the sample holder was put in the cryostat. A main pumping system was used to control the helium vapour pressure. An additional pumping system was designed specially for cryostat 2. Both cases were connected to helium and nitrogen transfer system.

(2) Magnetic field: a wide range of magnetic field was applied by means of a superconducting solenoid. Low magnet currents were obtained from a stabilized d.c. current supply while high currents were obtained from a three-phase power supply with sweep unit.

(3) Detection system: the main parts are a pulse bridge, a pulse generation system and a null-detecting oscilloscope.

3.4.2 General Procedure

The general procedure for manipulating the bridge device is given in the following way:-

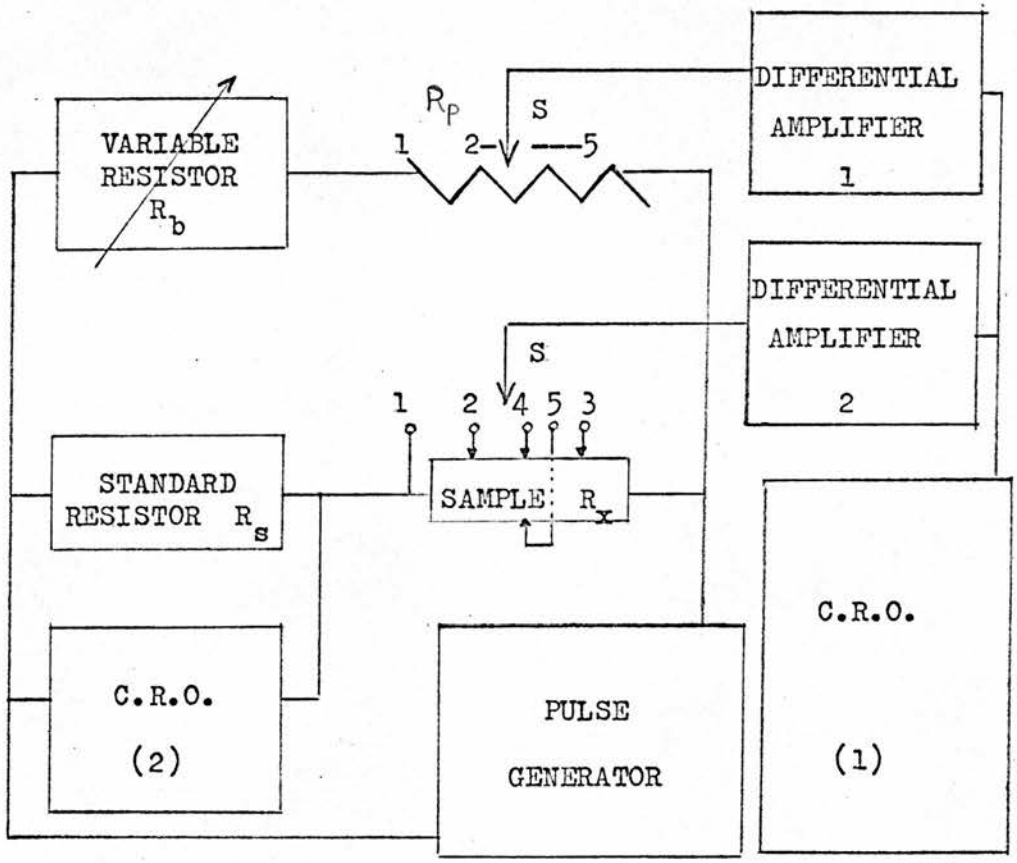
VARIABLE
RESISTOR
R_b
R_P
S
1
2
5
DIFFERENTIAL
AMPLIFIER
1
DIFFERENTIAL
AMPLIFIER
2
S
1
2
4
5
3
STANDARD
RESISTOR R_s
SAMPLE
R_x
C.R.O.
(2)
PULSE
GENERATOR
C.R.O.
(1)

FIG. 3.6

(1) A suitable pulse is selected by adjusting the pulse generator. This includes the rise-time, repetition-frequency and the pulse height which is controlled by the output power via an attenuator. For the delay-line unit the pulse height can be adjusted by the stabilized power supply.

(2) The absolute value of the pulse height is measured by a fast CRO across a standard resistor R_s; from the value we get, we can easily calculate the electric field across the sample.

(3) For balancing the bridge we refer to diagram 3.6. With the double switch in position 1 the bridge is balanced by adjusting R_b. This gives $V_s = R_s I_s = R_b I_b$ where V_s is the potential drop across the standard resistance and I_s and I_b are the sample current and the potentiometer current respectively under the balanced condition.

In balancing the bridge, the sensitivity of the differential amplifier may be increased in order to detect whether a good balance has been obtained. When the balance is perfect, the pulse on the CRO 1 will completely vanish.

(4) The switch is now moved to the position 2 and R_p is adjusted to get the balance point at R_{p2}.

(5) Similar operations are done for the second resistance probe 3 and R_{p3} is obtained.

(6) Similarly, for Hall probes 4 and 5, R_{p4} and R_{p5} are obtained.

(7) During the above procedure, a magnetic field can be applied by a superconducting solenoid. Operations should be repeated after reversing the field.

3.4.3 The measurement of resistivity, magnetoresistivity, Hall coefficient and the electric field across the sample.

From the above experimental data, one can easily calculate the following quantities:

(1) Resistivity and magnetoresistivity

$$\rho = \left(\frac{w \cdot d}{l}\right) R_s \left(\frac{R_{p2} - R_{p3}}{R_b}\right)$$

(2) Hall coefficient

$$R_H = \left(\frac{d}{B}\right) R_s \left(\frac{R_{p4} - R_{p5}}{R_b}\right) \times 10^8$$

(3) External electric field

$$E = \left(\frac{1}{L}\right) V_s \left(\frac{R_{p2} - R_{p3}}{R_b}\right)$$

where, in laboratory units, w is the width, d, the thickness, L, the distance between two resistance probes of the sample, respectively and B is the intensity of the applied magnetic field.

3.4.4 The measurement of carrier concentration of the samples at room temperature.

The carrier concentration and the carrier sign are determined by the conventional D.C. Hall measurement. The main instrument is an accurate potentiometer. Then the Hall coefficient

can be measured by

$$R_H = \frac{V_y \cdot d}{I \cdot B}$$

where V_y is the corrected Hall voltage given by

$$V_y = \frac{1}{2}\left\{ \frac{1}{2}(V_y(+H+I) - V_y(-H+I)) - \frac{1}{2}(V_y(+H-I) - V_y(-H-I)) \right\}$$

and by introducing the Hall field factor we have

$$R_H = \frac{\gamma_H}{ne}$$

therefore,

$$n = \frac{\gamma_H \, I \, B}{e \, V_y \, d}$$

In our calculation we take the approximation $\gamma_H = 3\pi/8$.

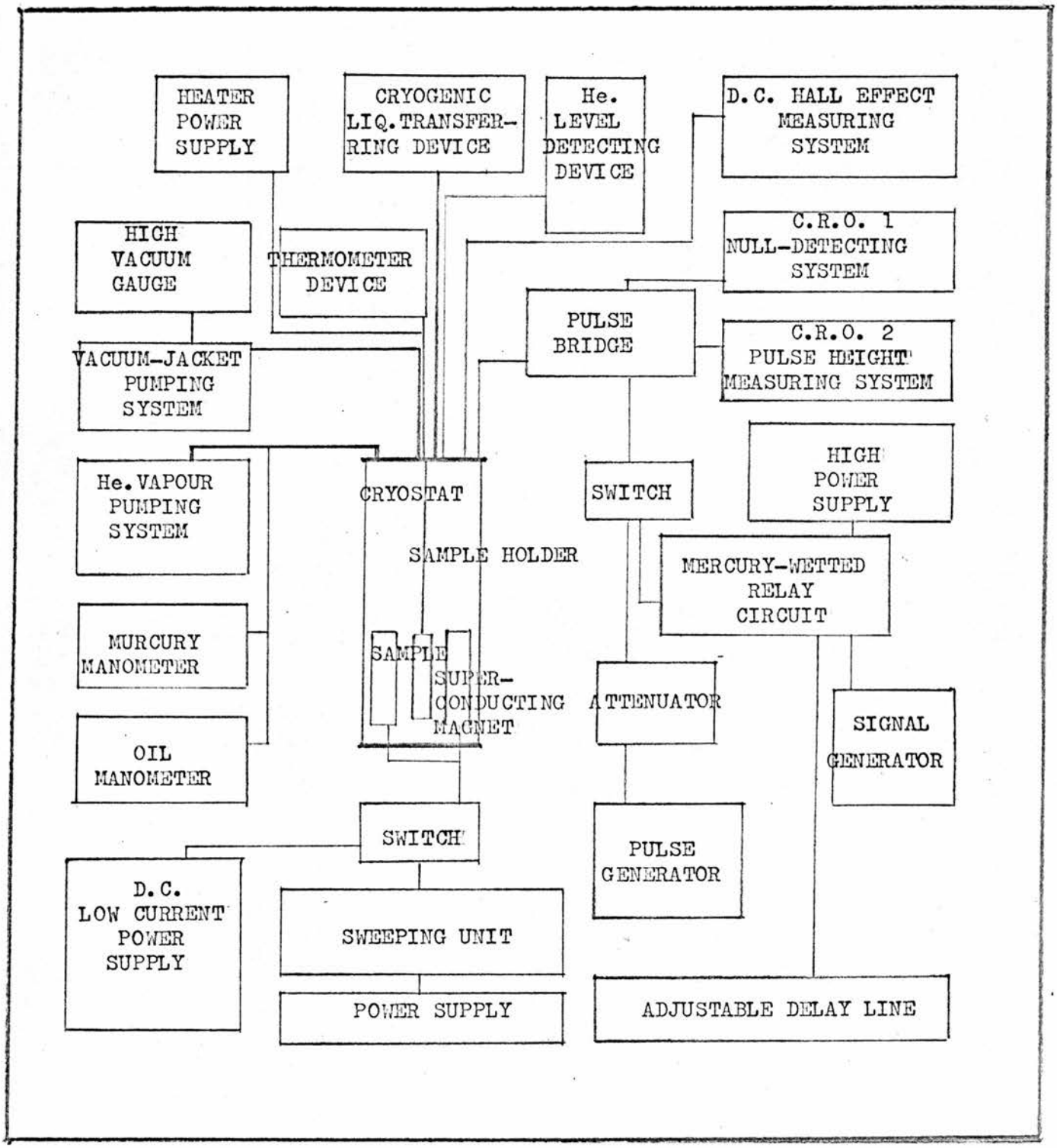
HEATER POWER SUPPLY
CRYOGENIC LIQ. TRANSFER-RING DEVICE
He. LEVEL DETECTING DEVICE
D.C. HALL EFFECT MEASURING SYSTEM
HIGH VACUUM GAUGE
THERMOMETER DEVICE
C.R.O. 1 NULL-DETECTING SYSTEM
PULSE BRIDGE
C.R.O. 2 PULSE HEIGHT MEASURING SYSTEM
VACUUM-JACKET PUMPING SYSTEM
He. VAPOUR PUMPING SYSTEM
CRYOSTAT
SAMPLE HOLDER
SWITCH
HIGH POWER SUPPLY
MERCURY-WETTED RELAY CIRCUIT
MURCURY MANOMETER
SAMPLE
SUPER-CONDUCTING MAGNET
ATTENUATOR
SIGNAL GENERATOR
OIL MANOMETER
SWITCH
PULSE GENERATOR
D.C. LOW CURRENT POWER SUPPLY
SWEEPING UNIT
POWER SUPPLY
ADJUSTABLE DELAY LINE

FIG. 3.7

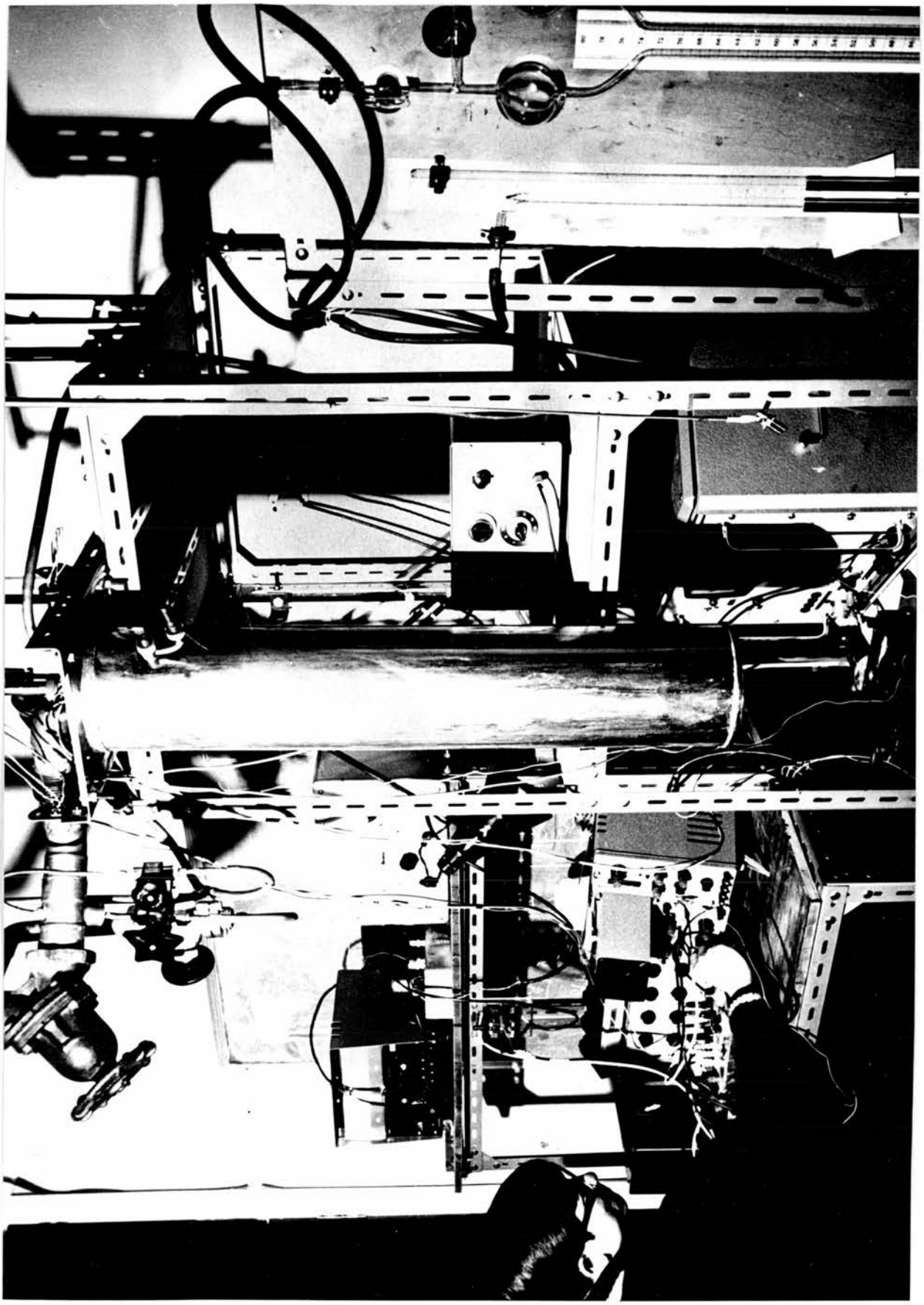

FIG. 3.8

CHAPTER 4

DISCUSSION OF THE RESULTS OBTAINED AT NITROGEN TEMPERATURE

4.1 Measurement of electron concentration

D.C. Hall measurements were carried out at room temperature in order to obtain the carrier concentrations of the samples used in this work. The results are listed in Table 4.1.

4.2 Measurements at nitrogen temperature

4.2.1 Resistivity measurements

Figure 4.1 shows a typical curve of resistivity against ln E at 77 deg. K in zero magnetic field. In the low field region an ohmic part can be observed. This is followed by a small dip before the resistivity begins to rise fairly steeply at high electric fields. For sample K'43 measurements were made up to fields of 2500 volts per cm. No sign of avalanche multiplication was observed up to this field. We note however that in lead telluride and lead selenide, avalanche multiplication was not observed until fields of order of 10^3 to 10^4 volts per cm. had been reached [45],[46] and might be higher for lead sulphide. Higher fields could not be obtained with our existing apparatus.

4.2.2 Resistivity in a longitudinal magnetic field.

Sample No.	Lab Index No.	Electron Concentration at Room Temp. (cm^{-3})	Low Field Resistivity at He. Temp. (ohm-cm)
1	Y 24	7.5×10^{15}	0.64
2	K 4	9.3×10^{15}	0.39
3	K 8	9.5×10^{15}	0.31
4	Y11	1.02×10^{16}	0.23
5	C'43	1.15×10^{16}	0.19
6	K'43	1.17×10^{16}	-
7	Y 23	1.19×10^{16}	-
8	C'38	1.31×10^{16}	0.053
9	J 100	1.4×10^{16}	-
10	K 1	1.47×10^{16}	0.052
11	K 3	1.48×10^{16}	-
12	K 7	1.53×10^{16}	0.05
13	Y''110	5.0×10^{17}	0.007

TABLE 4.1

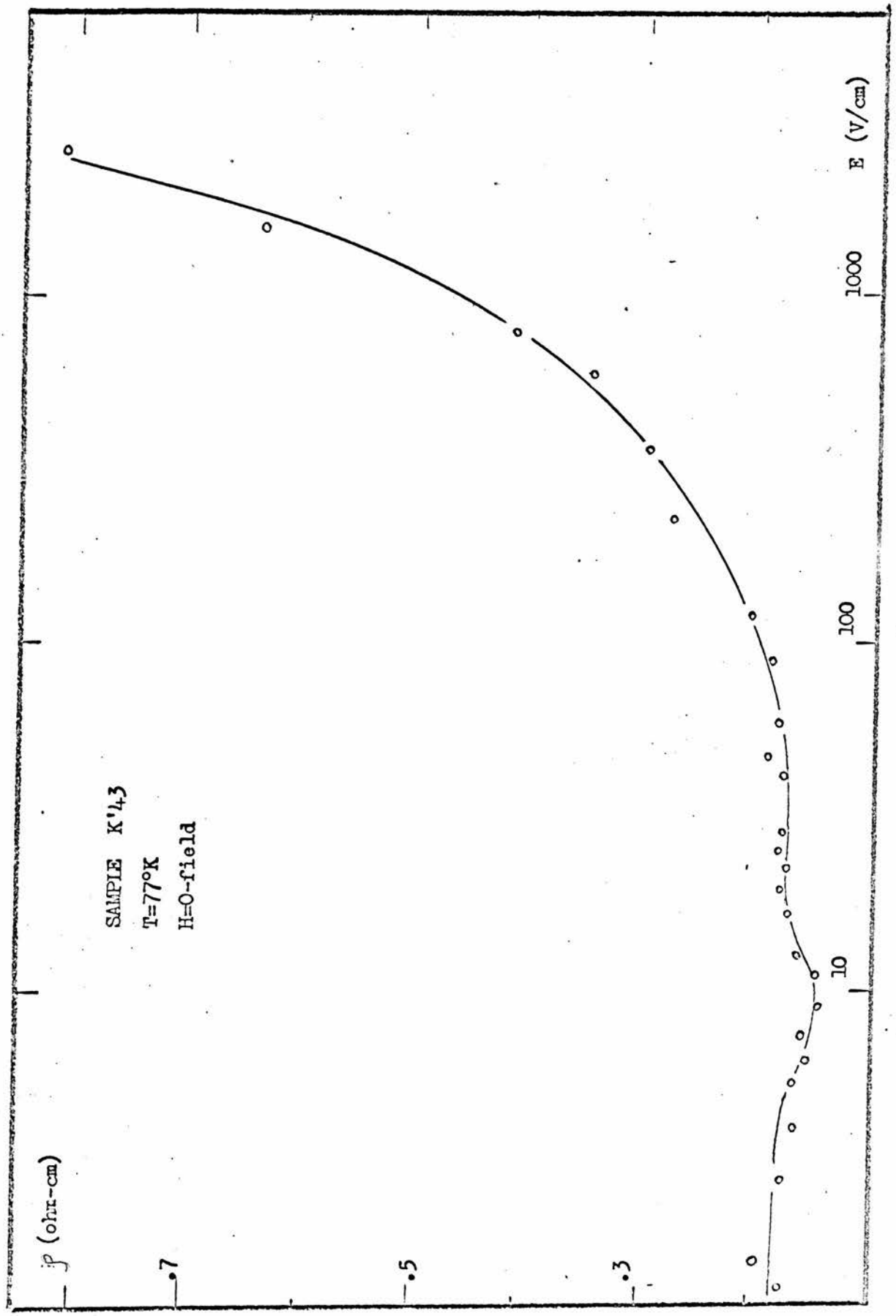

FIGURE 4.1

Because of space limitation in the 77deg. K cryostat measurements were made only in the longitudinal configuration.

The variation of resistivity for samples Y23 and K3 as a function of both magnetic and electric field is shown in Figures 4.2 and 4.3 respectively. Comparing Figures 4.1, 4.2 and 4.3 we note that the steep rise in resistivity begins at higher electric fields for samples of lower electron concentration.

To illustrate the dip in resistivity we have plotted ρ_L against ln E for sample J100 on a bigger scale in Figure 4.5

4.3 The displaced Maxwell-Boltzmann distribution function

At 77 deg. K the electrons with sufficient energy in the sample will interact with the lattice vibrations, absorbing and emitting phonons. In the absence of an external electric field absorption balances emission when the electrons have the Maxwell-Boltzmann distribution

$$f_o \sim e^{-\mathcal{E}/KT} \qquad \text{.....(4.3.1)}$$

and the number of phonons $\overline{N}_q$ with wave vector $\underline{q}$ is given by

$$\overline{N}_q = 1/(e^{\hbar\omega_q/KT} - 1) \qquad \text{.....(4.3.2)}$$

where K is the Boltzmann constant, T, lattice temperature,

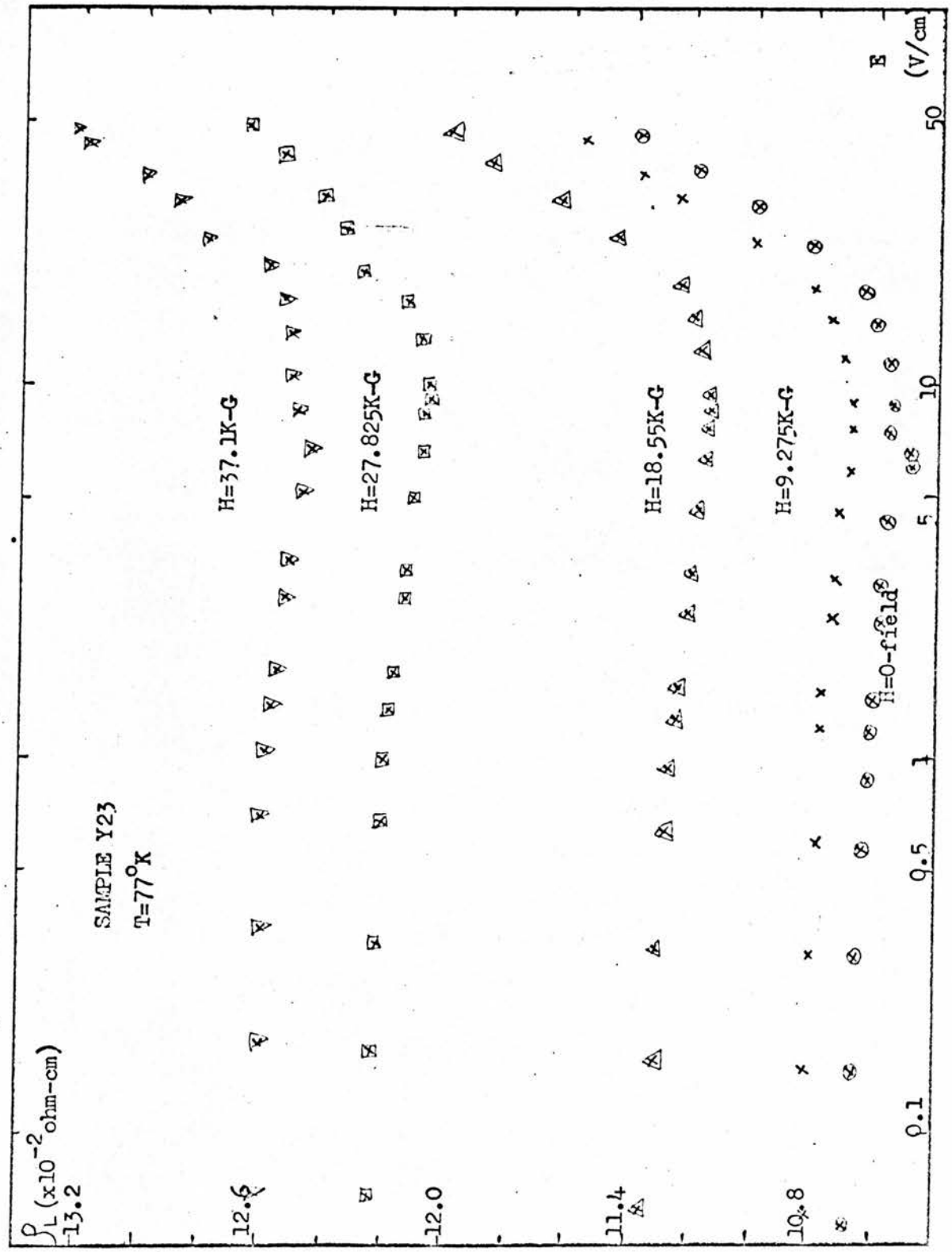
ρ_L (x10^{-2} ohm-cm)
13.2
12.6
12.0
11.4
10.8
SAMPLE Y23
T=77°K
H=37.1K-G
H=27.825K-G
H=18.55K-G
H=9.275K-G
H=0-field
0.1
0.5
1
5
10
50
(V/cm

FIGURE 4.2

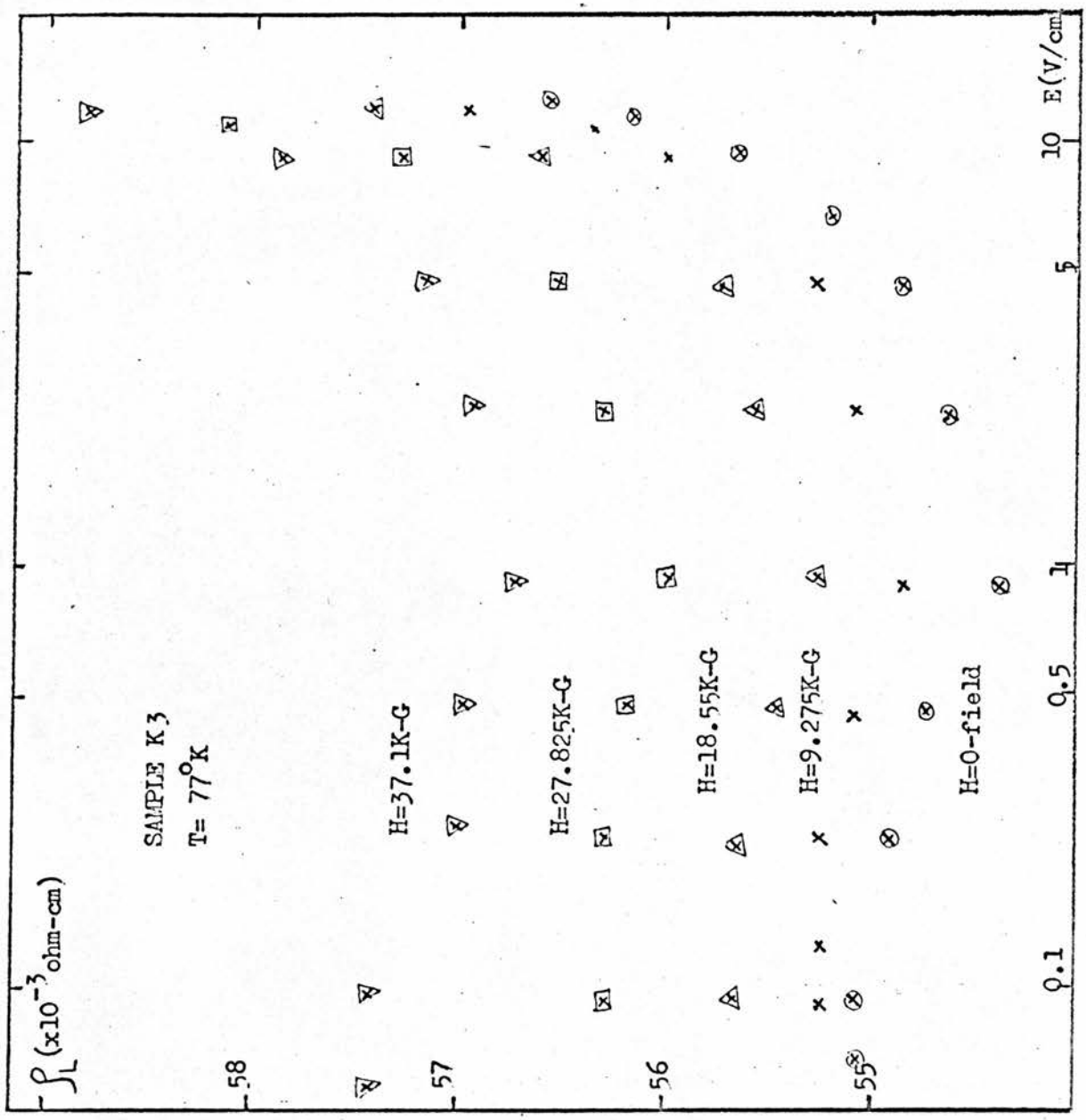
SAMPLE K3
T= 77°K
H=37.1K-G
H=27.825K-G
H=18.55K-G
H=9.275K-G
H=0-field
ρL (x10⁻³ ohm-cm)
E(V/cm)
58
57
56
55
0.1
0.5
1
5
10

FIGURE 4.3

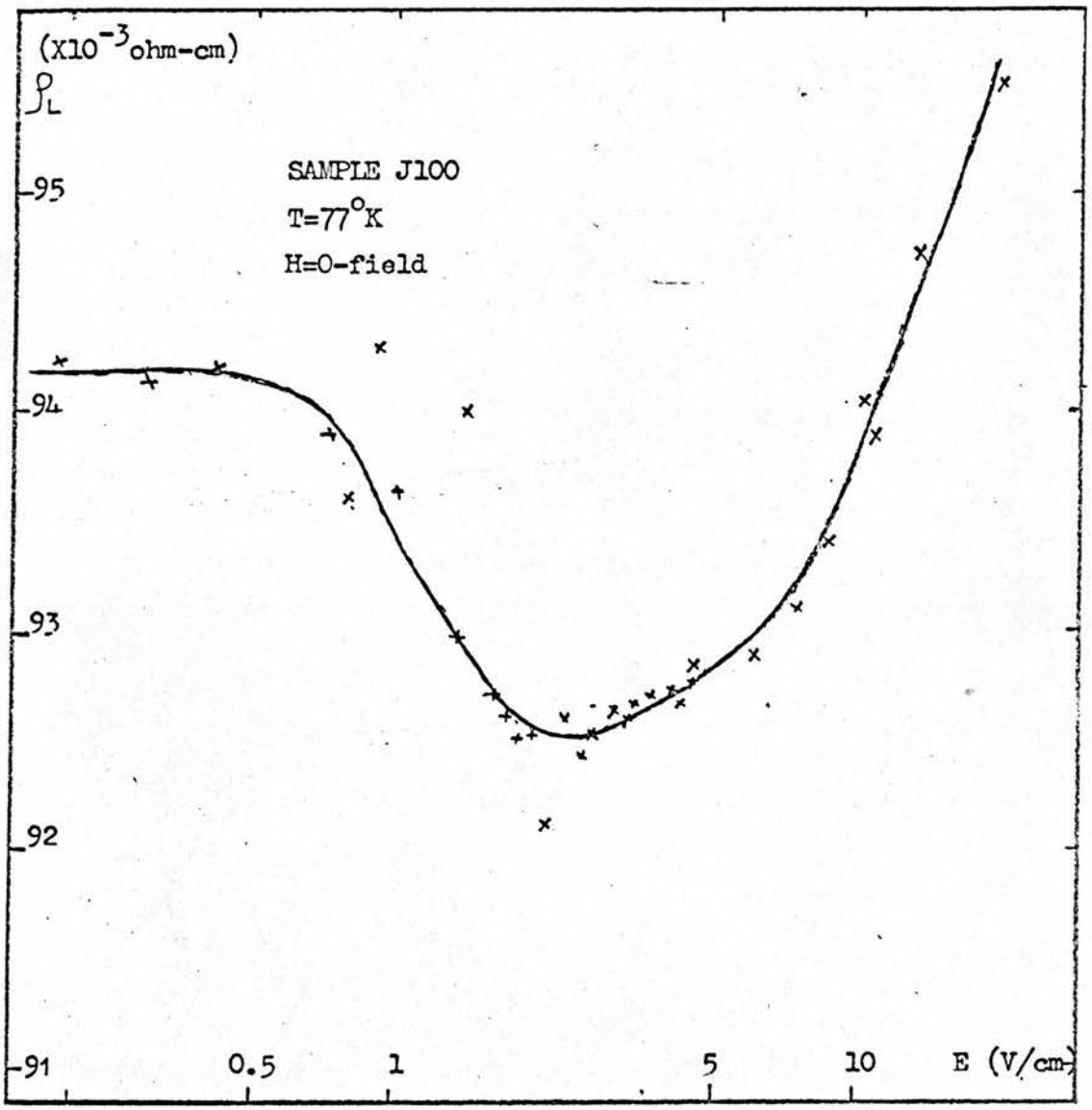
(X10^{-3}ohm-cm)
ρ_L
SAMPLE J100
T=77°K
H=0-field
95
94
93
92
91
0.5
1
5
10
E (V/cm)

FIGURE 4.5

$\hbar\omega_q$, the energy of a phonon and $\mathcal{E}$, the energy of an electron.

However when an electric field E is applied the rate of energy supplied to the electrons increases. So the average energy of the electrons and also the average rate of phonon emission will be increased. A steady state is reached when the average rate of energy loss equals the rate of gain from the field, ie.

$$\left\langle \frac{d\mathcal{E}}{dt} \right\rangle_{gain} = \left\langle \frac{d\mathcal{E}}{dt} \right\rangle_{loss} = e\mu E^2 = eEv \quad \ldots\ldots\ldots(4.3.3)$$

This requires a change in the distribution function (4.3.1). Usually we may introduce a perturbation term f_1, depending on the details of band structure and scattering mechanism, added to the thermal equilibrium distribution function for the case of small electric fields, ie.

$$f = f_o + f_1 \qquad f_1 \ll f_o \quad \ldots\ldots\ldots(4.3.4)$$

On the other hand, if high electric fields are applied neither (4.3.1) nor(4.3.4) can be used. However, in a steady state, if electron-electron collisions are frequent enough the shape of the distribution function will be modified. For these collisions result in a sharing of the energy gained from the field and in building up an internal thermal equilibrium condition among the electron gas. Then the distribution will be a Maxwell-Boltzmann one at a temperature T_e displaced in momentum space, ie.

$$f \sim e^{-\frac{\frac{1}{2}m(v - v_d)^2}{KT_e}} \qquad \text{.....(4.3.5)}$$

where $\frac{1}{2}mv_d^2$ is the drift energy of the electron gas, T_e, the hot electron temperature which we have mentioned in Chapter 1.

T_e, physically is a measure of the average energy of the electrons, since

$$\langle \mathcal{E} \rangle = 3/2KT_e + 1/2mv_d^2 \cong \frac{3}{2}KT_e \qquad \text{.....(4.3.6)}$$

For the case in which we are interested the drift velocity, v_d is comparatively small; and the dependence of external electric field, E on T_e can be found experimentally.(85) (86)

Assuming that the use of T_e is justified, then the nature of the $\rho \sim T_e$ and hence $\rho \sim E$ (or $\rho \sim \mathcal{E}$) characteristics as shown in Figure 4.1 and etc. will then yield direct information on the type of electron-phonon interaction responsible.

4.4 The critical electron concentration for the Electron Temperature Model

The application of a displaced Maxwell-Boltzmann distribution at T_e is based on the fact that electron- electron collisions are frequent enough which means that the electron concentration should be high enough. To get some idea of the critical concentration n_c required for this to occur, one may compare the rate at which a carrier faster than the average would lose energy to the other carriers, to the rate at which

it would lose its energy in all other processes. For acoustic modes the calculation was carried out by Stratton [47] giving $n_c \simeq 2 \times 10^{14}(T_e/293)^2$ cm^{-3} for germanium and by Yamashita[48], $n_c \simeq 10^{15}$ cm^{-3} for n-type Ge at 78°K; while Koenig [49] found experimentally $n_c \simeq 6 \times 10^{15}$ cm^{-3}.

Estimates have been made also for polar crystals. For polar optical modes Conwell[50] was able to give an expression

$$n_c \simeq \frac{eE_o \hbar\omega_l \epsilon^2}{2\pi e^4} \left[(N_q+1)\sinh^{-1}\left(\frac{\mathcal{E}-\hbar\omega_l}{\hbar\omega_l}\right)^{\frac{1}{2}} - N_q \sinh^{-1}\left(\frac{\mathcal{E}}{\hbar\omega_l}\right)^{\frac{1}{2}} \right] \qquad \ldots\ldots\ldots\ldots (4.4.1)$$

where $eE_o = \dfrac{m^* c^2 \hbar\omega_l}{\hbar^2}\left(1/\epsilon_\infty - 1/\epsilon_o\right)$

$$N_q = \frac{1}{e^{\frac{\hbar\omega_l}{KT}} - 1}$$

and ϵ is an average dielectric constant of ϵ_∞ and ϵ_o .

For our case we assume $\mathcal{E} \lesssim \hbar\omega_l$ and for lead sulphide we have,

$m = 0.1\, m_o = 0.1 \times 9.1 \times 10^{-28}$ gm

$\epsilon_\infty = 18$

$\epsilon_o = 190$

$T = 77$ deg. K

$\omega_l = 7.13 \times 10^{12}$ sec^{-1}

Therefore $n_c \lesssim 2.72 \times 10^{16}$ cm^{-3}.

For higher lattice and electron temperatures, n_c calculated from 4.4.1 will be slightly higher. However, recalling the results in Table 4.1 we notice that all the concentrations are somewhat lower than this n_c. It should be noted however that even when the concentrations are not high enough to justify the use of displaced Maxwell-Boltzmann distribution, calculations based on this distribution are likely to yield results correct as to order of magnitude [51]. Since in our case the difference between our electron concentrations and the critical value is fairly small we shall assume that the electron temperature model can be applied.

4.5 Possible scattering mechanisms and a summary of the theories on phonon scattering.

It is necessary to review the various theoretical predictions about the behaviour of $1/\tau$ and hence ρ due to different types of scattering, in order to know which type of scattering is predominant in our lead sulphide samples in a given temperature and field range.

4.5.1 Ionized impurity scattering:

This is an important scattering mechanism at rather low temperatures (eg. helium temperatures). It gives

$$\rho \sim \frac{1}{\tau} \sim \varepsilon^{-3/2} \qquad \text{.....(4.5.1)}$$

4.5.2 Neutral impurity scattering:

This is another important scattering mechanism at low temperatures for high concentration samples. It shows an independence of electron energy on relaxation time,

$$\rho \sim 1/\tau \sim \delta^{0} \qquad \text{.....(4.5.2)}$$

Recalling the results at nitrogen temperature in Figures 4.1, 4.2, 4.3 and 4.4 which show the resistance increasing with field the above scattering mechanisms cannot be applied. (They will be however discussed in more detail in Chapter 5.) So the discussion is now concentrated on the phonon scattering.

4.5.3 Phonon scattering:

Conduction electron-phonon scattering can be thought of , in a polar crystal, as due to the strain produced by the lattice vibrations and an electrical polarization produced by this lattice strain; the latter gives rise to an additional scattering that may be stronger than that of the former.

For acoustic modes we have:

(1) Deformation potential scattering : due to the strain.

(2) Piezoelectric scattering : due to the polarization.

And for optical modes we have:

(3) Nonpolar optical scattering: due to the strain.

(4) Polar optical scattering: due to the polarization.

Now we will summarize the theories for simple models as follows.

4.5.3.1 Acoustic deformation potential scattering

Considering the shift of the band edge energy, Conwell gave the expression,(52)

$$\rho \sim \frac{1}{\tau_{ac}} = \frac{2^{\frac{1}{2}}}{\pi} \frac{E_1^2 (m^*)^{3/2} KT}{\hbar^4 c_1} \varepsilon^{\frac{1}{2}} \sim \varepsilon^{\frac{1}{2}} \quad \text{.....(4.5.3)}$$

where E_1 is the shift of the band edge per unit dilatation and c_1 is the average longitudinal elastic constant.

It shows that the relaxation time τ of the electrons decreases as $\varepsilon^{-\frac{1}{2}}$ and this results in mobility and hence conductivity decreasing when the average energy of the electrons increases.

4.5.3.2 Acoustic piezoelectric scattering

By calculating the direction and magnitude of the electric field arising from a plane acoustic wave propagating in a piezoelectric material, the relaxation time can be shown as,(53)

$$\rho \sim \frac{1}{\tau_{pz}} = \frac{(m^*)^{\frac{1}{2}} e^2 K T}{2^{3/2} \pi \hbar^2} \left\langle \frac{P^2}{\epsilon^2 c_1} \right\rangle \frac{1}{\varepsilon^{\frac{1}{2}}} \sim \varepsilon^{-\frac{1}{2}}$$

.....(4.5.4)

where P is the piezoelectric tensor and ϵ , the dielectric constant.

It simply shows that τ_{pz} increases as $\varepsilon^{\frac{1}{2}}$ which would result in an increase in mobility, and hence in conductivity, with increasing energy of the electrons. An increase in mobility, however, means that this scattering process is less effective for hot electrons. Thus for weakly pieoelectric materials such as lead sulphide, it can be completely ignored even for the low-energy electrons.

4.5.3.3 Nonpolar optical scattering

Following an approach similar to that of the deformation potential due to the optical strain which is now defined as the displacement of the sublattice containing one type of atom with respect to the sublattice containing the other, divided by the unit cube edge, the mean free time was given by (54)

$$\rho \sim \frac{1}{\tau_{op}} = \frac{D_t^2 K^2 (m^*)^{3/2}}{2^{\frac{1}{2}} \pi \hbar^3 \rho_o \omega_q} \left[N_q (\varepsilon + \hbar\omega_o)^{\frac{1}{2}} + (N_q + 1)(\varepsilon - \hbar\omega_q)^{\frac{1}{2}} \right]$$

$$\sim \varepsilon^{\frac{1}{2}} \qquad \text{.....(4.5.5)}$$

where D_t is an interaction constant having the dimensions of energy and K, a reciprocal lattice vector, ρ_o, the density of the crystal.

It shows that the mobility and hence conductivity always decreases with heating of the electrons, just as it does for the above mentioned acoustic deformation potential scattering; it is, for this reason, that one cannot distinguish between acoustic and optical mode scattering in the qualitative discussions of mobility variations in nonpolar materials.

4.5.3.4 Polar optical scattering

The consideration of the polarization of the crystal arising from the vibrations of the longitudinal optical branch will give an additional interaction with the electrons; it is called polar optical scattering. Then the mean free time of an electron being scattered out of the initial state by a polar optical phonon can be calculated as[55]

$$\frac{1}{\tau_{pop}} = \frac{2^{\frac{1}{2}}(m^*)^{\frac{1}{2}} e^2 \omega_q}{\hbar \, \mathcal{E}^{\frac{1}{2}}} \left(\frac{1}{\epsilon_\infty} - \frac{1}{\epsilon_o}\right) \left[N_q \sinh^{-1}\left(\frac{\mathcal{E}}{\hbar\omega_q}\right)^{\frac{1}{2}} + (N_q+1) \sinh^{-1}\left(\frac{\mathcal{E}-\hbar\omega_q}{\hbar\omega_q}\right)^{\frac{1}{2}} \right] \quad \ldots.(45.6)$$

where ϵ_∞ and ϵ_o are the dielectric constants for infinite and zero frequencies respectively.

Qualitatively it tells us that for $\mathcal{E} \ll \hbar\omega_q$, τ_{pop} is a constant, independent of $\mathcal{E}$, but when $\mathcal{E}$ increases emission becomes possible and τ_{pop} decreases. We note that in the limit

$\mathcal{E} \gg \hbar\omega_q$, τ_{pop} increases with increasing $\mathcal{E}$, essentially as $\mathcal{E}^{\frac{1}{2}}$ since the remaining dependence on $\mathcal{E}$ is small. However, for our case, the lattice temperature is well below the Debye temperature, $T \ll \theta_D$, and we have a not very high energy region, $\mathcal{E} \lesssim \hbar\omega_q$. (This will be shown in section 4.9.) The mobility is then expected to decrease with electron heating. For simplification we have

$$\rho \sim \frac{1}{\tau_{pop}} \sim \mathcal{E}^r \qquad \text{.....(4.5.7)}$$

with $0 < r < \frac{1}{2}$.

(The validity of a relaxation time will be discussed in section 4.8).

It is generally expected that the polar optical scattering is much stronger than the nonpolar one for not very high energy carriers in a polar crystal since the factor $(1/\epsilon_\infty - 1/\epsilon_o)$ in equation (4.5.6) is large and on the other hand the factor D_t^2 in (4.5.5) is small for polar materials.

4.6 The predominant scattering mechanism

From the preceding discussion in section (4.5) only acoustic deformation potential scattering ($\rho \sim \mathcal{E}^{\frac{1}{2}}$) and polar optical scattering ($\rho \sim \mathcal{E}^r$) are likely to be the important scattering mechanisms responsible for the behaviour of lead

sulphide at nitrogen temperature. It is impossible to distinguish between these two scattering mechanisms by a qualitative discussion. Therefore we have to try some calculations.

4.6.1 The order of magnitude of mobilities due to optical phonon and acoustic phonon scattering

Following Kinch's [56] estimation for optical phonon scattering

$$\mu(0) = \frac{3T_o \left(\frac{K}{\theta m^*}\right)^{\frac{1}{2}}}{2x\sqrt{2}\,E_o} \left[\exp\left(\frac{\theta}{T_o}\right) - 1 \right] \quad \text{.....(4.6.1)}$$

where $E_o = (\epsilon_\infty^{-1} - \epsilon_o^{-1})K\theta/a_o e$

$\theta = hf/K$

we put in the values for lead sulphide in our experiment

$m^* = 0.1x9.1x10^{-28}$ gm

$\epsilon_\infty = 18$

$\epsilon_o = 190$

$f = 7.13x10^{12}$ sec^{-1}

$T_o = 77$ deg.K

$a_o = 5x10^{-9}$ cm

to get the mobility which has been extrapolated to zero electric field,

$\mu(0) = 1.27x10^3$ cm^2/volt-sec

From our experiments we got mobilities at low fields

$\mu_{J100} = 4.7 \times 10^3$ cm^2/V-sec for sample J100

$\mu_{Y23} = 5.4 \times 10^3$ " " for sample Y23

$\mu_{K3} = 7.4 \times 10^3$ " " for sample K3.

From Conwell's relation given by the equation (4.5.3) we calculate the mobility for the acoustic mode. If we take the deformation potential [57] = 6.9 ev
longitudinal sound velocity $u_l = 4 \times 10^5$ cm/sec
density of the crystal $n_o = 7.6$ gm/cm^3
average longitudinal elastic constant $c_l = u_l n_o \doteq 3 \times 10^6$ gm/cm^2-sec
we find [52] that

$$\mu_{ac} \simeq 1.3 \times 10^5 \text{ cm}^2/\text{ V-sec}$$

So comparing the experimental values with the theoretical ones we may conclude that the scattering by the optical phonons plays a very important role.

4.6.2 The further comparison of experimental and theoretical values

We understand that so far in the literature no firm conclusion has been reached as to the predominant scattering mechanism in lead chalcogenides. However, some recent experiments seem to contradict the widespread opinion that all the available data at moderately low temperatures can be explained

by acoustic scattering. By measuring the Nernst-Ettingshausen coefficient, Kaidanov et al [58] obtained a value for the scattering parameter which is closer to the predicted value for optical scattering rather than to that for acoustic scattering. Recently Ravich et al [59] concluded that lead chalcogenides at concentrations of the order of 10^{18} cm^{-3} and below, polar scattering played a significant role over the temperature range 77--600 deg. K.

In order to go into the problem more quantitatively the method used here is to compare the experimentally observed field-dependence of the mobility with the dependence predicted theoretically for the two scattering processes and the combination of them.

Figure 4.4 shows the comparison of the experimental(E>1 V/cm) and theoretical results. The theoretical curves are calculated by computer according to well known theories recently brought up to date by Stokoe and Cornwell.[60] The broken line gives the acoustic phonon scattering; the solid line gives the polar optical phonon scattering when the calculation includes consideration of nonparabolicity but without the correction of screening effect; the dash-dotted line represents the combination of the above two curves. The data of the present work for samples K'43, K3 and Y23 show a fairly good fit to the combination curve. This confirms the importance of the

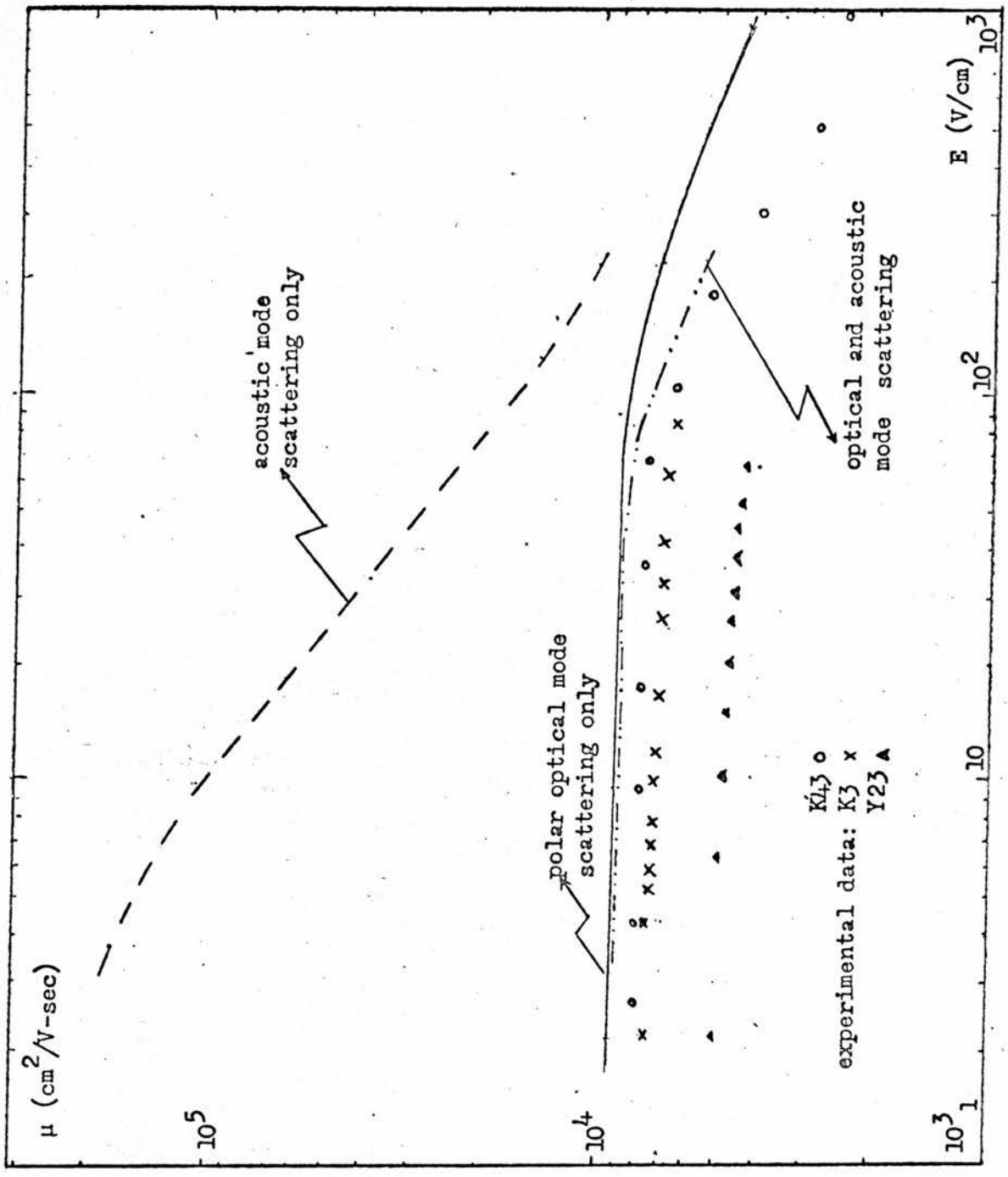
μ (cm²/V-sec)
10⁵
10⁴
10³
1
10
10²
10³
E (V/cm)
acoustic mode scattering only
polar optical mode scattering only
optical and acoustic mode scattering
experimental data: K43 o
K3 x
Y23 ▲

FIGURE 4.4

polar optical scattering mechanism at 77 deg. K for n-type lead sulphide over the warm electron region.

4.7 Further discussion on the polar optical phonon scattering in lead sulphide (also see Appendix A)

4.7.1 The consideration of nonparabolicity and screening effect

Since this mechanism has shown its importance experimentally and theoretically for lead sulphide at 77 deg. K, it is worthwhile to have a further discussion.

Lead sulphide posesses some unusual properties. One of these is the pronounced nonparabolicity of the energy band. This is manifested not only in a change in the dependence of the carrier energy on the electron wave vector but also leads to a change in the form of the wave function. The other important property is the appreciable effect of screening of polar vibrations by the conduction electrons. The screening not only has a considerable effect on the value of the matrix element for the interaction of an electron with an optical phonon and its dependence on the wave vector of the phonon, but it also gives rise to a dispersion of long-wavelength longitudinal optical phonons. The latter effect is especially large in lead sulphide because of the great difference between the static and high-frequency dielectric constants [61].

Considering these two effects, we may have,

$$\frac{1}{\tau_{pop}} = (\text{I}) \times (\text{II}) \times (\text{III}) \quad \ldots\ldots\ldots\ldots (4.7.1)$$

where (I) has been given in the equation (4.5.6)

(II) contains the correction terms for the non-parabolicity [62]

(III) contains the correction terms for the screening effect [62] which can be shown as

$$\left[1-\delta \ln(1+1/\delta)\right] - \frac{2\mathcal{E}(\mathcal{E}_g+\mathcal{E})}{(\mathcal{E}_g+2\mathcal{E})^2}\left[1-2\delta+2\delta^2\ln(1+1/\delta)\right] \quad \ldots(4.7.2)$$

where $1/\delta$ is a measure of the screening effect and

$$\delta \sim T_e^2 \quad \text{or} \quad \delta = C_\delta T_e^2 \quad \ldots\ldots\ldots\ldots\ldots (4.7.3)$$

C_δ is defined as screening effect coefficient.

4.7.2 The minimum in resistivity due to the screening effect

From the preceding theory we can predict that in the term (III) there is a minimum in $1/\tau_{pop}$ when

$$(T_e)_{min} \doteq \left(\frac{\frac{1}{2}+\frac{1}{2}\sqrt{7}}{C_\delta}\right)^{\frac{1}{2}} \qquad \text{if } \mathcal{E} \gtrsim \mathcal{E}_g$$

and correspondingly there should also be a resistivity minimum, ρ_{min} in the experimental data.

As shown in Figures 4.1, 4.2 and 4.3 the ρ_{min} are at

$E_{K'43} = 10$ V/cm for sample K'43

$E_{Y23}=7$ V/cm and $E_{K3} = 1$ V/cm for samples Y23 and K3.

4.8 The validity of a relaxation time

The way we used the relaxation time for optical phonon scattering is arguable. In the theory we used for the present work the relaxation time assumption was employed. This treatment has proved to be fairly applicable to most scattering processes occurring in elemental semiconductors. An important condition pointed out by Howarth and Sondheimer (63) is that the energy emitted or absorbed by an electron at collision must be small compared with its initial energy.

However, for lead sulphide, recalling its electronic nature, two unlike atoms, Pb being positive and S, negative in a unit cell, the optical vibrations may produce significant electric polarization. For such polar optical scatterings where the energy changes are large compared to the initial average energy of the electrons, a universal time of relaxation cannot be defined. So the relaxation time τ_{pop} used in this work is a pseudo-relaxation time which can be understood as the probability per unit time of an electron being scattered out of its initial state by a polar optical interaction. It is also noticible that the expression $\rho \sim \frac{1}{\tau_{pop}}$ can be only used to give a qualitative picture of the variation of ρ with electron heating.

The way the mean free time τ is used in this chapter and the next chapter can be summarized in the following manner:

(1). $\rho \sim 1/\tau \sim f(\varepsilon)$.

This sort of formula is really very crude and only gives the general qualitative argument.

(2). They should have the following meanings

$$1/\tau \sim f(\varepsilon)$$

$$\mu \sim \frac{e}{m}\langle\tau\rangle$$

$$\langle\tau\rangle \sim \left[\int \tau \exp(-\varepsilon/KT_e) N(\varepsilon) d\varepsilon\right] / \left[\int \exp(-\varepsilon/KT_e) N(\varepsilon) d\varepsilon\right]$$

$$\rho \sim 1/ne\mu \qquad \text{.....(4.8.1)}$$

4.9 The field dependence of the mobility

In warm electron range, if one were to represent the mobility by an expansion in powers of the field intensity, it should be well approximated by[65]

$$\mu = \mu_o(1+\beta E^2) \qquad \text{.....(4.10.1)}$$

where coefficient β is independent of field.

The behaviour of μ predicted by this relation has been verified by many experiments.[66] [67]

It is seen that β should be negative for our samples in which lattice scattering dominates in this range for μ decreases with the increase of field.

Figures 4.8 and 4.9 show the electric field dependence of the mobility for samples K3 and Y23 respectively. Fairly good straight lines can be fitted from which the coefficients for samples K3 and Y23 are calculated.

$$(\beta)_{K3} = -0.244 \times 10^{-3} \quad cm^2/V^2$$

$$(\beta)_{Y23} = -0.038 \times 10^{-3} \quad "$$

For all samples β is negative as we should expect for lattice scattering. The difference in the values of β may be due to the electron concentration dependence of the coefficients.[68] [69] However some impurity scattering in addition to the lattice scattering may also be responsible for the difference in β.

4.10 The effect of the magnetic field on phonon scattering.

Attention must be drawn to the effect of magnetic field on the longitudinal magnetoresistivity as shown in Figures 4.2 and 4.3. When magnetic fields are applied a higher field gives higher resistivity. This can be interpreted by the fact that the conduction electrons in the sample describe spiral orbits about the axis of the applied magnetic field H; and the angular frequency of rotation is $\omega_c = eH/m^*$

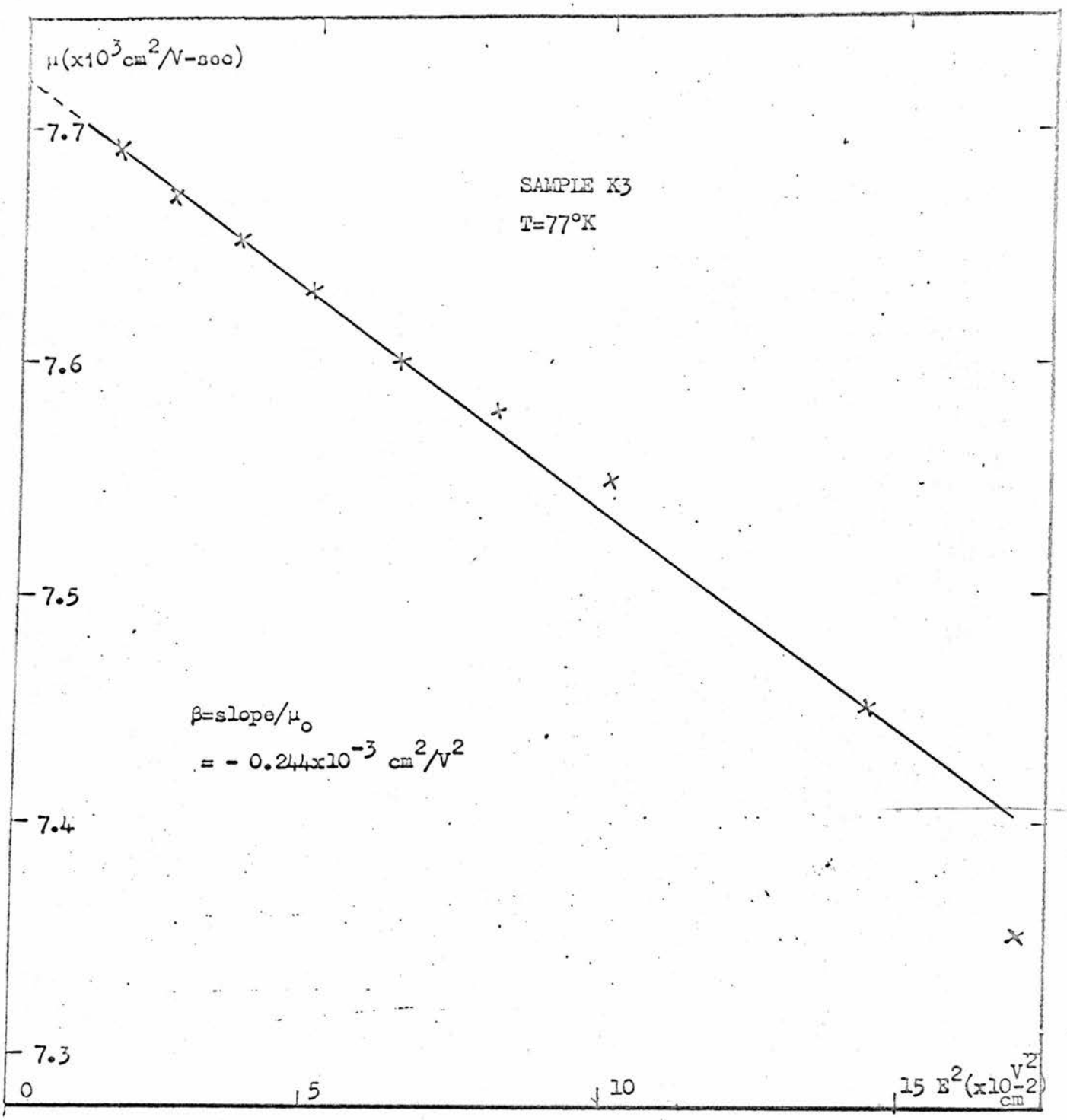
μ(x10³cm²/V-sec)
7.7
7.6
7.5
7.4
7.3
SAMPLE K3
T=77°K
β=slope/μ₀
= - 0.244x10⁻³ cm²/V²
0
5
10
15 E²(x10⁻² V²/cm²)

FIGURE 4.8

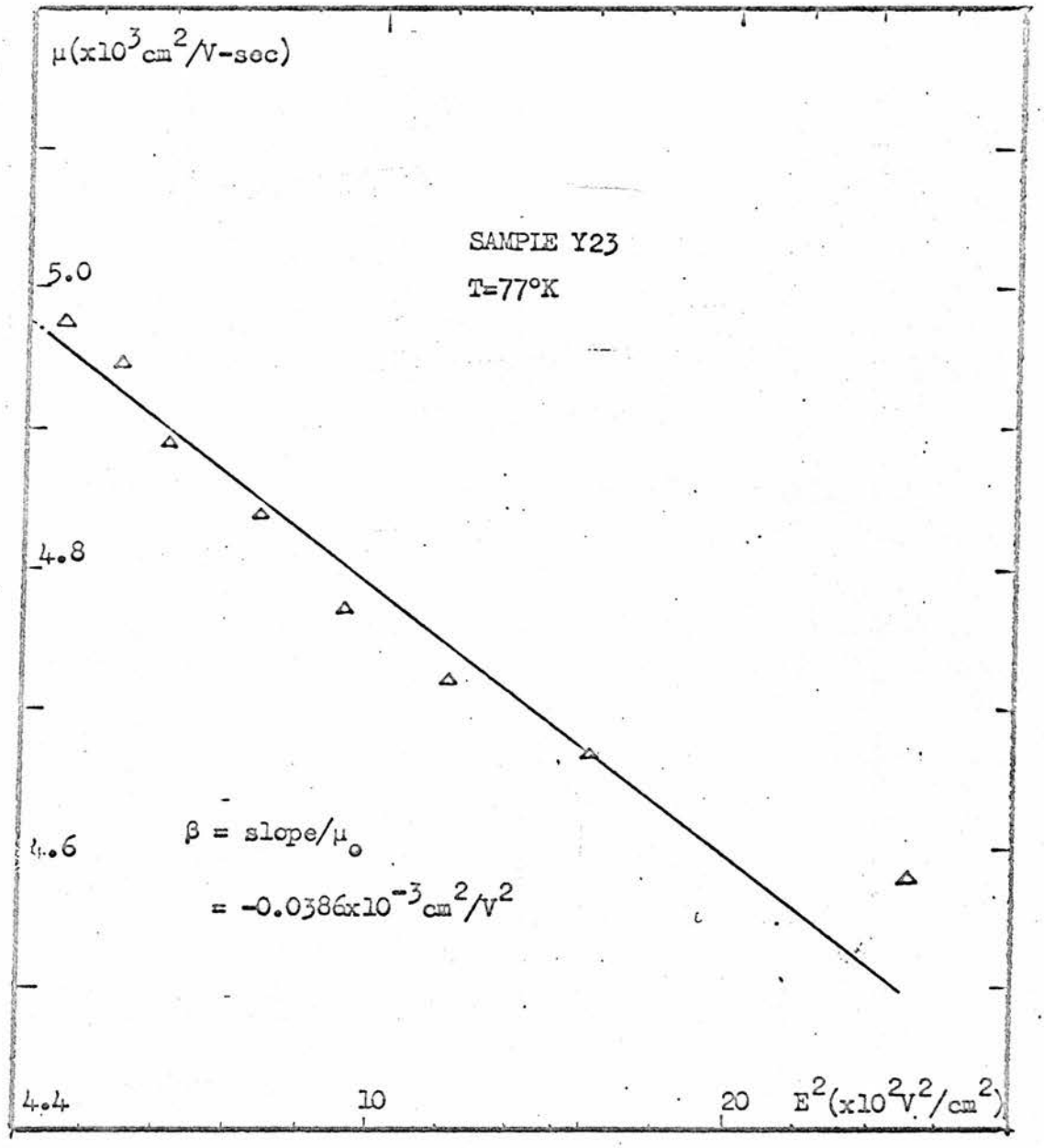
μ(x10³cm²/V-sec)
SAMPLE Y23
T=77°K
5.0
4.8
4.6
4.4
β = slope/μ₀
= -0.0386x10⁻³cm²/V²
10
20
E²(x10²V²/cm²)

FIGURE 4.9

In fact, quantization of energy levels should be taken into account in the high magnetic field case. This quantization changes somewhat the nature of the scattering of the electrons by the optical phonons. The quantum limit is usually defined as

$$KT_e \ll \hbar\omega_c \qquad \text{.....(4.11.1)}$$

For example, if we take

$H = 40$ K-gauss and $T_e = 200^\circ$ K

then we have

$$\omega_c = eH/m^* = \frac{1.6\times10^{-19}\,\text{coul}\times40\times10^{3}\,\text{gauss}}{0.1\times9.1\times10^{-28}\,\text{gm}}$$

$$\simeq 8\times10^{11}\ \text{sec}^{-1}$$

$$\hbar\omega_c \cong 0.8\times10^{-15}\ \text{erg}$$

while $KT_e = 1.36\times10^{-16}\ \text{erg deg}^{-1}\times200\ \text{deg}$

$$\simeq 2.72\times10^{-14}\ \text{erg.}$$

Therefore, in our present work (ie. $H < 40$ K-gauss and $T_e \lesssim 200^\circ$K) the quantum limit has not been reached when the experiments are carried out at 77 deg.K.

Furthermore, at this relatively high temperature we would not expect freeze-out effects to be important and since we have shown that we are in the low field region we would

expect the usual H^2 dependence of resistivity.(70)

In Figure 4.10 the resistivity is plotted against H^2. Parallel straight lines are obtained for three values of electric field. This shows that the H^2 dependence does hold and furthermore this dependence is independent of electric field since the parallel straight lines give a similar slope.

In Figure 4.11 the mobility is plotted against E^2 and again a set of parallel lines are obtained. Similarly it shows that the coeffecient in equation (4.10.1), β is independent of magnetic field.

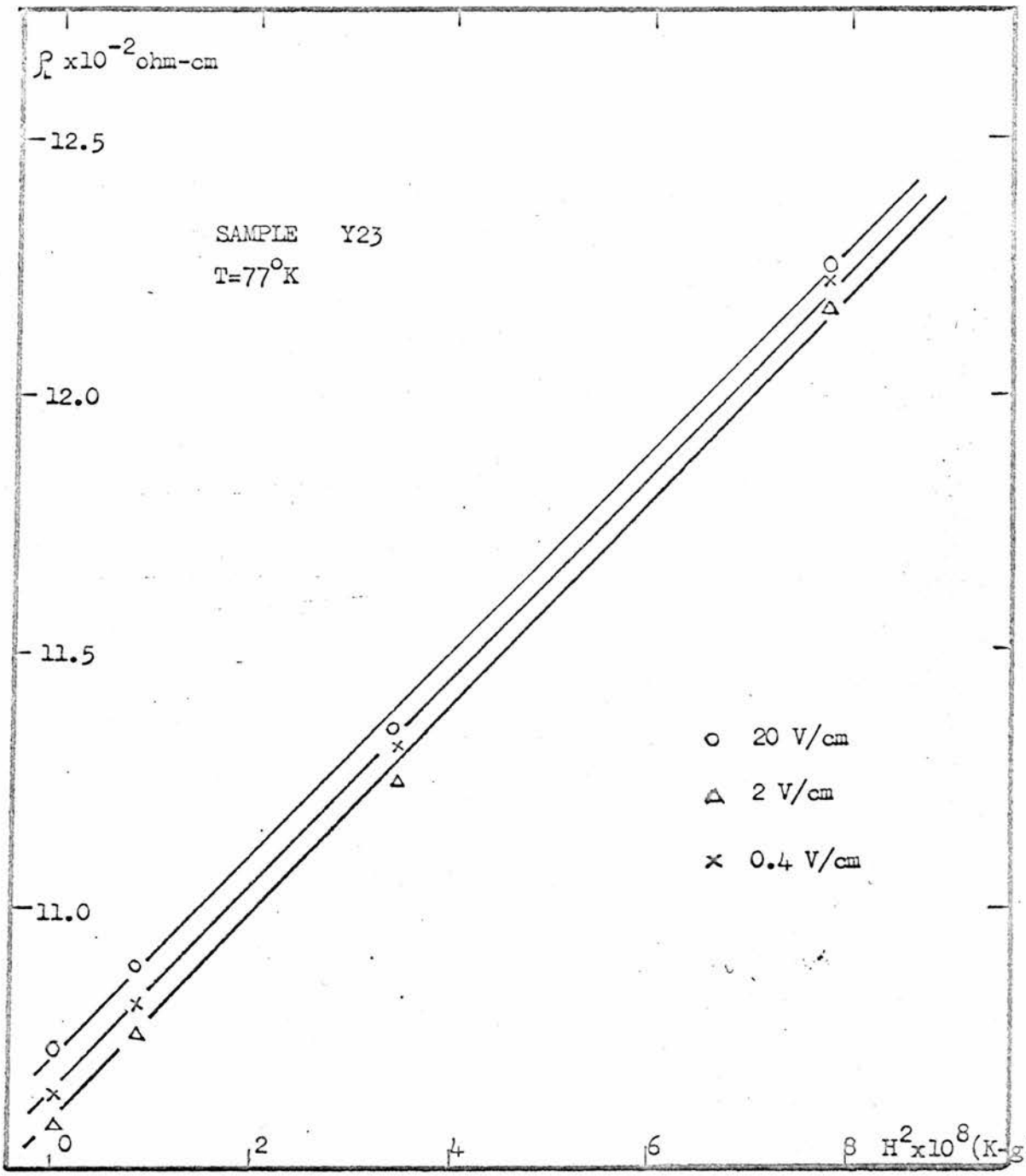
ρ x10^-2 ohm-cm
12.5
12.0
11.5
11.0
SAMPLE Y23
T=77°K
o 20 V/cm
Δ 2 V/cm
× 0.4 V/cm
0
2
4
6
β H^2 x10^8 (K-g)^2

FIG. 4.10

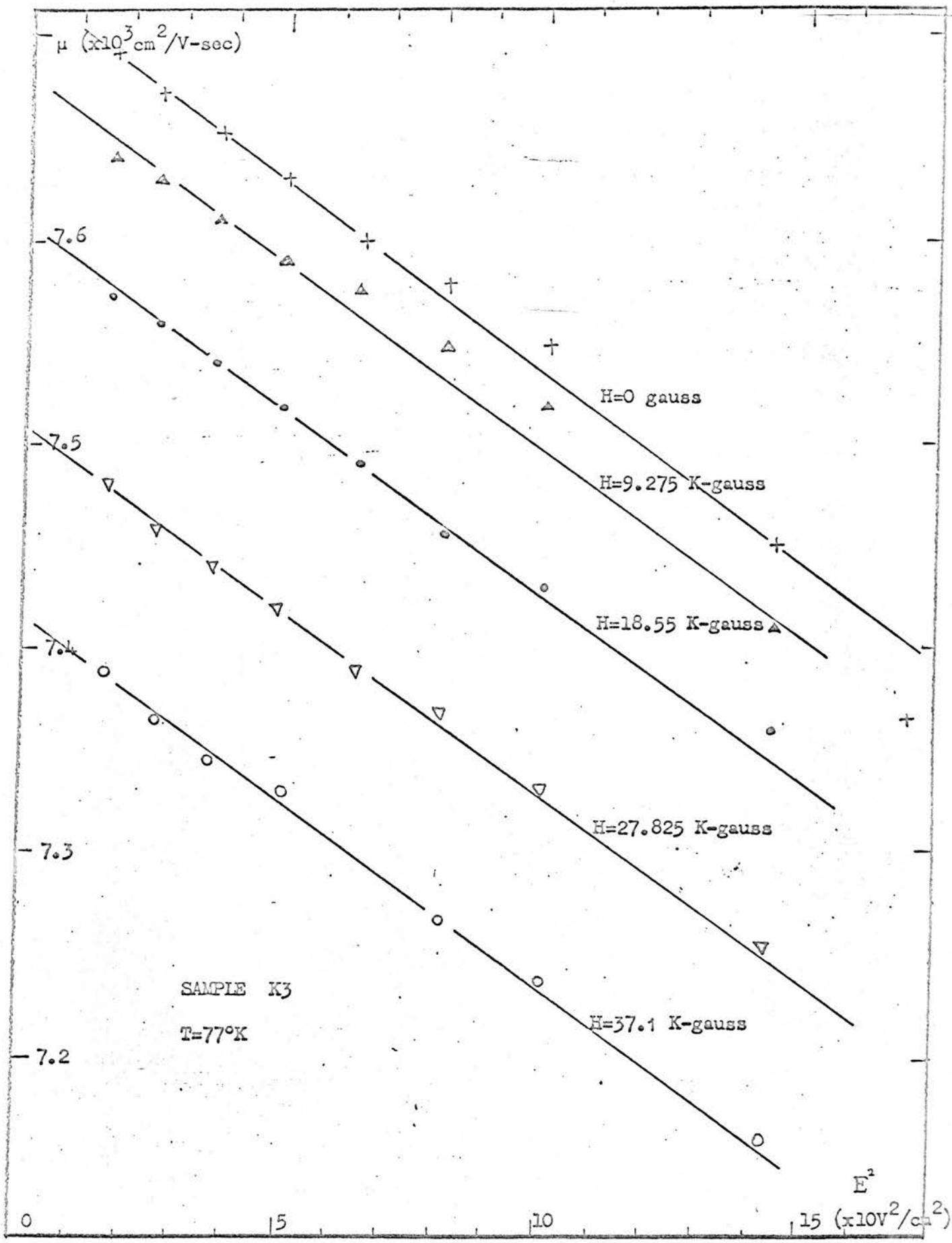
μ (x10³cm²/V-sec)
7.6
7.5
7.4
7.3
7.2
H=0 gauss
H=9.275 K-gauss
H=18.55 K-gauss
H=27.825 K-gauss
H=37.1 K-gauss
SAMPLE K3
T=77°K
0
5
10
15 (x10V²/cm²)
E²

FIGURE 4.11

CHAPTER 5

DISCUSSION OF THE RESULTS OBTAINED AT HELIUM TEMPERATURES

5.1 Measurements at helium temperatures

5.1.1 Resistivity in a transverse magnetic field

Figures 5.1, 5.2, 5.3 and 5.4 show the typical relationship between resistivity ρ and ln E for samples K4 and C'43 for different magnetic fields at 4.2 deg.K and 1.4 deg. K. In each case the resistivity curve starts at low fields with a constant ohmic value but begins to decrease for fields greater than 0.5—1 volt/cm. This decrease continues to fields in the region of 50—100 volt/cm after which the resistivity appears to be again constant with field.

In the low electric field region (ie. $E < 0.5$ volt/cm) a small magnetic field gives rise to a negative magnetoresistance while large magnetic fields give rise to a substantial positive magnetoresistance. In the high electric field region (ie. $E > 50$ volt/cm) the magnetoresistance effect is very much reduced.

In Figure 5.5 the temperature variation of the resistivity with electric field is shown for a single sample K4 at a fixed magnetic field. In the low field region, a resistivity minimum can be observed at about 3.15 deg.K.

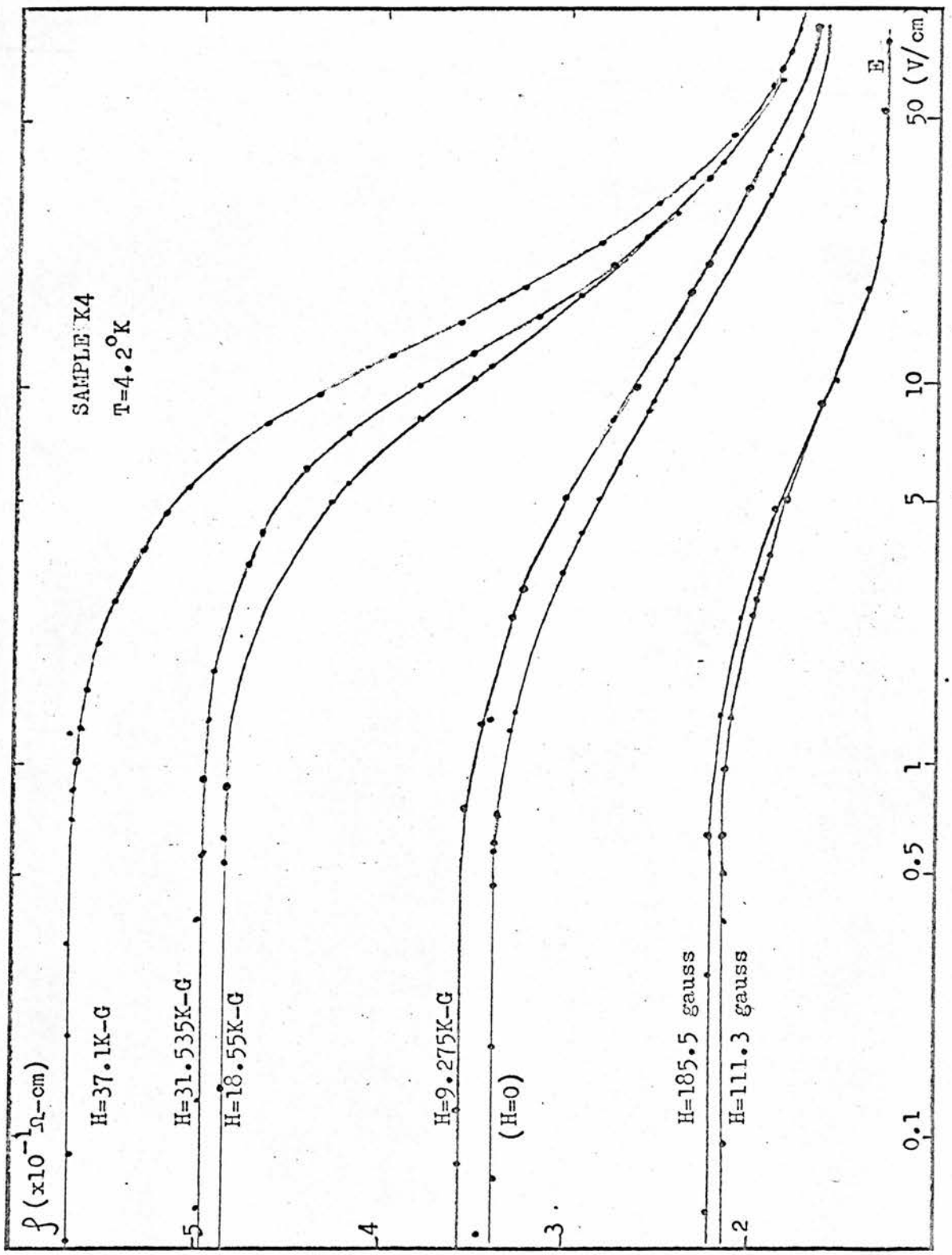
SAMPLE K4
T=4.2°K
ρ (x10⁻¹Ω-cm)
H=37.1K-G
H=31.535K-G
H=18.55K-G
H=9.275K-G
(H=0)
H=185.5 gauss
H=111.3 gauss
5
4
3
2
0.1
0.5
1
5
10
50 (V/cm
E

FIG. 5.1

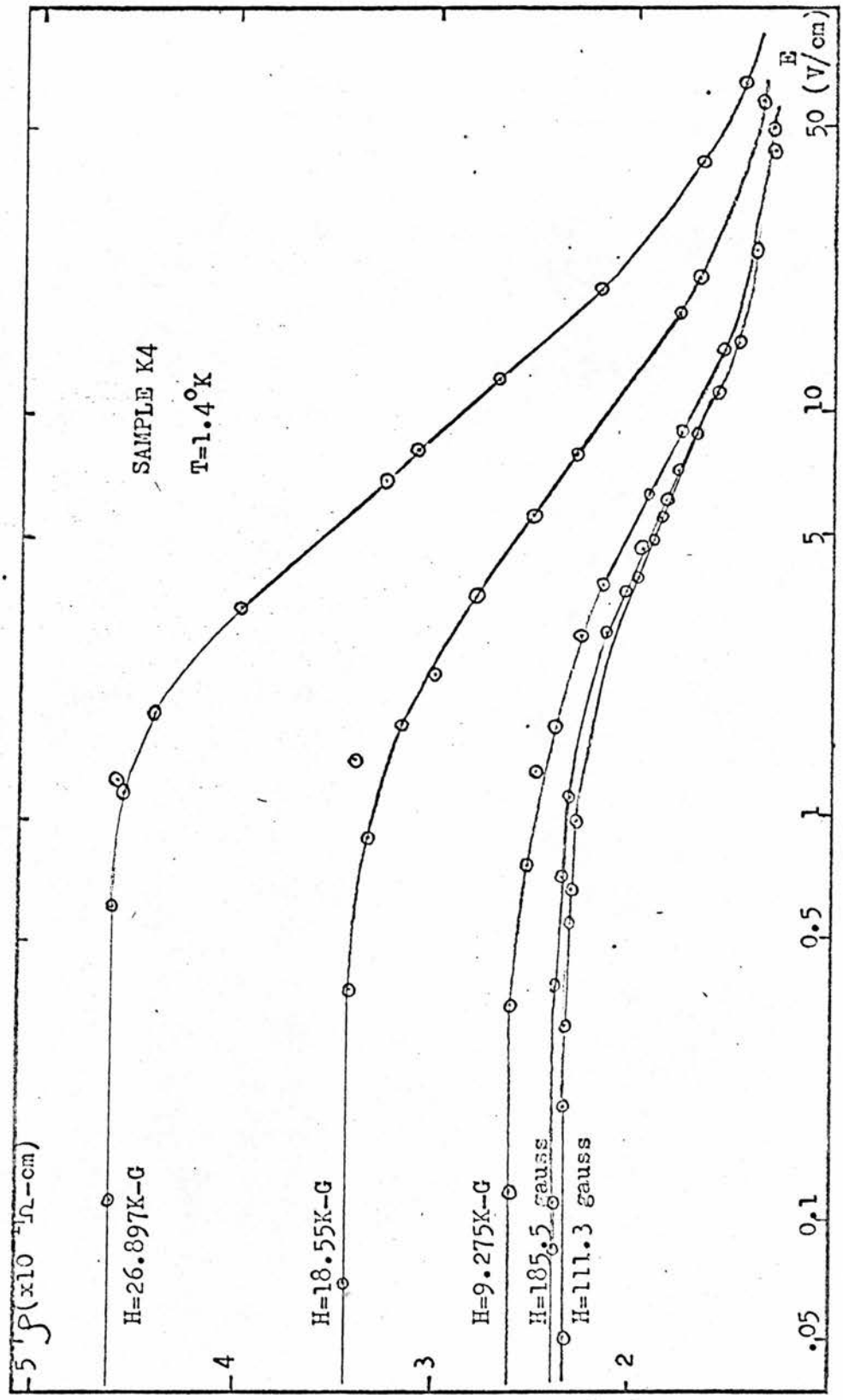
SAMPLE K4
T=1.4°K
H=26.897K-G
H=18.55K-G
H=9.275K-G
H=185.5 gauss
H=111.3 gauss
ρ(x10⁻⁴Ω-cm)
E (V/cm)
.05
0.1
0.5
1
5
10
2
3
4

FIGURE 5.2

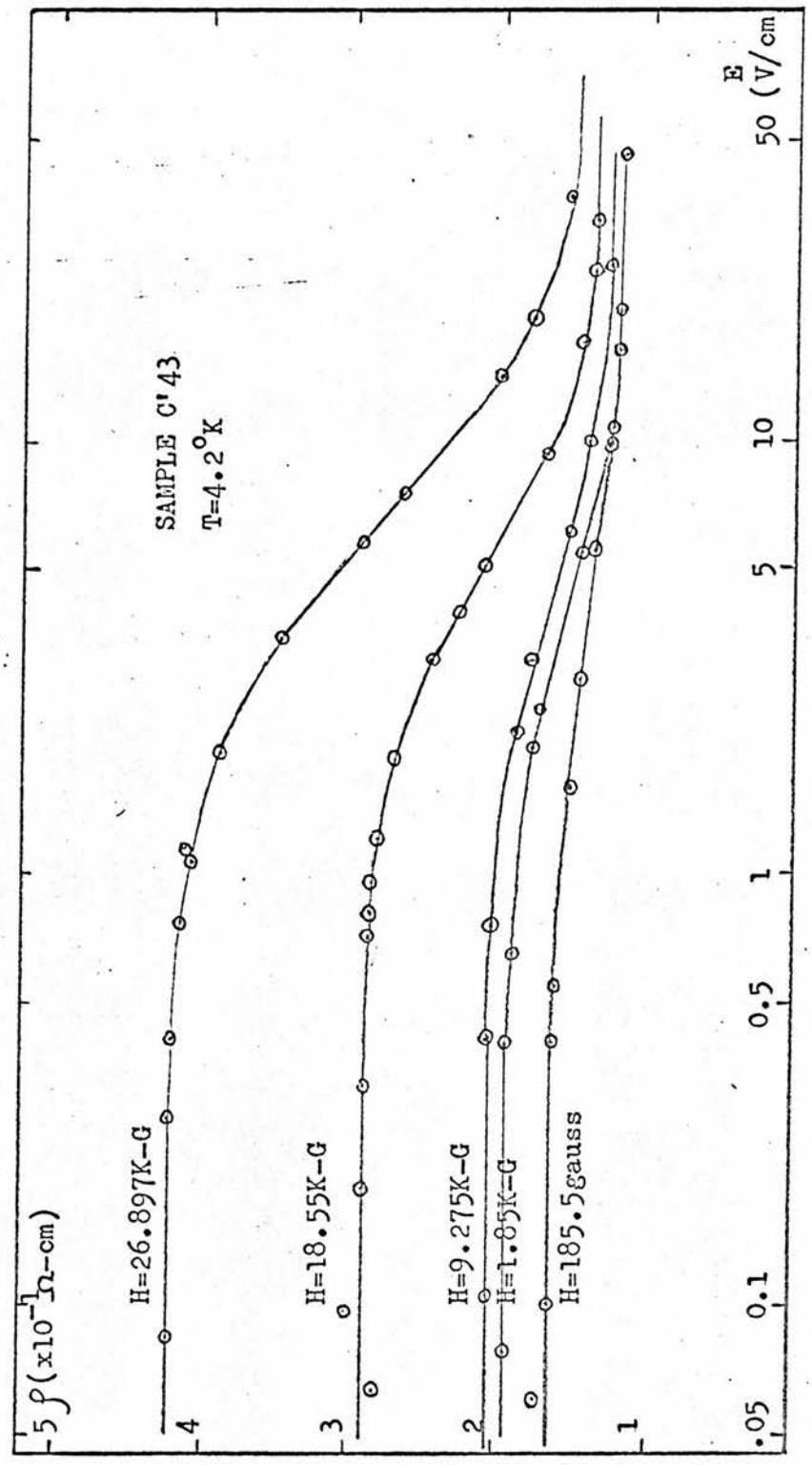
SAMPLE C'43
T=4.2°K
H=26.897K-G
H=18.55K-G
H=9.275K-G
H=1.85K-G
H=185.5gauss
5 ρ (x10⁻⁷Ω-cm)
E (V/cm)
4
3
2
1
.05
0.1
0.5
1
5
10
50

FIGURE 5.3

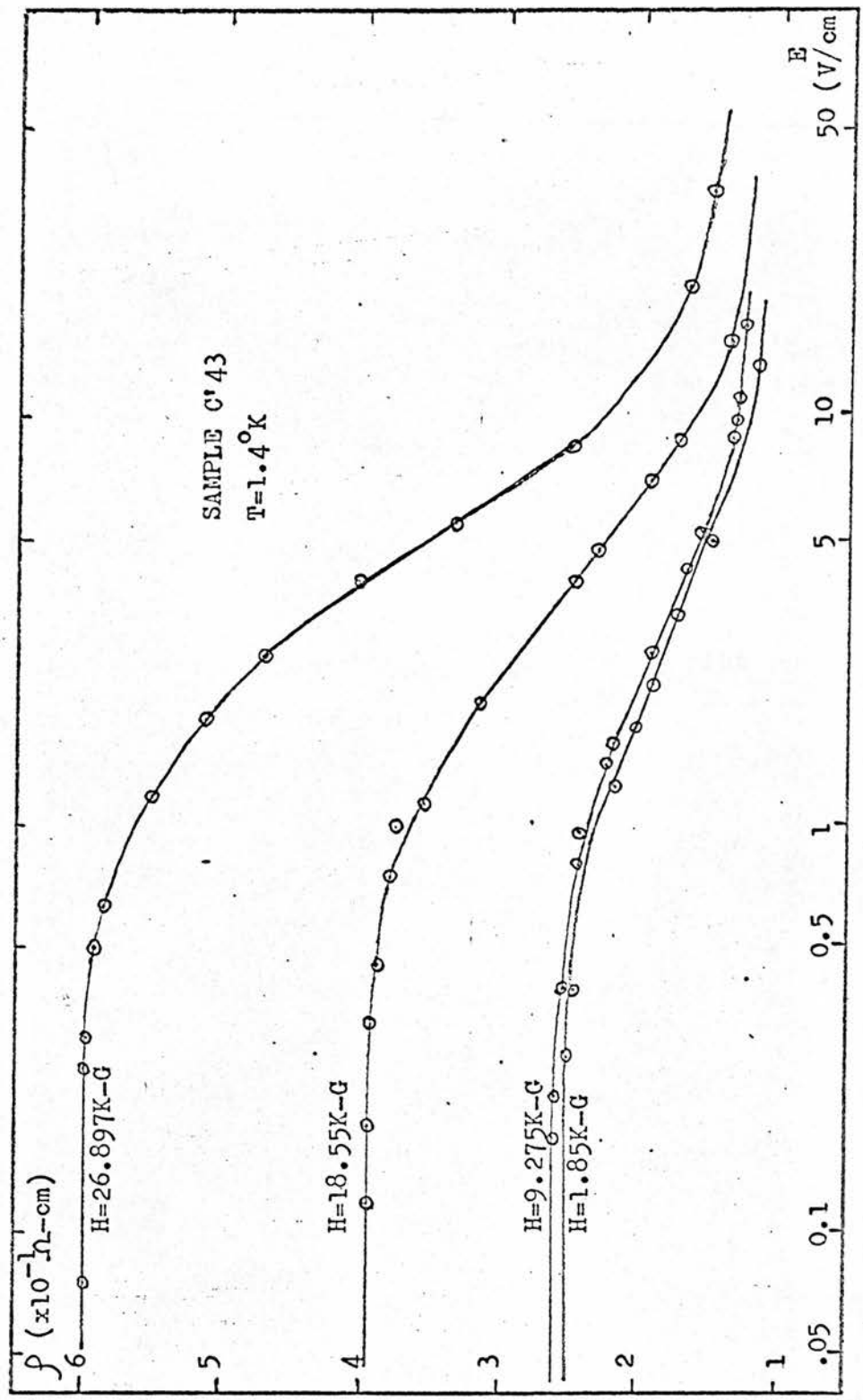
SAMPLE C'43
T=1.4°K
H=26.897K-G
H=18.55K-G
H=9.275K-G
H=1.85K-G
ρ (x10⁻¹Ω-cm)
E (V/cm)
6
5
4
3
2
1
.05
0.1
0.5
1
5
10
50

FIGURE 5.4

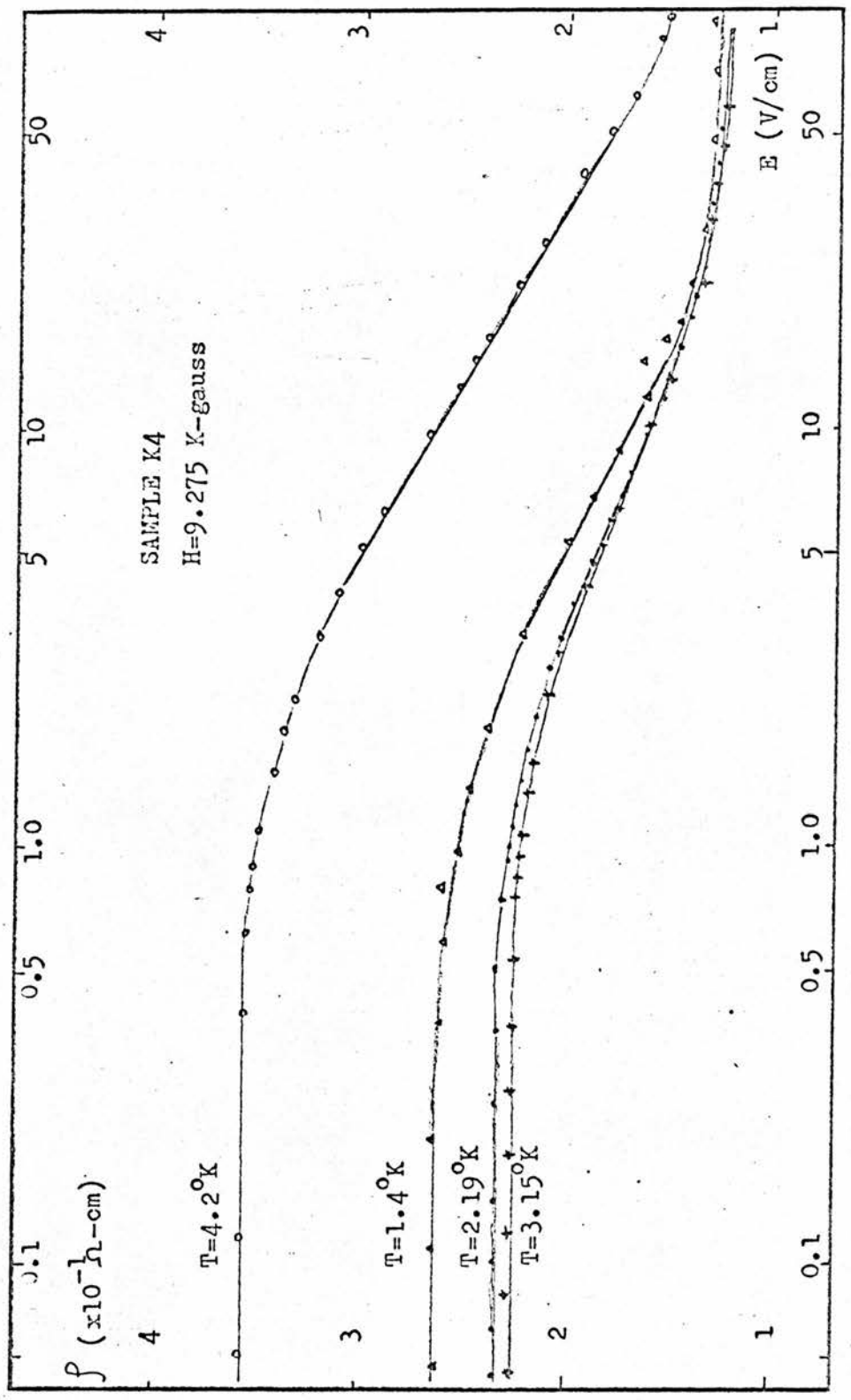
SAMPLE K4
H=9.275 K-gauss
T=4.2°K
T=1.4°K
T=2.19°K
T=3.15°K
ρ (x10⁻¹Ω-cm)
E (V/cm)
0.1
0.5
1.0
5
10
50
1
2
3
4

FIGURE 5.5

In Figure 5.6 we give a plot of resistivity against ln E at zero magnetic field and temperature 1.4 deg.K for carrier concentrations ranging from $7.49 \times 10^{15} cm^{-3}$ to $5 \times 10^{17} cm^{-3}$ (see Table 4.1). In the region where the resistivity is falling sharply with increasing electric field we note that , for each carrier concentration, there is a substantial linear portion. In other words, the resistivity is here proportional to the logarithm of the electric field and we can write

$$\rho = C - D \ln E \qquad \text{.....(5.1.1)}$$

where C and D are constants.

The value of D obtained from the slope of the curves in this region is seen to decrease as the carrier concentration increases.

On the other hand if we refer to Figure 5.5 we see that D is not strongly dependent on the lattice temperature.

5.1.2 Resistivity in a longitudinal magnetic field

In Figure 5.7 and 5.8 are given the plots of resistivity against ln E for different values of longitudinal magnetic field at 4.2 deg.K and 1.4 deg.K. The behaviour

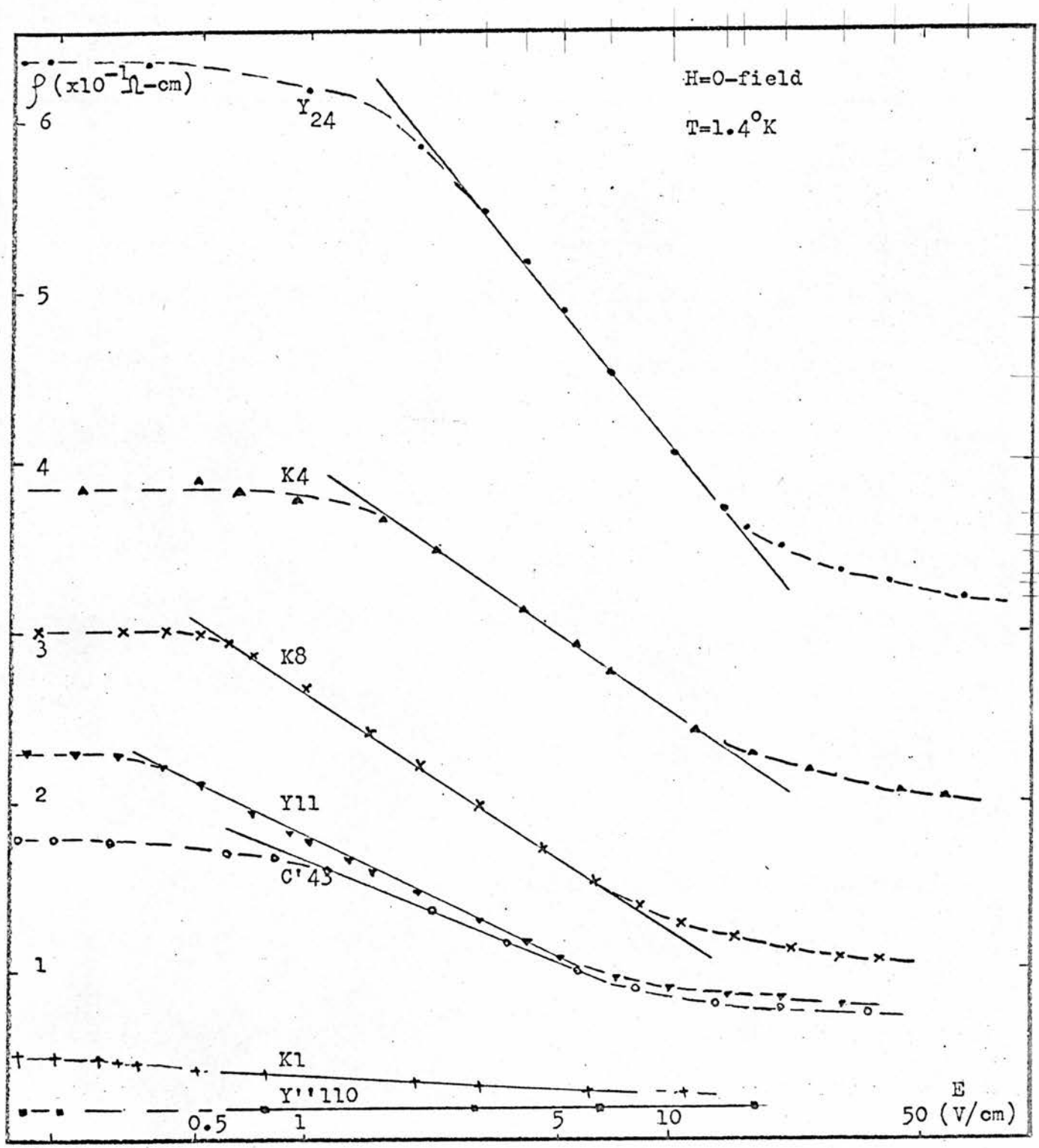
ρ (x10⁻³Ω-cm)
H=0-field
T=1.4°K
Y24
K4
K8
Y11
C'43
K1
Y''110
6
5
4
3
2
1
0.5
1
5
10
E
50 (V/cm)

FIGURE 5.6

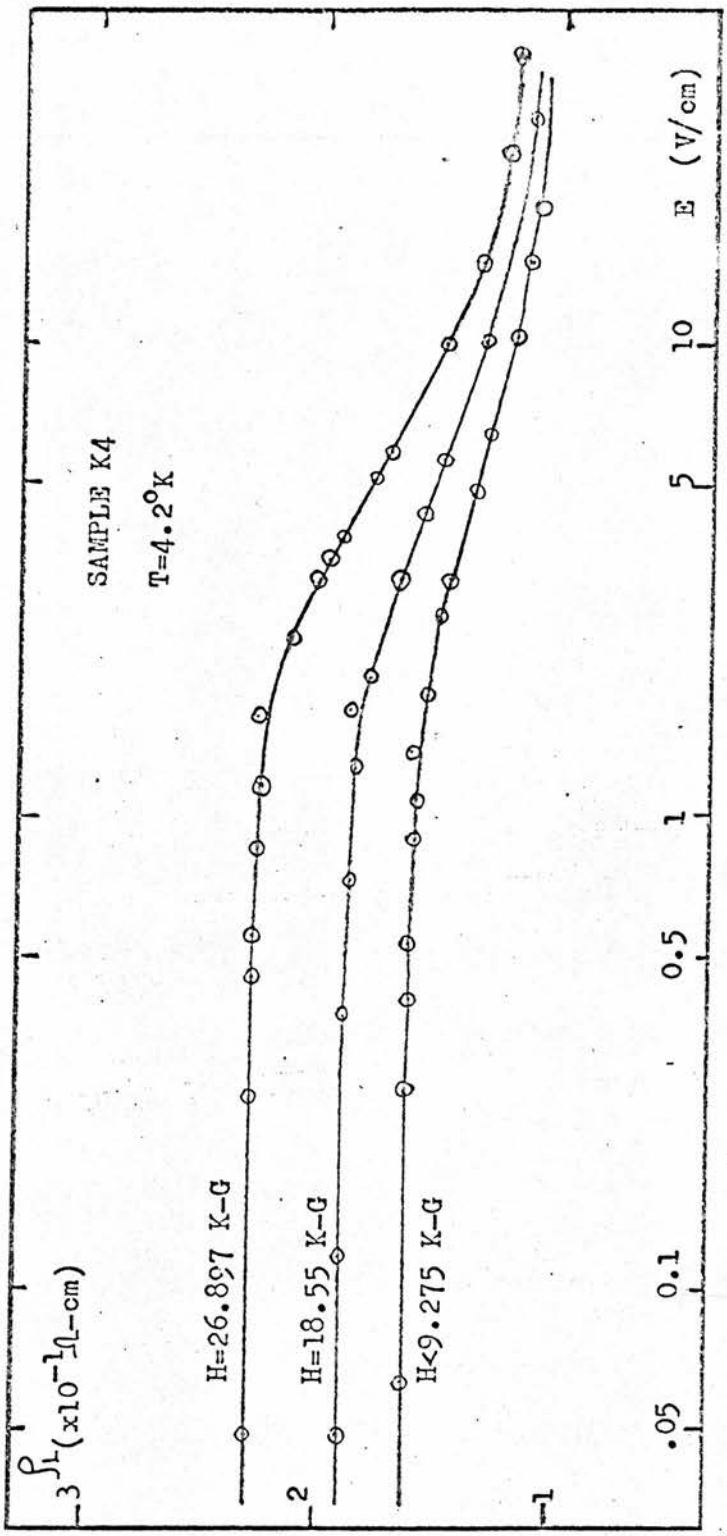
SAMPLE K4
T=4.2°K
H=26.897 K-G
H=18.55 K-G
H<9.275 K-G
$\rho_{\perp}$ (x10^{-1}Ω-cm)
E (V/cm)
3
2
1
.05
0.1
0.5
1
5
10

FIGURE 5.7

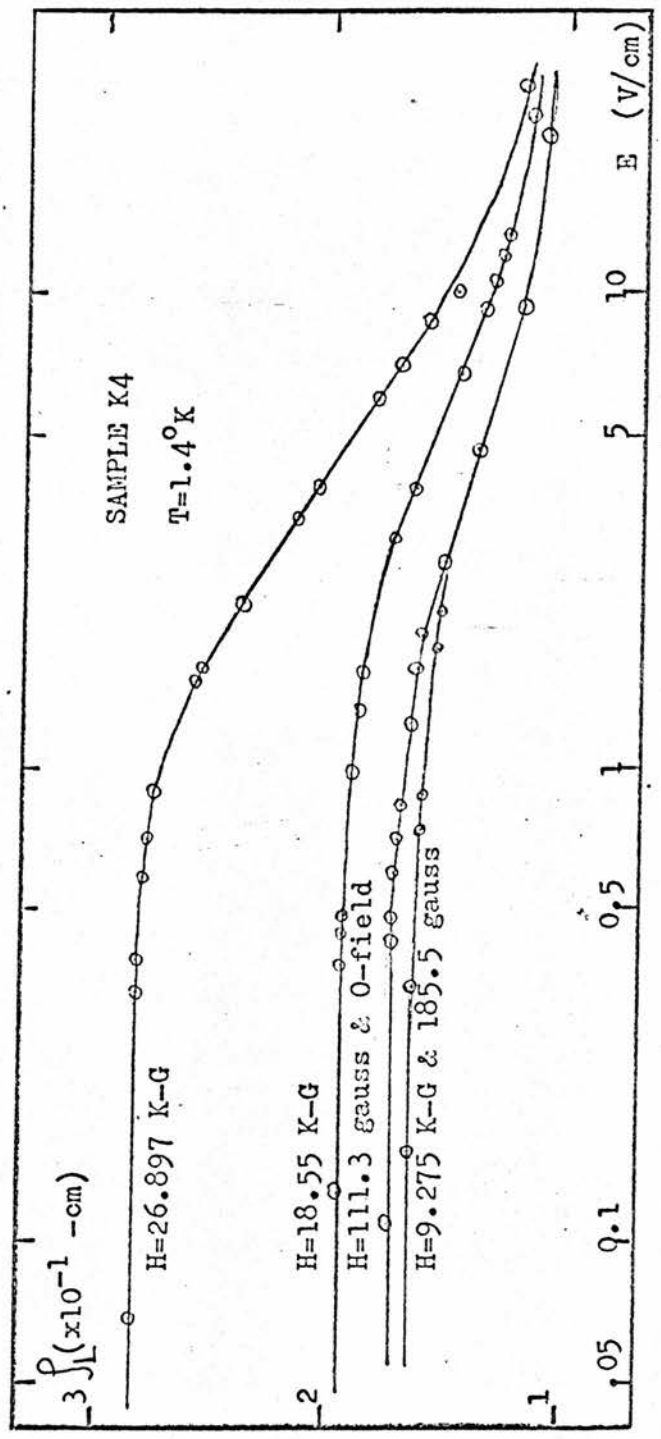
SAMPLE K4
T=1.4°K
H=26.897 K-G
H=18.55 K-G
H=111.3 gauss & 0-field
H=9.275 K-G & 185.5 gauss
ρ_{JL} (x10^{-1} -cm)
E (V/cm)
3
2
1
.05
0.1
0.5
1
5
10

FIGURE 5.8

is somewhat similar to that found in the transverse case. However the change of resistivity in magnetic field at low electric fields is smaller in the longitudinal case but negative magnetoresistance is again observed.

In Figure 5.9 (similar to Figure 5.5) the temperature variation of the resistivity with electric field is shown for the same sample K4 at a higher fixed longitudinal field. A resistivity minimum in the low field region is again observed at about 2.19 deg.K.

5.1.3 Anisotropy of magnetoresistivity

Subtracting the data given in sections (5.1.1) and (5.1.2) gives

$$\Delta\rho = \rho - \rho_L \qquad \text{.....(5.1.2)}$$

In Figure 5.10 this quantity is plotted against ln E for sample K4 at two magnetic fields and two temperatures. It is seen that at high electric fields the difference vanishes.

5.1.4 Hall coefficient

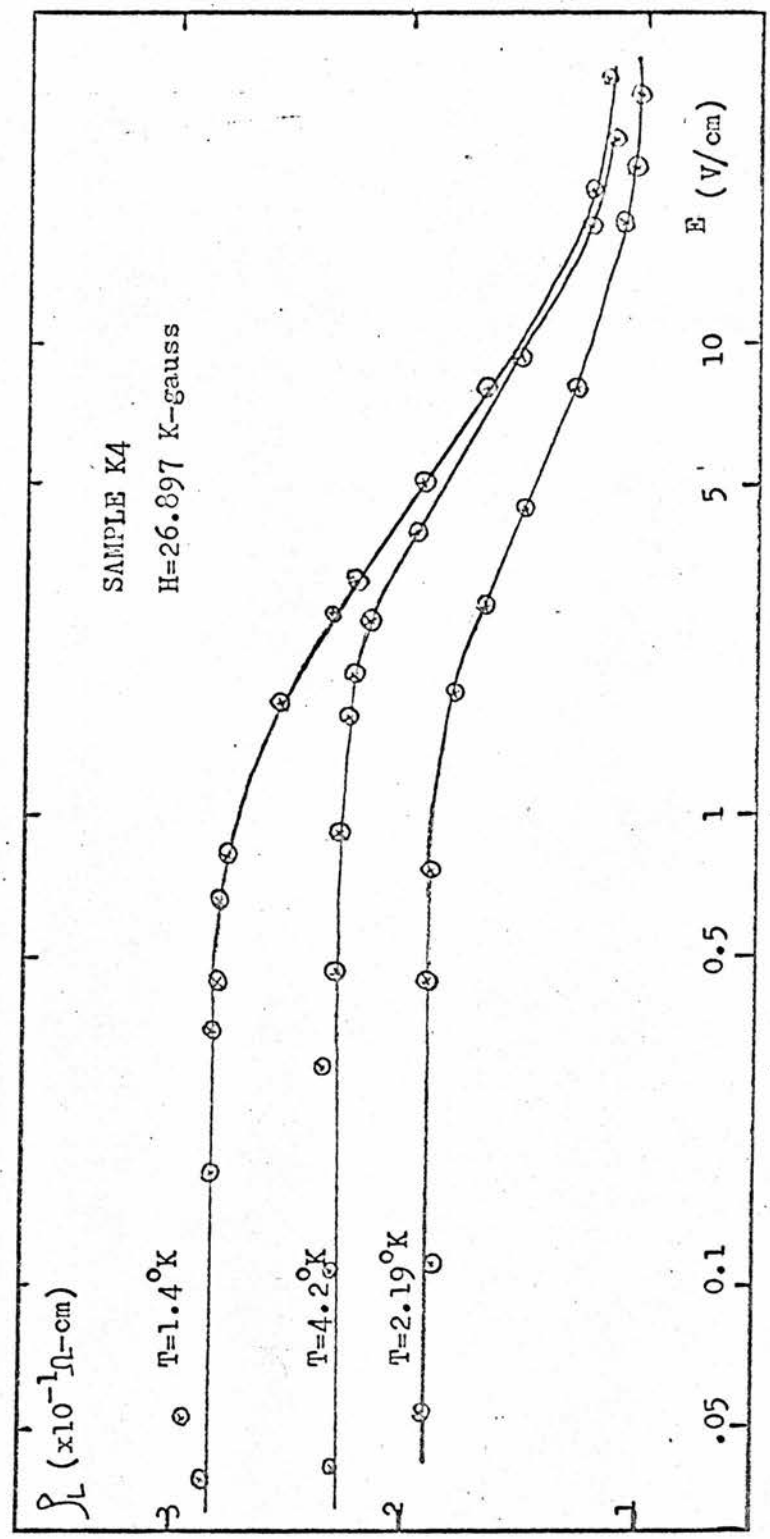
SAMPLE K4
H=26.897 K-gauss
T=1.4°K
T=4.2°K
T=2.19°K
ρ_L (x10$^{-1}\Omega$-cm)
E (V/cm)
.05
0.1
0.5
1
5
10
1
2
3

FIGURE 5.9

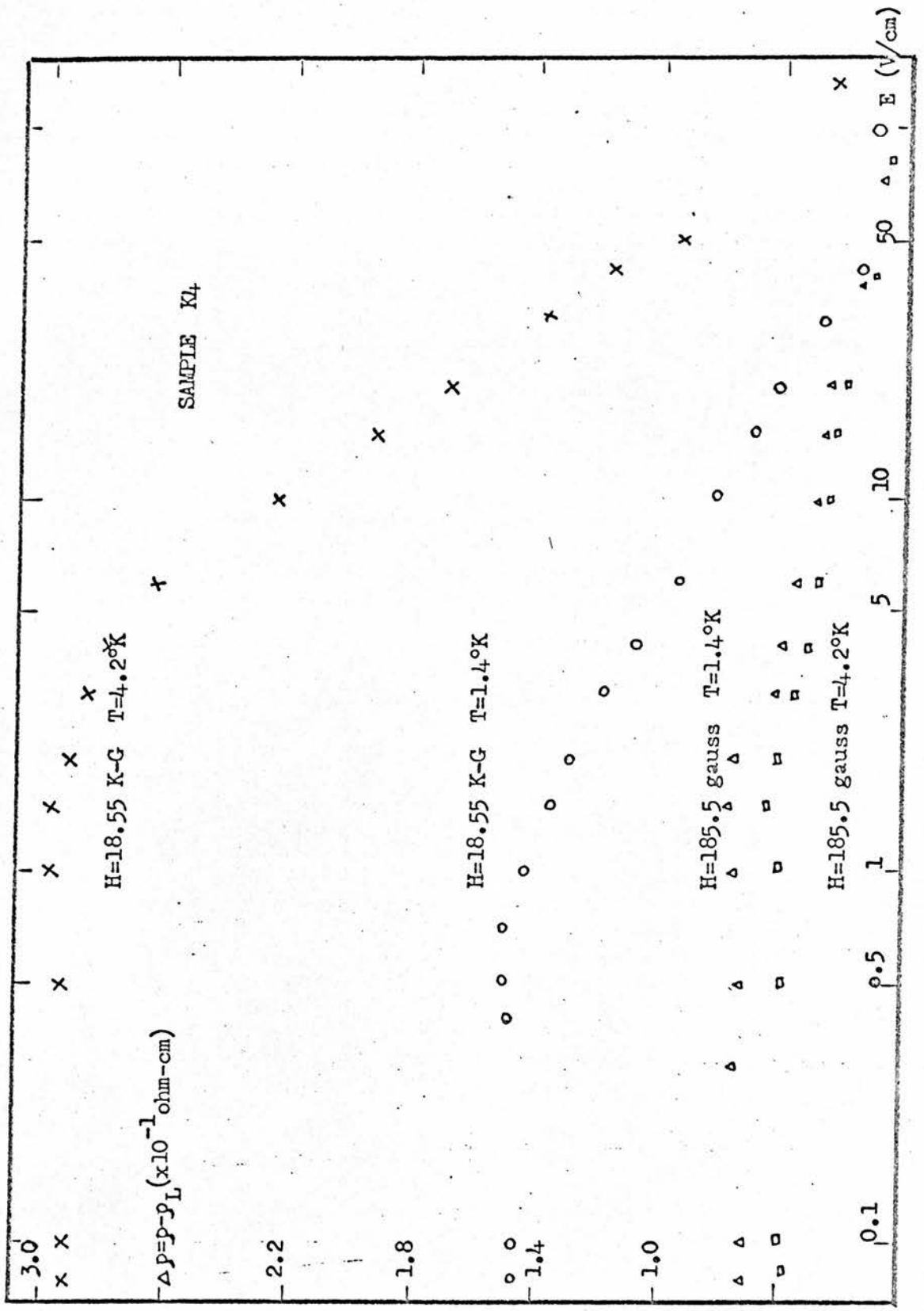
SAMPLE K4
H=18.55 K-G T=4.2°K
H=18.55 K-G T=1.4°K
H=185.5 gauss T=1.4°K
H=185.5 gauss T=4.2°K
Δρ=ρ-ρL (x10⁻¹ ohm-cm)
E (V/cm)
3.0
2.2
1.8
1.4
1.0
0.1
0.5
1
5
10
50

FIGURE 5.10

5.1.4 Hall coefficient

Figure 5.11 gives a plot of the Hall coefficient as a function of electric field for these different concentrations. In this range of electric field we see that the Hall coefficients are approximately constant. This result is not surprising since at these temperatures the samples are essentially degenerate.

Figure 5.12 is plotted on a bigger scale to show that in the helium temperature range, the lattice temperature does not affect the value of the Hall coefficient very much.

Figure 5.13 shows the influence of magnetic field on the Hall coefficient. This slight decrease in Hall coefficient with increase in lattice temperature or decrease in magnetic field may be interpreted as a consequence of changing statistics and will be discussed in the section (5.9.3).

5.2 Possible scattering mechanisms for lead sulphide at helium temperatures

Since the resistivity is now a good deal lower than that at 77 deg.K the maximum field that can be applied to

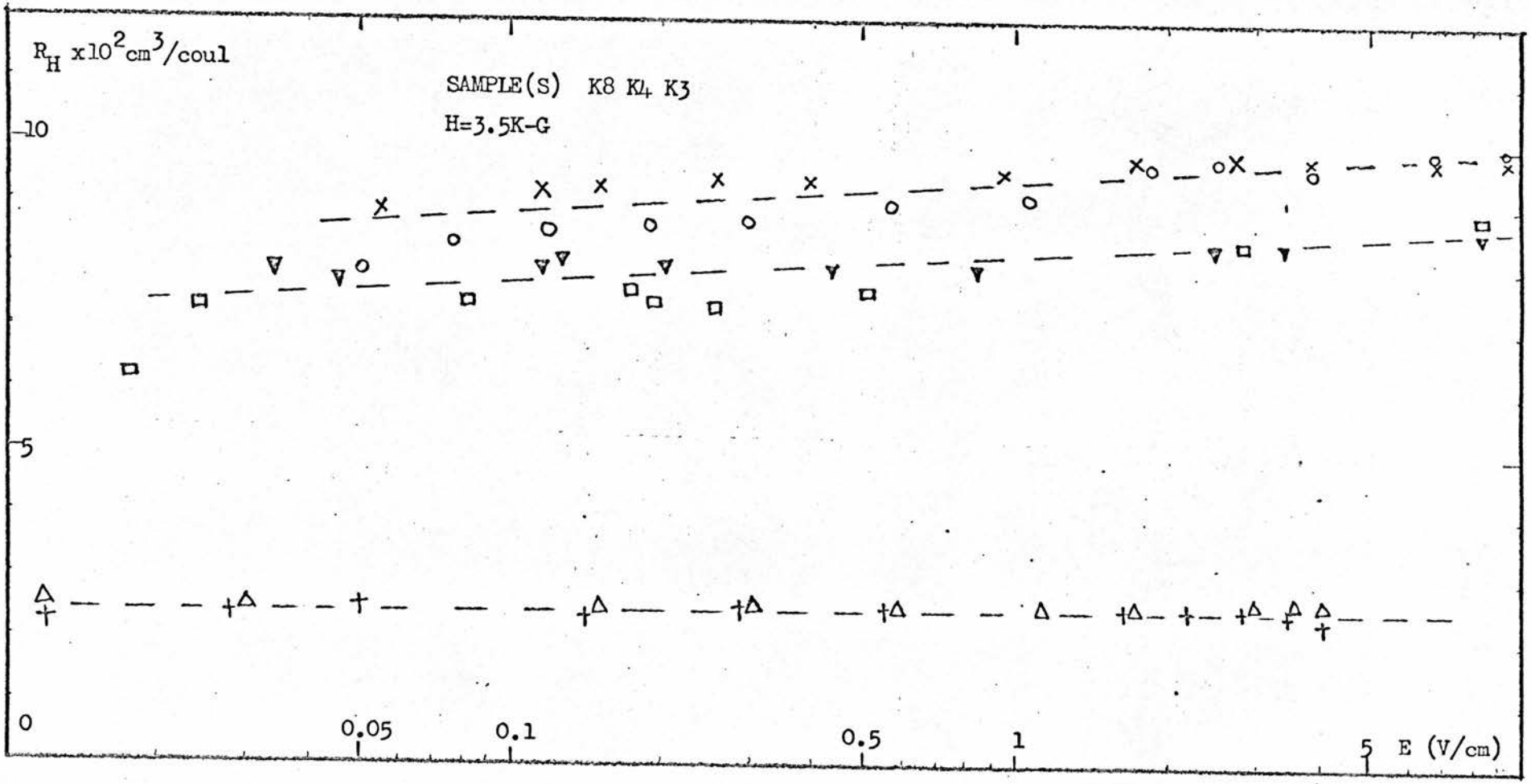

FIG. 5.11.

K8 4.2°K ▽
1.4°K □
K4 4.2°K ×
1.4°K ○
K3 4.2°K +
1.4°K △

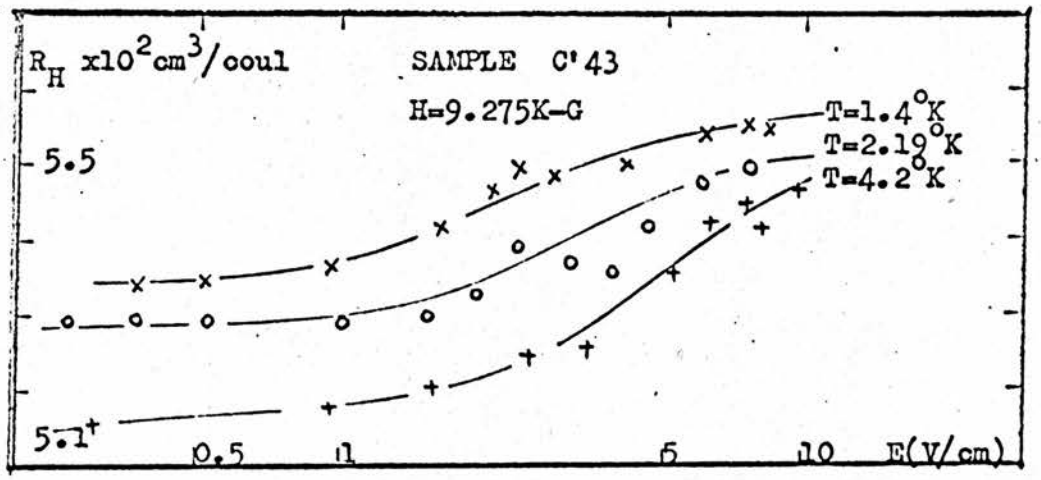
R_H x10^{2}cm^3/coul
SAMPLE C'43
H=9.275K-G
T=1.4°K
T=2.19°K
T=4.2°K
5.5
5.1
0.5
1
5
10
E(V/cm)

FIGURE 5.12

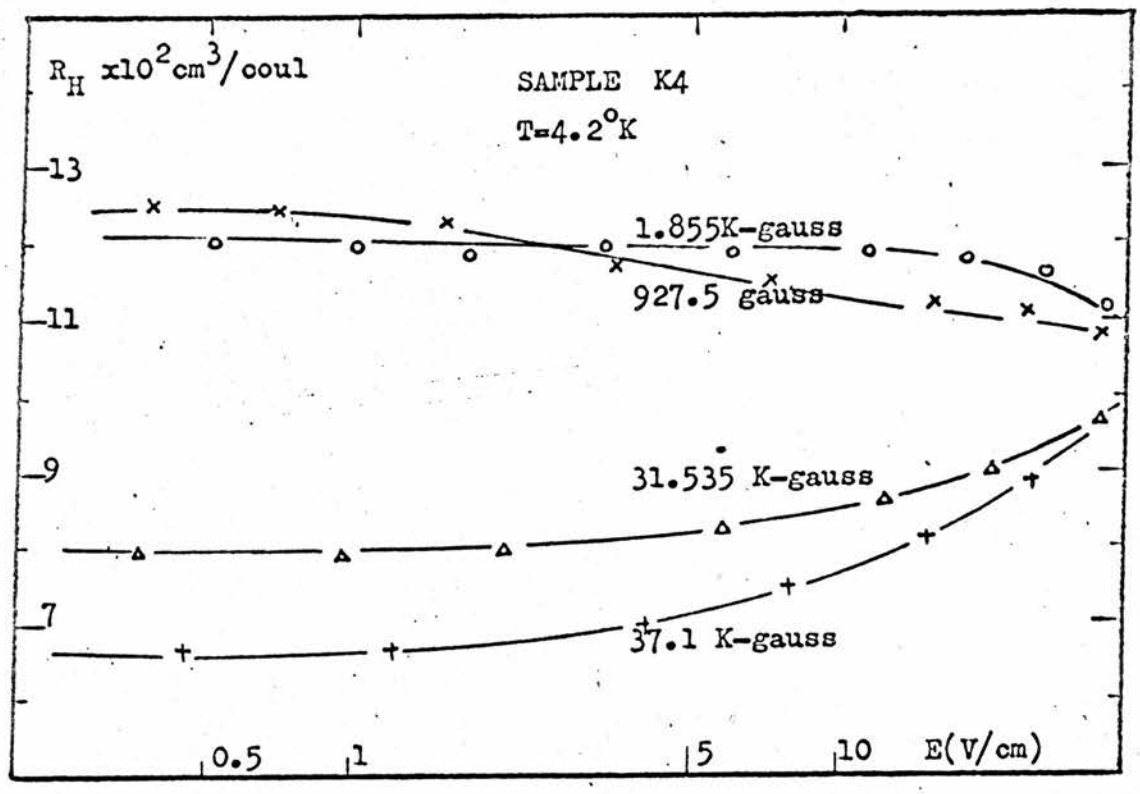
R_H x10^{2}cm^3/coul
SAMPLE K4
T=4.2°K
13
11
9
7
1.855K-gauss
927.5 gauss
31.535 K-gauss
37.1 K-gauss
0.5
1
5
10
E(V/cm)

FIGURE 5.13

the crystal is correspondingly reduced. However it is immediately clear that the variation of resistivity with field is now qualitatively different. In particular the drop in resistivity in the range 0.5—50 volt per cm shown in Figure 5.1 , 5.2 , 5.3 , 5.4 and etc. is not observed at 77 deg.K. First of all we consider explanations in terms of well known scattering mechanisms.

5.2.1 Phonon scattering

As we have shown in section (4.5.3) the lattice vibrations can give four kinds of phonon scattering for lead sulphide, a polar compound.

(a) Acoustic deformation potential scattering gives

$$\rho \sim \frac{1}{\langle \tau_{ac} \rangle} \sim \varepsilon^{\frac{1}{2}}$$

(b) Acoustic piezoelectric scattering gives

$$\rho \sim \frac{1}{\langle \tau_{pz} \rangle} \sim \varepsilon^{-\frac{1}{2}}$$

(c) Nonpolar optical scattering gives

$$\rho \sim \frac{1}{\langle \tau_{op} \rangle} \sim \varepsilon^{\frac{1}{2}}$$

(d) Polar optical scattering gives

$$(\rho) \sim \frac{1}{\langle \tau_{pop} \rangle} \sim \varepsilon^{r}$$

Obviously (a), (c) and (d) will not give a drop in resistivity as the electric field goes up in the specified range, for the higher the field the higher the energy of the electrons and thus the higher the resistivity.

So it seems that only (b) gives rise to the negative resistivity gradient at first sight. However, we understand that piezoelectric scattering is important for piezoelectric materials and furthermore, the piezoelectric effect is inversely proportional to the square of ϵ , the dielectric constant. Lead sulphide, having a large value of ϵ, is a very weak piezoelectric material and therefore its piezoelectric scattering can be ignored.

5.2.2 Ionised impurity scattering

An ionised impurity in a semiconductor can be treated as a net charge in a neutral background and its effect upon the conduction electrons can be considered as if there is a screened potential which falls off exponentially with distance with a screening radius $1/\lambda$. It means that this ionized impurity cannot be seen by the electrons in effect beyond this radius (or some multiples of this radius). Then the resistivity of the semiconductor can be calculated in

the following manner.(71)

$$\rho \sim \frac{1}{\tau} \simeq nv2\pi \left(\frac{Ze^2}{\epsilon \mathcal{E}} \right)^2 \int_0^1 \frac{\frac{1}{2}z^3 dz}{(z^2 + \lambda^2 h^2/8m^* \mathcal{E})^2} \qquad \ldots\ldots\ldots\ldots(5.2.1)$$

where n is the concentration of impurity , v, the averaged velocity of the electrons, $z=\sin\frac{1}{2}\theta$, θ being the scattering angle.

If we evaluate the integral we find that it varies only slowly with $\mathcal{E}$. τ depends on the energy of an electron through the factor $\mathcal{E}^2/v \sim \mathcal{E}^{3/2} (m^*)^{\frac{1}{2}}$. When we put this into equation (5.2.1) we have

$$\rho \sim \mathcal{E}^{-3/2} (m^*)^{-\frac{1}{2}} \epsilon^{-2} \qquad \ldots\ldots\ldots\ldots(5.2.2)$$

It shows that ionised impurity scattering is important at low energies. We note that considerable effects due to ionised impurities have been observed in the transport properties of materials having fairly low dielectric constants, such as ZnSe ($\epsilon \simeq 9.1$) and InSb ($\epsilon \simeq 17.5$). However, lead sulphide is notable for the very high value of dielectric constant combined with fairly low effective mass. These factors render the contribution of ionised impurity scattering to resistivity negligible in all ranges of temperature.

5.2.3 Possibilities arising from two-band conduction

On the two-band conduction theory, two kinds of carriers, namely electrons in the donor band and electrons in the normal conduction band coexist in the region of weak electric fields at liquid helium temperatures and both contribute to conduction with a density n_i and mobility μ_i in the impurity donor band and n_c in the conduction band with a higher mobility μ_c respectively. It is assumed that at a low lattice temperatures and in a low electric field, most of the carriers are in the impurity band and the resistivity is high. As the field is increased carriers are transferred to the conduction band by impact ionisation, resulting in a decrease in ρ. After this drop in resistivity all the carriers are in the conduction band and the resistivity-electric field curves for different lattice temperatures converge.

Experimental data for InSb at low temperatures have been sucessfully interpreted by Danilychev in 1965[72] and Miyazawa and Ikoma in 1967 [73] by means of the existence of a separate impurity donor band, even in the absence of a magnetic field. Later Sandercock in 1968 [74] suggested that this interpretation is open to criticism and worked out from his experimental measurements for InSb the ratio of

mobilities μ_c/μ_i equaling 1/3 , implying that the impurity band mobility is not smaller than the conduction band mobility. The agreement with the resistivity drop as the field is increased entirely breaks down. The argument about the interpretation of the InSb results has not yet been settled.

However for lead sulphide the energy gap between donor band and conduction band is so small that the two bands overlap. Taking the dielectric constant $\epsilon = 190$ and the effective mass, $m^* = 0.1m_o$ the PbS binding energy is estimated by the hydrogen atom model to be 0.00004 ev. (for InSb is 0.00069 ev.) Hence it is virtually certain that the donor band is merged with the conduction band if the donor concentration exceeds 10^{15} cm^{-3}. We believe that, unless a very strong magnetic field is applied, the electrons remain in the conduction band as free carriers at helium temperatures to produce a degenerate system even for the purest crystals available in the present work.

5.2.4 Neutral impurity scattering

At low temperatures many of the impurities in a semiconductor may not be ionised and these will have a different

scattering effect on an electron.

By applying the approximate methods used for the calculation of the collisions of slow electrons with a hydrogen atom[75] the relaxation time τ_n due to neutral impurity scattering is then given by

$$\rho \sim \frac{1}{\tau_n} \sim \frac{20\,\hbar^3 e\, N_n}{(m^*)^2 e^2} \sim \varepsilon^0 \qquad \text{.....(5.2.3)}$$

where N_n is the concentration of neutral impurities.

Thus we see that the τ_n is independent of the energy of the carrier and also does not vary with the temperature. This is obviously not the model to explain the energy dependence of resistivity.

Since the above mentioned scattering mechanisms do not seem to provide a satisfactory explanation of the experimental results we must look to other mechanisms.

5.3 Localised spin scattering

To explain the negative magnetoresistance observed in n-type Ge a localised spin system was suggested by Toyozawa in 1962.[76] He predicted the existence of localised spins

embedded in the impurity band and located at those impurity sites which are relatively isolated from other sites.

In 1964 the well known resistance minimum in dilute alloys was first explained by Kondo [77] in terms of localised spin scattering. He worked out the transition probability for scattering of the conduction electron by localised spins in dilute magnetic alloys using the hamiltonian for the s-d exchange coupling given by Kasuya.[78] When this was done in the second Born approximation a logarithmic temperature dependence of the resistivity was obtained.

In 1967 Tanaka and Katayama [79] used both these ideas to explain the low temperature behaviour of InSb. We propose to use a similar approach to discuss the behaviour of warm electrons in PbS at low temperatures following the discussion of resistance minimum and negative magnetoresistance given by Finlayson et al. [80] [81]

5.4 The summary of Kondo-Toyozawa theory (see Appendix B)

5.4.1 The localized spin system

Consider a semiconductor with random distribution of impurities and label the impurity sites by subscript n. The expectation value of the occupation number operator for spin

up is $\langle m_{n+} \rangle$ and for spin down is $\langle m_{n-} \rangle$ which can be interpreted as the average number of electrons with spin up or spin down respectively at the n^{th} site. If

$$\langle m_{n+} \rangle = \tfrac{1}{2} \quad \text{and} \quad \langle m_{n-} \rangle = \tfrac{1}{2} \qquad \ldots\ldots\ldots\ldots (5.4.1)$$

that means there are equal numbers in spin up and spin down electrons, hence no net localized spin ; but if

$$\langle m_{n+} \rangle \sim 1 \quad \text{and} \quad \langle m_{n-} \rangle \sim 0 \qquad .$$

or

$$\langle m_{n+} \rangle \sim 1 \quad \text{and} \quad \langle m_{n-} \rangle \sim 0 \qquad \ldots\ldots\ldots\ldots (5.4.2)$$

and if the site is sufficiently isolated from neighbouring sites, there will be a localized spin pointing in the up direction or down direction respectively appearing at the site n. Furthermore we assume that the localized orbital is always occupied by just one electron.

5.4.2 The Hamiltonian

The Hamiltonian of the exchange coupling between the i^{th} conduction electron and the localized spin at n^{th} site is

$$H_{ex} = -2 \sum_{i,n} J (r_i - R_n) (s_i \, S_n) \qquad \ldots\ldots\ldots (5.4.3)$$

where s_i, r_i and S_n, R_n are respectively the spin operators

and lattice vectors of the conduction electron and localized spin. J is a measure of the exchange coupling strength.

Assuming $\mathcal{E}_F > kT$ at very low temperature

$$H_{ex} = -1/N \sum_{\underline{k}\underline{k}'n} J(\underline{k},\underline{k}')\, e^{i(\underline{k}-\underline{k}')\,\underline{R}_n} \cdot \left[(a^*_{\underline{k}'+} a_{\underline{k}+} - a^*_{\underline{k}'-} a_{\underline{k}-}) S_{nz} + a^*_{\underline{k}'+} a_{\underline{k}-} S_{n-} + a^*_{\underline{k}'-} a_{\underline{k}+} S_{n+} \right] \quad \ldots.(5.4.4)$$

where $a^*_{\underline{k}+}$ is interpreted as creation operator for the conduction electron in the initial state $\underline{k}$ with energy $\hbar\omega_{\underline{k}}$ and spin up; similarly $a^*_{\underline{k}-}$ for spin down, a's for destruction operators and suffice $\underline{k}'$ for the final state k'.

5.4.3 Transition probability

To the 2nd Born approximation, the transition probability per unit time from the initial state "k" to the final state "k' " is given by

$$W(k \to k') = \frac{2\pi}{h} \delta(\mathcal{E}_k - \mathcal{E}_{k'}) \left[H'_{kk'} H'_{k'k} + \sum_{q,k} \frac{(H'_{kq} H'_{qk'} H'_{k'k} + c.c)}{\mathcal{E}_k - \mathcal{E}_q} \right] \quad \ldots\ldots\ldots(5.4.5)$$

where c.c. denotes complex conjugate and $H'_{kk'}$ etc. , the matrix

element of H_{ex} between the two specified states.

In the first term in the bracket the matrix elements involved are $H'_{kk'}$ and $H'_{k'k}$ which will be interpreted as the contribution due to direct transition from state k to k' and vice versa. It can be shown that it is independent of the initial energy of the conduction electrons.

The second term in the bracket represents the second Born approximation for the transition probability. It will be found that it involves a factor which has a dependence on the electron energy.

For the direct transition terms, there are four processes:

(1) Electron with wave number $\underline{k}$ and up spin(which will be denoted by $|\underline{k}+\rangle$) is scattered to the final state k' with up spin ($|\underline{k}'+\rangle$).

(2) $|\underline{k}-\rangle \longrightarrow |\underline{k}'-\rangle$

(3) $|\underline{k}+\rangle \longrightarrow |\underline{k}'-\rangle$

(4) $|\underline{k}-\rangle \longrightarrow |\underline{k}'+\rangle$

(3) and (4) processes involve the spin flip down and spin flip up of the conduction electron during the scattering.

The second term, including H'_{kq} and $H'_{qk'}$ can be interpreted as a 2-step process. Considering the initial, inter-

mediate and final states we also have the following four processes; each process can be divided into four groups:

(1) $|\underline{k}+\rangle$ —— $|\underline{k}'+\rangle$

(a) The electron $|\underline{k}+\rangle$ is first scattered to the unoccupied state $|\underline{q}'+\rangle$ and then to $|\underline{k}'+\rangle$.

(b) One of the occupied electrons $|\underline{q}+\rangle$ is first scattered to $|\underline{k}'+\rangle$ and then the electron $|\underline{k}+\rangle$ fills up the state $|\underline{q}+\rangle$ which is now empty.

(c) In the intermediate states, the sign of the spin may be changed. The electron $|\underline{k}+\rangle$ is scattered to the unoccupied state $|\underline{q}'-\rangle$, while the z-component of the spin of the n^{th} impurity which shall be denoted by $|M_n\rangle$, is increased by unity (ie. from $|M_n\rangle$ to $|M_n+1\rangle$) due to the conservation of angular momentum. After that the electron is again scattered to $|\underline{k}'+\rangle$, while the impurity is from $|M_n+1\rangle$ to $|M_n\rangle$.

(d) One of the occupied electrons $|\underline{q}-\rangle$ is scattered to the state $|\underline{k}'+\rangle$, while $|M_n\rangle$ to $|M_n-1\rangle$. The electron $|\underline{k}+\rangle$ then fills $|\underline{q}-\rangle$. $|M_n-1\rangle$ returns to $|M_n\rangle$.

Note that in (c) and (d) , spin flip up or down is involved during scattering.

(2) $|\underline{k}-\rangle$ —— $|\underline{k}'-\rangle$ with the similar four groups.

(3) $|\underline{k}+\rangle$ —— $|\underline{k}'-\rangle$

(a) Electron $|\underline{k}+\rangle$ is first changed to $|\underline{q}'-\rangle$, while the z-component of the n^{th} impurity S_{nz} is increased from $|M_n\rangle$ to

$|M_n+1\rangle$ and then $|\underline{q}'-\rangle$ to $|\underline{k}'-\rangle$, S_{nz} remaining to be $|M_n+1\rangle$.

(b) One of the occupied states $|\underline{q}-\rangle$ is changed to $|\underline{k}'-\rangle$, the localized spin S_{nz} being unchanged. Then the electron $|\underline{k}+\rangle$ fill up the empty state $|\underline{q}-\rangle$, while S_{nz} from $|M_n\rangle$ to $|M_n+1\rangle$.

(c) Electron $|\underline{k}+\rangle$ is scattered to the unoccupied state $|\underline{q}'+\rangle$, S_{nz} of localized spin being unchanged; and then to the final state $|\underline{k}'-\rangle$ while $|M_n\rangle \dashrightarrow |M_n+1\rangle$.

(d) One of the occupied state $|\underline{q}+\rangle$ is changed to $|\underline{k}'-\rangle$ while $|M_n\rangle$ --- $|M_n+1\rangle$; then electron $|\underline{k}+\rangle$ is scattered to the empty state $|\underline{q}+\rangle$, S_{nz} remaining $|M_n+1\rangle$.

(4) $|\underline{k}-\rangle$ —— $|\underline{k}'+\rangle$, with the similar four groups.

Note that 8 groups in processes (3) and (4) involve spin-flip during scattering.

In the calculation of transition probability some important assumptions must be recalled.

1. The localized spins are randomly oriented and the correlation between any pair of localized spins can be neglected.

2. The scattering is elastic ie. energy conservation is taken into account ($\varepsilon_k \doteq \varepsilon_{k'}$).

3. The scattering through intermediate states without change of the spin direction may be regarded of the similar

nature as the potential scattering and has little dependence on the initial electron energy $\mathcal{E}_k$ and hence will be neglected.

4. The two processes (d)'s (ie. S_{nz} of localized spin first decreases then increases) and (c)'s (S_{nz} first increases and then decreases) do not give the same answer. This is the basic dynamical character of the localized spin system.

Then the transition probability can be calculated as

$$W(\underline{k}^{\pm} \longrightarrow \underline{k}'^{\pm}) = 2\pi J^2 s(s+1)\frac{C}{3\hbar N}\left[1+4Jg(\mathcal{E}_{\underline{k}})\right]\delta(\mathcal{E}_{\underline{k}}-\mathcal{E}_{\underline{k}'}) \qquad \text{.....(5.4.6)}$$

$$W(\underline{k}^{\pm} \longrightarrow \underline{k}'^{\mp}) = 4\pi J^2 s(s+1)\frac{C}{3\hbar N}\left[1+4Jg(\mathcal{E}_{\underline{k}})\right]\delta(\mathcal{E}_{\underline{k}}-\mathcal{E}_{\underline{k}'}) \qquad \text{.....(5.4.7)}$$

where $g(\mathcal{E}_k) = \frac{1}{N}\sum_{\underline{k}'} f^{o}_{k'}/\mathcal{E}_{k'}-\mathcal{E}_k$

and $f_{k'}$ is the Fermi distribution function for the electron with energy $\mathcal{E}_{k'}$; C is the number of localized spin per atom which can also be defined as the probability of an atom being an localised impurity atom. N is total number of atoms in the crystal, hence CN is the total number of localized impurity atoms.

5.4.4 The logarithmic temperature dependence of resistivity

With the use of the conventional Boltzmann transport equation together with the relaxation time approximation we have

$$\rho = -\frac{12\pi^2}{e^2}\left(\int \tau v^2 \frac{df_k}{d\varepsilon_k} d^3k\right)^{-1} \qquad \text{.....(5.4.9)}$$

$$\frac{1}{\tau} = \sum_{k'} \left[W(\underline{k}^{\pm} \longrightarrow \underline{k}'^{\pm}) + W(\underline{k}^{\pm} \longrightarrow \underline{k}'^{\mp}) \right] \text{...(5.4.10)}$$

From equations (5.4.6), (5.4.7) and $(1+4Jg)^{-1} \simeq (1-4Jg)$ ...(5.4.8) we have,

$$\tau = \left(\frac{Cs(s+1)3\pi nJ^2V}{2\varepsilon_F \hbar N}\right)^{-1} \left[1 - 4Jg(\varepsilon_k)\right] \qquad \text{.....(5.4.11)}$$

We put (5.4.11) into (5.4.9) and calculate

$$\int v^2 \frac{df_k}{d\varepsilon_k} d^3k = -\frac{12\pi^3 n}{m} \qquad \text{.....(5.4.12)}$$

$$\int g(\varepsilon_k) \frac{df_k}{d\varepsilon_k} d^3k \doteq \iint \ln \frac{\varepsilon_k - \varepsilon_{k'}}{4\varepsilon_F} \frac{df}{d\varepsilon_k}\frac{df}{d\varepsilon_{k'}} d\varepsilon_k d\varepsilon_{k'}$$

$$= \text{const} + \ln T \qquad \text{.....(5.4.13)}$$

If we assume the distribution function

$$f = \frac{1}{e^{\frac{\varepsilon - \varepsilon_F}{KT}} + 1} \qquad \text{.....(5.4.14)}$$

then equation (5.4.9) becomes

$$\rho \sim c\rho_M \left(1 + \frac{3zJ}{\varepsilon_F} \ln T \right)$$

$$\sim a - b \ln T \qquad \text{.....(5.4.15)}$$

where $a = c\rho_M$

$$\rho_M = \frac{3\pi m J^2 s(s+1)\, z}{2e^2 \hbar \varepsilon_F n} \qquad \text{.....(5.4.16)}$$

$$b = - c\rho_M \frac{3z J}{\varepsilon_F} \qquad \text{.....(5.4.17)}$$

and z = number of conduction electrons per atom $= n/N_o = n/(\frac{N}{V})$

N_o = number of atom per unit volume

n = number of conduction electrons per unit volume

= carrier concentration.

The above mentioned theory is based on the ideas of Toyozawa and Kondo;[76] [77] so we call it " Kondo—Toyozawa theory ".

5.4.5 The theory applied to the hot electron problem

In the hot electron problem the conduction electrons travel along the sample with their energy characterised by electron temperature T_e which is higher than lattice temperature T. At low temperature, if the energy is not too high

the conduction electrons are supposed to be scattered by these localized spins. The calculation of the effect of this scattering on the electrical resistivity is similar to the preceding section (5.4.4). Only instead of using equation (5.4.14) we use the modified Maxwell-Boltzmann distribution function

$$f \sim \frac{1}{e^{\frac{\varepsilon-\varepsilon_F}{KT_e}} + 1} \qquad \text{.....(5.4.18)}$$

then finally we have

$$\rho \simeq C \rho_M \left(1 + \frac{3zJ}{\varepsilon_F} \ln T_e \right)$$

$$\simeq A - B \ln T_e \qquad \text{.....(5.4.19)}$$

Since the electron temperature T_e is a function of E we can rewrite (5.4.19) in the form

$$\rho \simeq C - D \ln E \qquad \text{.....(5.4.20)}$$

where A,B,C and D are positive constants.

5.5 The negative magnetoresistance and the logarithmic temperature dependence of the resistivity

A negative magnetoresistance and a logarithmic temperature dependence of the resistivity have been observed in a number of semiconductors at low temperatures. These measurements have most readily been explained by localised spin scattering in terms of the above mentioned Kondo-Toyozawa theory.

In our fast pulse technique we observe these two phenomena in the low electric field region. From the experimental result shown in section (5.1.1) we plot the curve $\Delta\rho/\rho$ against H^2 at low-pulsed field in Figure 5.14. A negative magnetoresistance is shown below 65$(K\text{-gauss})^2$ and a positive one at the higher magnetic fields. It is supposed to be the resultant of the normal positive contribution proportional to H^2 and a negative contribution which tends to saturate at higher magnetic fields in the manner discussed by Finlayson and Mathewson. (80) The negative magnetoresistance can be understood as follows. At sufficiently low temperatures a fraction of the impurity electrons exists as magnetic states at somewhat isolated sites. The spin, randomly orientated in zero magnetic field, become more ordered when a field is applied. Their scattering efficiency is thereby decreased due to the magnetic freeze-out of the spin-flip scattering (this will be discussed in section 5.8) and a decrease in

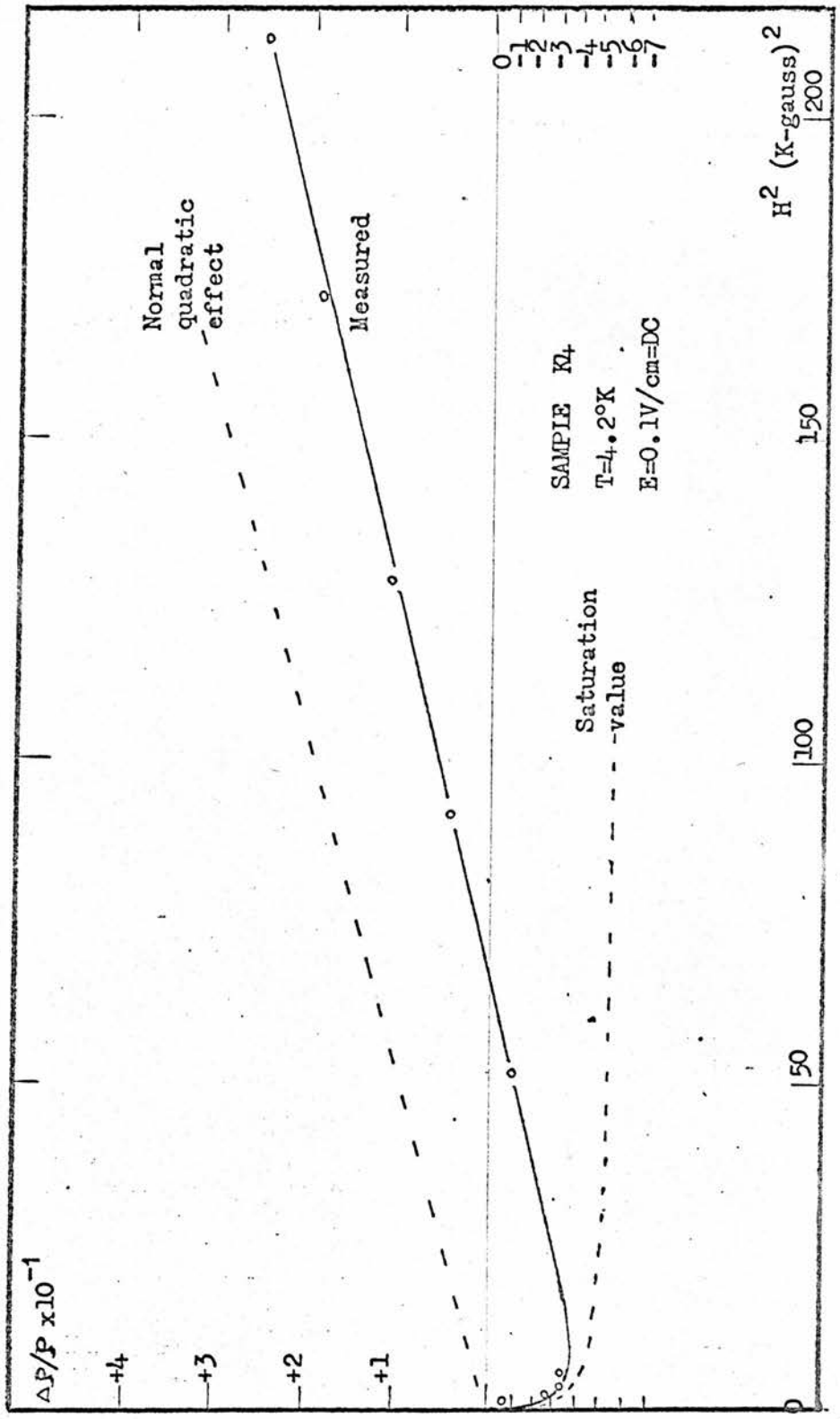
Normal quadratic effect
Measured
Saturation value
SAMPLE K4
T=4.2°K
E=0.1V/cm=DC
$\Delta P/P \times 10^{-1}$
+4
+3
+2
+1
0
-1
-2
-3
-4
-5
-6
-7
50
100
150
200
H^2 (K-gauss)^2

FIGURE 5.14

resistance is observed.

The temperature dependence of resistivity is plotted in Fig.5.15 for the sample K8 at very low electric field and zero magnetic field. A resistance minimum is obtained at the Kondo temperature, about 30deg.K for sample K8 . The negative resistivity gradient can be easily proved to be the logarithmic temperature dependence. In Figure 5.16 the resistivity below the minimum is plotted against lnT. A straight line is obtained over a range of temperature and can be fitted to the expression

$$\rho = a - b \ln T \qquad \text{.....(5.5.1)}$$

This can be understood as the conduction electrons undergo the same localised spin scattering; they tend to spin-flip as they approach the localised spins. At low temperature more spin-flip means more scattering which in turn implies higher resistance. When temperature increases spin-flip scattering is expected to decrease due to thermal agitation. It gives rise to a decrease in resistivity.(also see section 5.8).

Experimentally we get from Figure 5.16

$a = 0.282$ ohm-cm

$b = 0.058$ ohm-cm/$\ln^{\circ}K$

For sample K8 $n = 9.54 \times 10^{15}$ per cm^3 it satisfies the empirical formula [82] pretty well

$$a \propto n^{-2.4} \; ; \; b \propto n^{-3.0} \qquad \text{.....(5.5.2)}$$

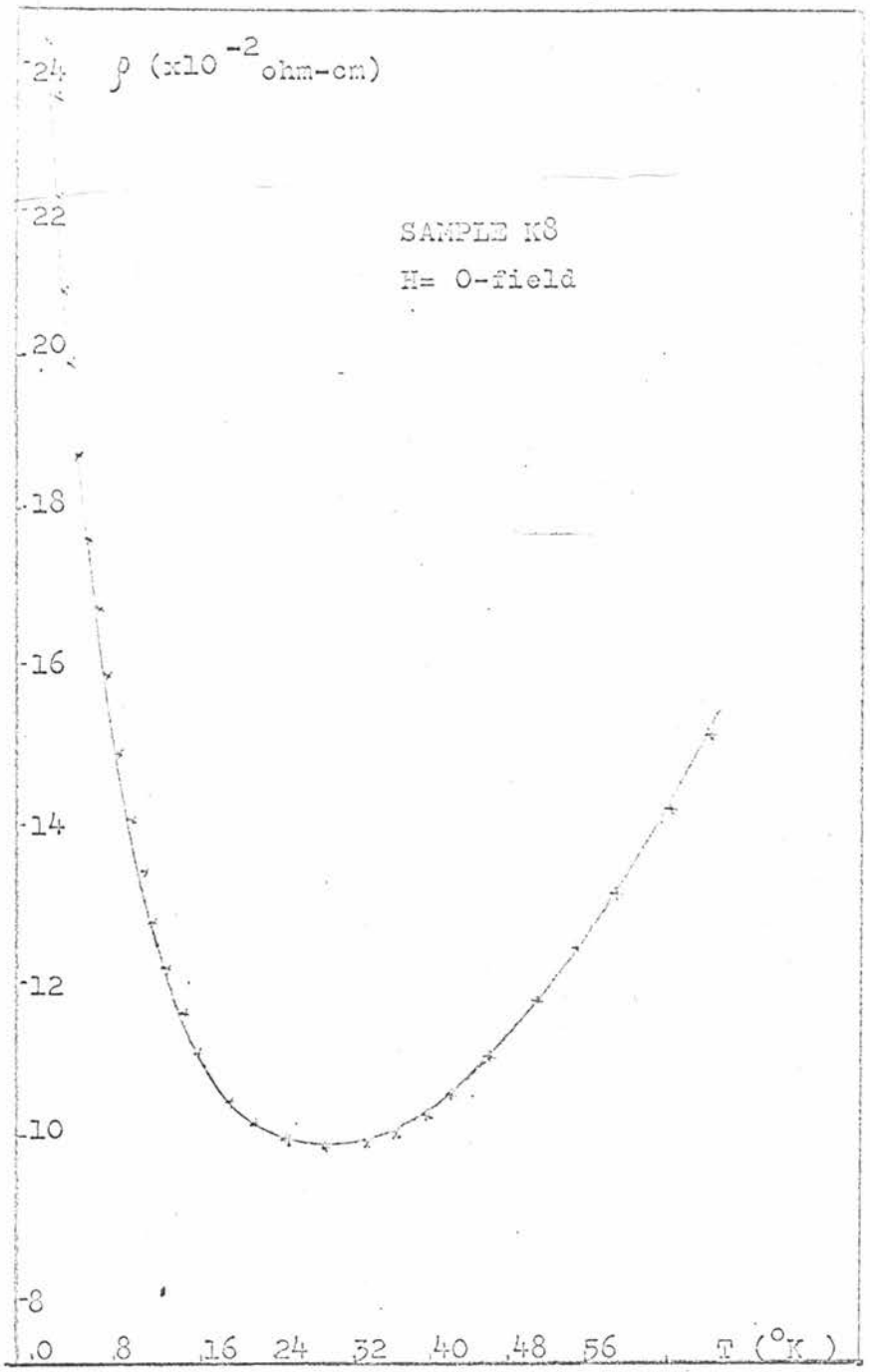
ρ (x10 -2 ohm-cm)
24
22
20
18
16
14
12
10
8
SAMPLE K8
H= 0-field
.0
.8
.16
.24
.32
.40
.48
.56
T (°K)

FIGURE 5.15

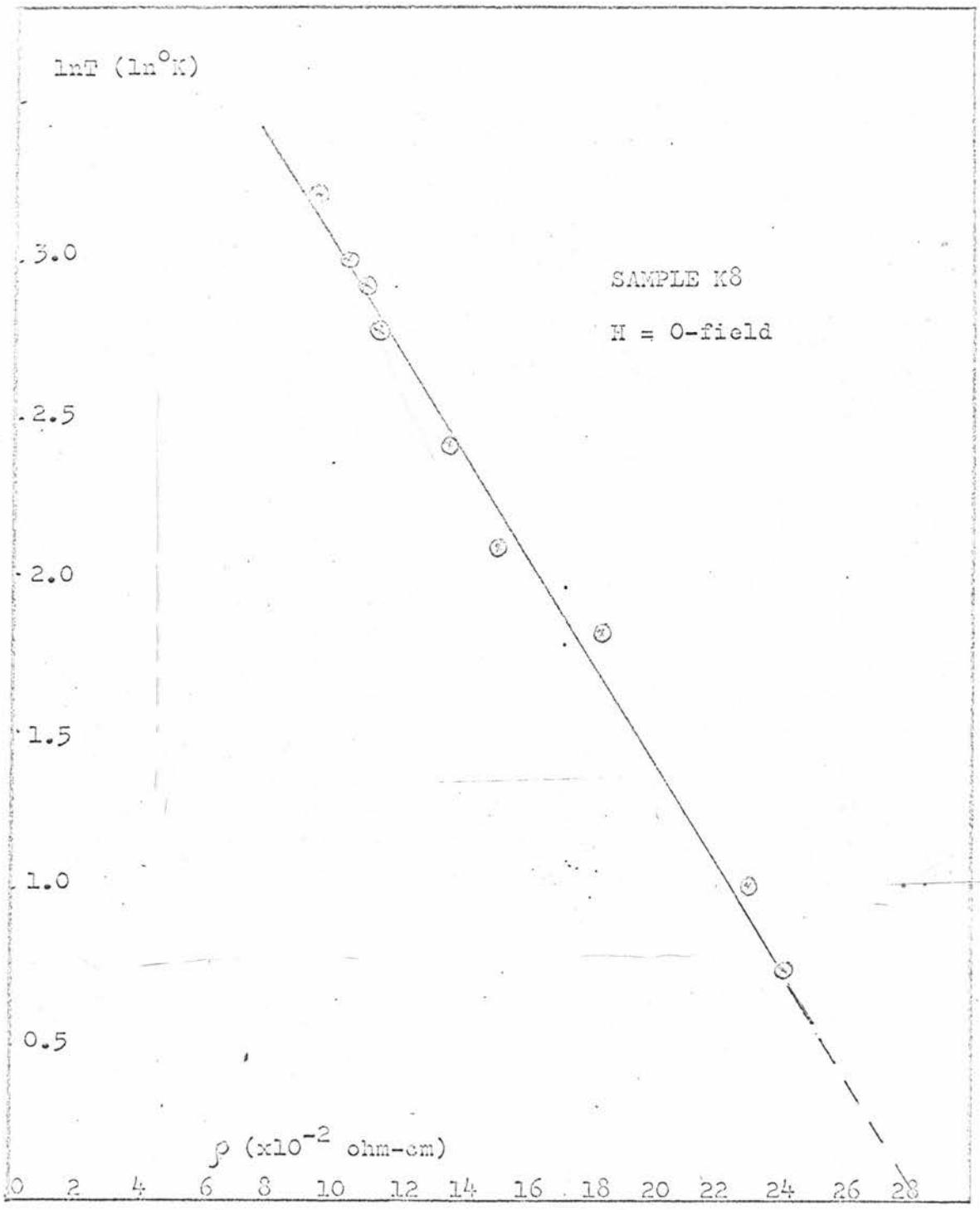
lnT (ln°K)
3.0
2.5
2.0
1.5
1.0
0.5
SAMPLE K8
H = O-field
ρ (x10⁻² ohm-cm)
0 2 4 6 8 10 12 14 16 18 20 22 24 26 28

FIGURE 5.16

The resistance minimum has already been investigated [82] and is not primarily part of the present work. However Figs.5.15 and 5.16 roughly show that our results are consistent with the earlier measurements.

5.6 Hot electron Kondo-behaviour

5.6.1 The logarithmic electric field dependence of resistivity

A logarithmic temperature dependence of resistivity is readily explained by localised spin scattering in terms of Kondo theory similar to that in dilute magnetic alloys. As pointed out by Kondo, this scattering depends strongly on the energy of the conduction electrons because of the dynamical character of the localised spin system. It seems more precise to emphasize the electrons' own energy, characterised by electron temperature T_e, rather than the lattice temperature T in order to study the nature of this mechanism. We suggest that the hot electrons will undergo the same scattering mechanism and give the electron temperature dependence of resistivity similar to that given in section (5.4.5) theoretically. Therefore in summary,

(1) For the thermal equilibrium

$$\rho \sim a - b \ln T \qquad \text{.....(5.6.1)}$$

(2) For the hot electron case

$$\rho \sim A - B \ln T_e \qquad \text{.....(5.6.2)}$$

(3) Electron temperature arises from an external field

$$\rho \sim C - D \ln E \qquad \text{.....(5.6.3)}$$

where a, b, A, B, C and D are positive constants.

This logarithmic field dependence of resistivity is observed in the present experiment and has been shown in Figures 5.1, 5.2, ...5.6 and etc. The very close correlation between the ln T dependence and ln T_e dependence of resistivity powerfully confirms that the latter arises from the same scattering mechanism. The observation of a substantial linear portion in Figure 5.6 for each carrier concentration as mentioned before in the section (5.1.1) therefore indicates a Kondo type explanation. It can be also understood that the localised spin scattering efficiency is decreased due to the thermal agitation (see section 5.8) when the electron is hotter and therefore a decrease in resistance is observed.

5.6.2 The variation of slope D with concentration n

The dependence of the negative magnetoresistance effect on carrier concentration n [80] and the dependence of the resistivity minimum on n [81] is somewhat similar to the dependence of the slope of the linear part in ρ—ln E curve on n. At the same lattice temperature the effect of negative magnetoresistance and resistivity minimum depth was strongest for the sample with the lowest carrier concentration under investigation. The effect decreased as carrier concentration increased, and for

carrier concentrations greater than about 5×10^{17} per cm^3 the negative magnetoresistance effect and the resistivity minimum were not observed. One can easily associate these facts with the variation of slopes in our case. The sample with the lowest concentration gives the greatest gradient, $(d\rho/d \ln E)$, and the gradient tends to be zero as n goes to 5×10^{17} per cm^3.

It was also shown experimentally that the negative magnetoresistance effect was temperature dependent. The effect tended to be weaker as temperature increased and disappeared at a temperature between 30°K and 40°K for samples with low concentration (ie. $n\simeq10^{16}$ per cm^3); while the Kondo temperature in the minimum resistivity measurements happened in the similar temperature range. This may be associated with the change of slope in the resistivity—ln E curves (see Figure 5.6 and etc.) which suggests a hot electron Kondo-temperature in the region of E = 20 volt/cm to 40 volt/cm.

In Figure 5.17 we plot ln n against $\ln(\overbrace{d\rho/d \ln E}^{=D})$ in order to work out the variation of D with n because

$$\rho \simeq C - D \ln E$$

$$D = -\frac{d\rho}{d(\ln E)} \qquad \text{.....(5.6.4)}$$

and found that it was reasonably good fit to a straight line.

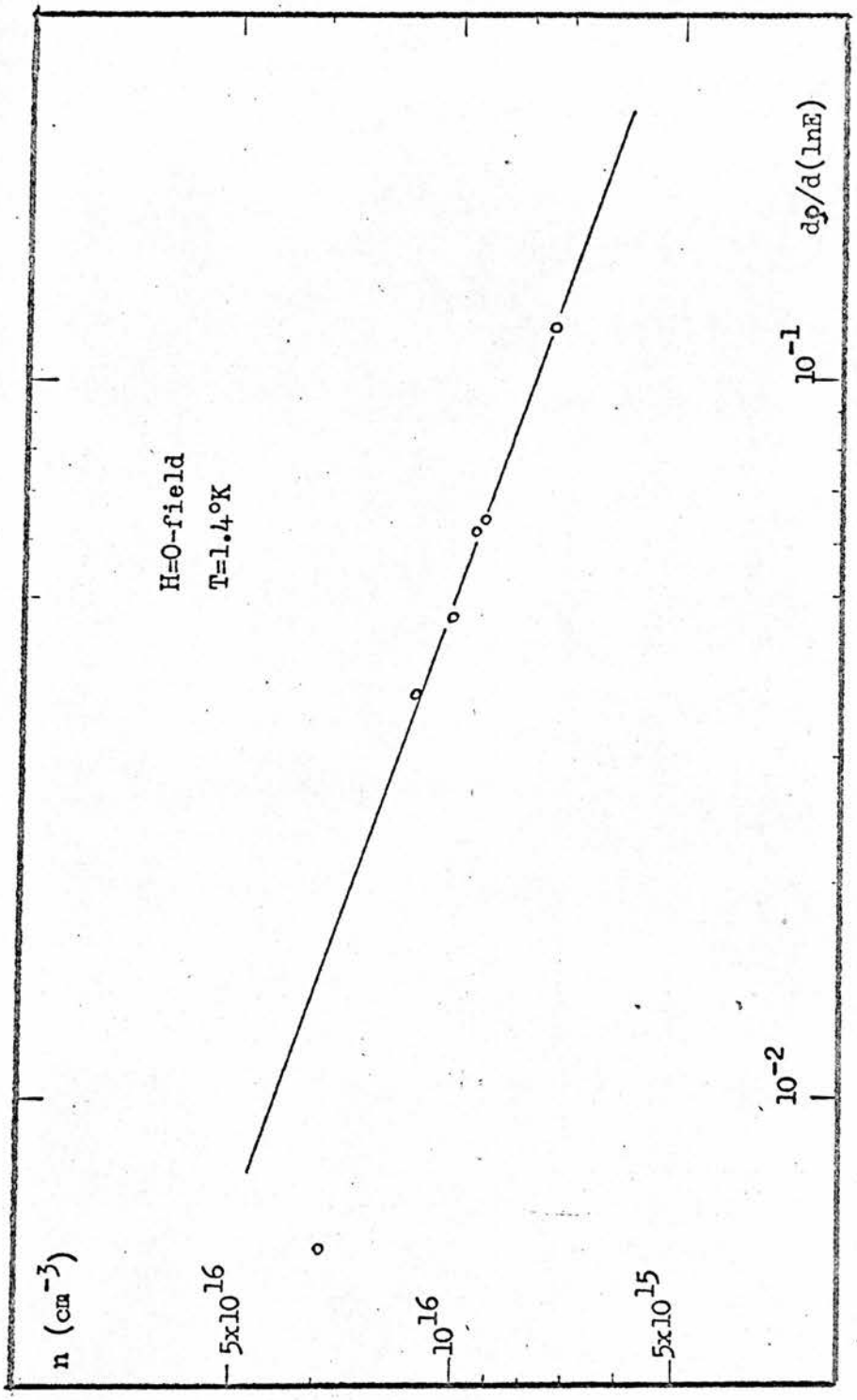
H=0-field
T=1.4°K
n (cm^{-3})
5×10^{16}
10^{16}
5×10^{15}
10^{-1}
10^{-2}
dρ/d(lnE)

FIGURE 5.17

If we assume, for zero magnetic field

$$D \sim n^{y} \qquad \text{.....(5.6.5)}$$

then $$\ln D = y \ln n \qquad \text{.....(5.6.6)}$$

and therefore empirically for hot electron case we have

$$D \sim n^{-2.92} \qquad \text{.....(5.6.7)}$$

5.6.3 An estimate of the concentration of localised spins

In fact, the concentration of localised spin should be involved in the above discussion. To study the problem more quantitatively we now estimate the concentration of localised spin for six different samples. From section (5.4) we have

$$D \sim B \simeq C \rho_M \frac{3z J}{\varepsilon_F}$$

$$\therefore, \quad D \simeq \frac{Cx3\pi xm^{*}x|J|^{3}s(s+1)z^{2}x3}{2e^{2}\hbar\, \varepsilon_F\, n}$$

where $\varepsilon_F = \frac{\hbar^2}{2m}(3\pi^2 n)^{\frac{2}{3}}$ ev

For PbS, a F.C.C. crystal we have

Volume of unit cell = $L^3/4$

L, lattice constant = 5.9×10^{-8} cm

N = the total number of atoms in the crystal

= the total number of unit cell

= the total volume/volume of unit cell

= $4V/L^3$

z = number of conduction electron per atom

$= n \frac{V}{N} = n \frac{L^3}{4} = nx(5.9x10^{-8})^3 x\frac{1}{4}$

n = carrier concentration

D = the slope in Figure 5.6 which can be calculated experimentally.

We also assume $s = 5/2$ (83)

and $J = 5x10^{-5}$ ev (82)

J here is considered as a constant since we understand that the coupling strength should be the same once the localised spin scattering happens even for samples with different concentrations.

Then $\mathcal{E}_F$ and C can be computed and C is also justified in the manner discussed by Tanaka. (79) The results are listed in Table 5.1.

This gives a reasonably good explanation of the fact that the number of localised spins decreases with increasing carrier concentration as the effect of localised spin scattering gets less pronounced.

TABLE 5.1

SAMPLE	CARRIER CONCENTRATION, n (cm^{-3})	SLOPE D IN lnE curve (ohm-cm^2/volt)	FERMI ENERGY LEVEL E_F^* (ev)	LOCALISED SPIN CONCENTRATION (cm^{-3})
Y 24	7.49×10^{15}	1.17×10^{-1}	1.19×10^{-3}	7.6×10^{14}
K 4	9.25×10^{15}	0.625×10^{-1}	1.35×10^{-3}	6.4×10^{14}
K 8	9.54×10^{15}	0.618×10^{-1}	1.37×10^{-3}	6.1×10^{14}
Y 11	1.02×10^{16}	0.453×10^{-1}	1.43×10^{-3}	5.7×10^{14}
C'43	1.15×10^{16}	0.363×10^{-1}	1.55×10^{-3}	5.0×10^{14}
K 1	1.47×10^{16}	0.06×10^{-1}	1.82×10^{-3}	2.9×10^{14}

5.7. The variation of the slope D with magnetic field H

So far we note that the coefficient D, the slope of our $\rho \sim \ln E$ plots, possesses an important physical meaning. It represents the change of resistivity with field; that means the change of efficiency of localised spin scattering with field. From the above discussion (see also Table 5.1) we can see that greater localised spin concentration gives greater change in scattering as the external field is varied.

Now if an external magnetic field H is applied the change of efficiency of localised spin scattering is expected to be higher since the "freezing-out" of localised spins is probably involved in the presence of magnetic fields due to the exclusion principle.

We plot ln D against ln H in Figure 5. 18 in order to show the relationship between $(d\rho) / d(\ln E)$ and H. We note that $(d\rho) / d(\ln E)$ is somewhat independent of H at low H and that at fields of the order of 10^4 gauss a sharp increase in slope is observed. Although straight lines have been drawn through the experimental points it may be that

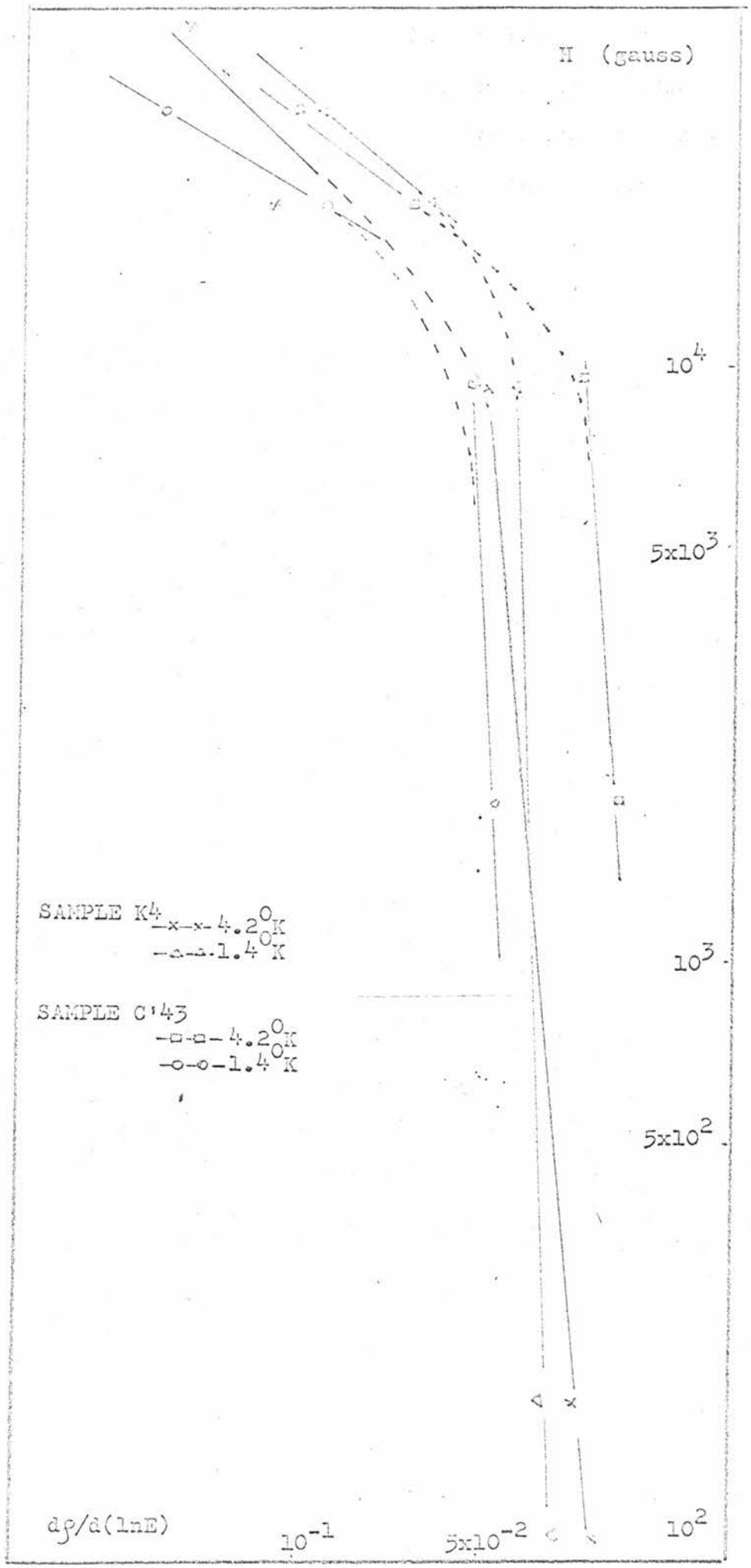
H (gauss)
10^4
$5x10^3$
10^3
$5x10^2$
SAMPLE K4
—x—x— 4.2°K
—a—a— 1.4°K
SAMPLE C'43
—□—□— 4.2°K
—o—o— 1.4°K
dρ/d(lnE)
10^{-1}
$5x10^{-2}$
10^2

FIGURE 5.18

smooth curves are more appropriate.

5.8 The consideration of the degeneracy of the system

In the preceding sections we have mentioned that the negative magnetoresistance and logarithmic temperature (ie. either electron temperature for hot electron case or lattice temperature for the thermal equilibrium case) dependence of resistivity are due to the spin-flip scattering. It is, in fact, only valid for degenerate semiconductors. When the degeneracy of the system is released the efficiency of this kind of scattering is reduced.

From the theory of semiconductors we know that generally the Fermi level is located at least a few kT below the bottom of the conduction band. It means that the electron gas is nondegenerate. However we understand that for our case the Fermi level may enter the conduction band at low temperature. Thus, the electron gas in the conduction band is, in fact, degenerate. The conditions favourable for this situation are (1) small ionization energy (2) small effective mass as mentioned before. Therefore the Fermi level varies with electron temperature. As the temperature is increased, the Fermi level moves down and then leaves the conduction band. This means that the degeneracy of the system is removed. Once the system becomes nondegenerate

the temperature dependence of spin-flip scattering vanishes. In fact, in this Kondo-type behaviour two-step-transitions are involved and a simplified picture is not easy to obtain.

In the negative magnetoresistance case we know that it is caused by the freezing out of spin-flip scattering due to the aligning of the impurity spins by the magnetic field.[87] Let us consider the following spin-flip scattering process: initial state of an electron of momentum k_i , spin down, and impurity with spin component M_s , going into the final state of an electron of k_f , spin up and impurity spin component M_s-1 . In a simple case, energy conservation gives $|k_i| = |k_f|$, so for electrons initially within kT of the Fermi surface which contribute to the resistivity, the final-state spin-up electron therefore has an energy below the Fermi energy if the external magnetic field is at "up" direction. This scattering process is forbidden by the Pauli exclusion principle because below the Fermi level states are supposed to be filled up. Since the field tends to align the impurity spins along the " up " direction, more of the spin flip processes are of this forbidden electron--spin--down into electron--spin--up type

than of the electron-spin-up into electron-spin-down type allowed by the exclusion principle. Therefore the total contribution of the spin-flip scattering amplitudes to the resistivity is reduced.

5.9 The effects due to a magnetic field

5.9.1 The cooling effect

From magnetoresistivity measurements (see Figures 5.1 , 5.2, 5.3 and 5.4) it is found that when higher transverse magnetic fields are applied then higher electric fields are required before the decrease in resistivity begins to appear.

For instance, for sample K4 at 4.2 deg.K we have

H:		E_s :	
37.1	K-gauss	2.8	Volt/cm
31.5	"	2.51	"
18.6	"	2.25	"
9.3	"	1.82	"
0	"	1.62	"

where H is the magnetic field intensity and E_s is the field for a 5% decrease in resistivity.

The plot of E_s against H is shown in Figure 5.21.

The effect of the magnetic field in this case is easily understood. Because of the curvature of the path of the electrons

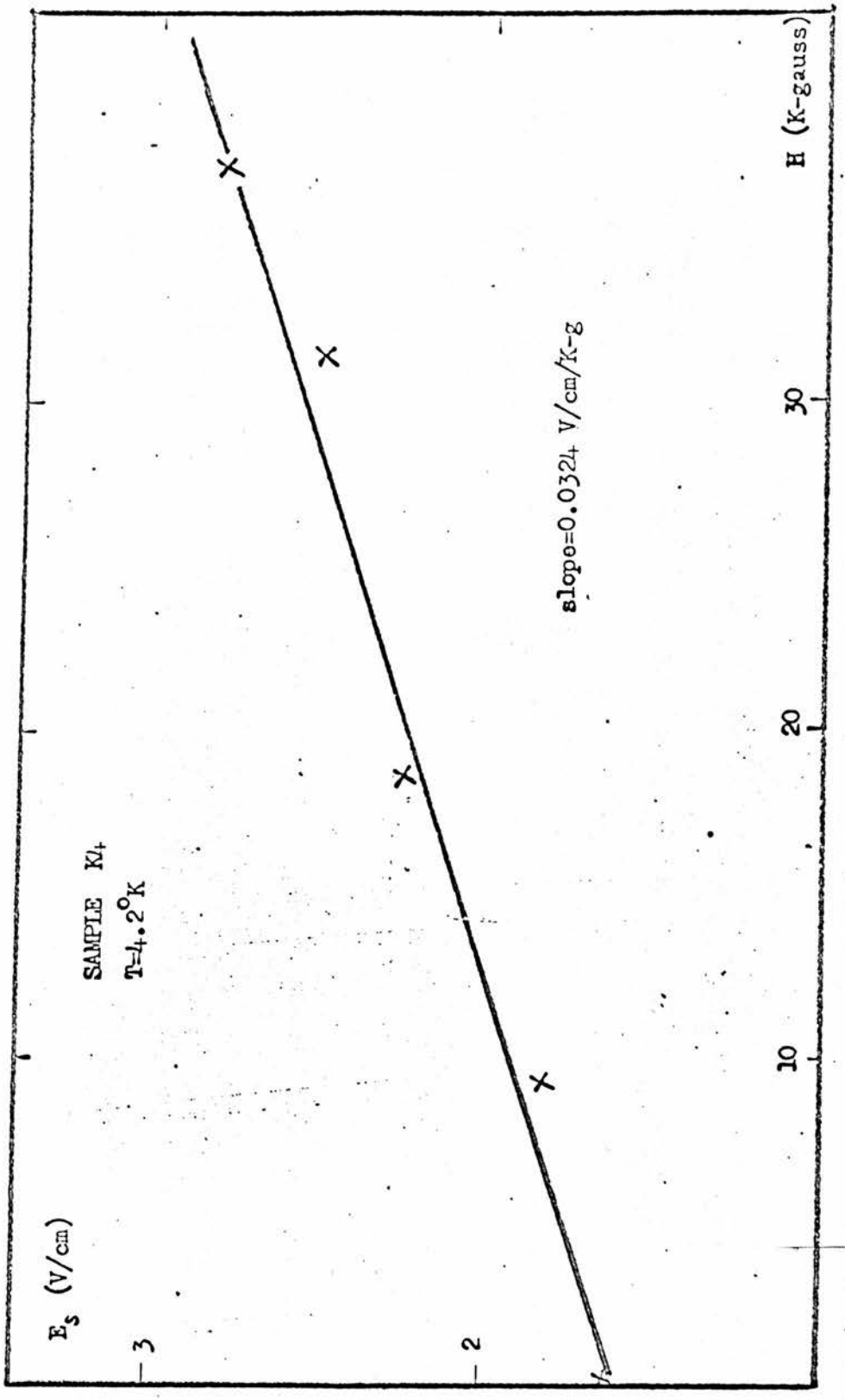

FIG. 5.21

by the Lorentz force, the rate at which they gain energy from the electric field is decreased in the presence of the magnetic field. Thus, the effect of a magnetic field is to cool the hot electron gas.

The power of this cooling effect can be estimated from the slope of the Figure 5.21 which gives

$$\text{Power} = 0.0324 \quad \frac{\text{volt/cm}}{\text{K-gauss}}$$

5.9.2 Effects of instability

The not-yet-understood instabilities of various kinds have not been found in our experiments for lead sulphide even with a magnetic field up to 37 K-gauss or an electric field to the order of magnitude of 10^3 volt.cm^{-1}. The only reason we can give is that the repetition frequency of pulse used in our bridge method is too low (100cps) to ignite the instability effect.

5.9.3 Effects on the Hall coefficient

We have mentioned before that when the magnetic field is low the Hall coefficient shows a little variation with field, E; it tells us that the electron concentration keeps contant as the field goes higher. However the Hall coefficient, R, may be written as

$$R = \gamma \frac{1}{ne}$$

where γ is the Hall coefficient factor of order of unity. Its exact value depends on the magnetic field intensity, the detail of scattering mechanism and the energy band structure.

The nature of the dependence of γ on magnetic field is determined by the dimensionless product of the mobility and the magnetic field intensity. This suggests why the Hall coefficient would change at high electric field even though electron concentration does not alter as shown in Figures 5.12 and 5.13. The change in the distribution function itself and changes in the relative importance of different scattering mechanisms would both affect R, because of the heating of electrons. For low magnetic field region ie. μH is small, γ and therefore R are independent of H while in the limit of large value of μH , $\gamma=1$ independent of the scattering mechanism and band structure.

Figure 5.13 shows the plot of Hall coefficient against electric field for sample K4 at helium temperatures. At lower magnetic fields, the Hall coefficient decreases with increasing electric field; while at the higher magnetic fields R is observed to increase with field. This behaviour can be understood by the consideration of μH dependence of γ. At low electric fields the considerable increase of R with decreasing H indicates that the μH product is small and hence γ is bigger than unity; while at

the higher magnetic fields μH at low electric fields is quite large so that the value of τ is close to unity. As the electric field increases, μ increases for Kondo type scattering, the μH product is substantial, and the Hall coefficients move toward each other.

Moreover, for a many-valley semiconductor, lead sulphide, there are possibilities for additional effects because different heating of electrons in different valleys would affect the Hall coefficient.

5.10 The anisotropy of magnetoresistivity

The experimental results of anisotropy of magnetoresistance of lead sulphide at helium temperatures were revealed in the present work as shown in Figure 5.10. The quantity $\Delta\rho=\rho-\rho_L$ was plotted against ln E for sample K4 at two magnetic fields and two temperatures. It is seen that the anisotropy vanishes at high electric fields. The nature of this phenomenon is studied as follows:

5.10.1 General considerations

The general idea for the transverse magnetoresistance of a semiconductor sample is based on the fact that inside the sample the Lorentz deflection of faster electrons (with longer τ than the average) wins over the built-in Hall field. This causes a

reverse current and so the total apparent current is reduced.

For a longitudinal case this idea is no longer applicable. We assume that the electrons are moving in spirals along the magnetic field direction in the sample. However the determination of magnetic anisotropy of resistance ie. the comparison of these two kinds of motion seems quite difficult even qualitatively.

5.10.2 Many-valley model

For a many-valley semiconductor, ie. its band edge (or minimum) is not at the centre but is at a number of equivalent points in the Brillouin zone. To a good approximation the surfaces of constant energy can be considered as ellipsoids with an axis of revolution which has rotational symmetry. Electrons with $\underline{k}$ vector parallel to the rotational axis of the spheroid have larger masses than that with $\underline{k}$ vectors perpendicular to the rotational axis. However, the population of electrons is still divided equally among the various valleys. If external electric field is applied the electrons with larger masses will make a small contribution to the current flow than the lighter ones. If the field is increased the lighter electrons gain more energy and get hotter. There is a tendency, therefore, for electrons in the hotter valleys to move into the cooler ones so that the cooler valleys gain in population.

If a directional magnetic field is applied in the same time to the sample the magnetic effect will give different influences to the hotter and cooler carrier flows. A magnetic anisotropy would be enhanced. When the electric field is high enough so that all valleys have high enough temperatures, transitions from the cool valleys to the hotter ones will occur in increasing number, tending to equalize the populations and temperatures of different valleys. Then the anisotropy decreases.

5.10.3 The model of spin-orbit interaction

When the conduction electrons encounter the localised spins, apart from the above discussed spin-spin exchange coupling, one should see the spin-orbit interaction coupling between the conduction electrons and the localised spins. We suggest that in the vicinity of the localised impurity sites the electrons are supposed to be in the outer orbits (ie., 6p-orbits for Pb impurity in PbS, which are similar to the unpaired d-orbits for ferromagnetics) and hence have certain amount of angular momentum. This becomes essentially a spin-orbit interaction coupling. The Hamiltonian is given as [88]

$$H_{int}(\underline{k},\underline{k}') = -\frac{1}{N}\sum_{\underline{k},\underline{k}',n} e^{i(\underline{k}-\underline{k}')\underline{R}_n}\Big[(a^*_{\underline{k}'+}a_{\underline{k}+} - a^*_{\underline{k}'-}a_{\underline{k}-})L^z(kk')S_{nz} + a^*_{\underline{k}'-}a_{\underline{k}+}L^-(kk')S_{n+} + a^*_{\underline{k}'+}a_{\underline{k}-}L^+(kk')S_{n-}\Big] \quad \ldots(5.10.1)$$

where L is the operator of obital angular momentum of electrons in the localised sites(see section 5.4 for the other symbols).

This part of Hamiltonian obviously will give an additional resistivity ρ_{int} to the resistivity measurements. We may write as follows

$$H'_{total} = H_{ex} + H_{int}$$

$$\therefore , \rho'_{total} = \rho_{ex} + \rho_{int} \qquad \text{and } \rho_{ex} \gg \rho_{int} \qquad \text{.....(5.10.2)}$$

Then in the case of anisotropy of magnetoresistance we have

$$\begin{aligned} \Delta\rho' &= \rho - \rho_L \\ &= \rho''_{total} - \rho^{\perp}_{total} \\ &= (\rho''_{ex} - \rho^{\perp}_{ex}) + (\rho''_{int} - \rho^{\perp}_{int}) \end{aligned} \qquad \text{.....(5.10.3)}$$

The first term equals zero since ρ_{ex} (it has been discussed in section 5.6) does not depend on the direction of the magnetic field and hence the anisotropy of magnetoresistance tells us only the information of the interaction coupling.

However different theories were given for this $\Delta\rho$-effect. The quantum theory was firstly given by Vonsovskii and Rodionov[89][90] in terms of the s-d model. As a consequence of this interaction coupling the effective mass of s-electrons is anisotropic which

explains the resistivity anisotropy. It was also shown that the $\Delta\rho$-effect is proportional to the square of magnetic field. Smith et al[91][92][93] later suggested that as a consequence of the mixing of parallel and antiparallel unpaired-states due to the perturbation of this spin-orbit interaction coupling, the transition probability for electrons moving in the direction of magnetization is different from that in the perpendicular direction. This gives also a magnetoresistivity anisotropy. In 1967 Vu Dinh Ky [88] calculated the $\Delta\rho$-effect by using the H_{int} Hamiltonian and showed that the temperature dependences of magnetoresistance anisotropy $\Delta\rho$ due to a spin-orbit interaction coupling and of the resistivity ρ_{ex} due to the exchange coupling resemble eaoh other but ρ_{ex} is much bigger than ρ_{int}. The $\Delta\rho$-effect is weakening as the localised spin scattering mechanism is vanishing when the temperature or the electron energy is going up.

From (5.10.1) for ETM model we then have [88]

$$\Delta\rho \sim \beta'\pi' T_e - \beta' T_e \ln T_e + \beta'\alpha' T_e^2$$

$$\sim \beta'\pi' T_e - \beta' T_e \ln T_e \qquad \text{.....(5.10.4)}$$

since $\alpha' \sim (m^*)^2$ is very small for lead sulphide compared to the other two terms in warm electron region.

In terms of external electric field, approximately we have

$$\Delta\rho \sim \beta\tau E - \beta E \ln E$$

Therefore when external field is not too high we have

$$\frac{\Delta\rho}{E} \sim \beta\tau - \beta \ln E$$

where β and τ are field-independent constants.

Figure 5.22 shows that when E increases the effect of anisotropy of magnetoresistance dies off. This can be understood in the light of our localised spin scattering model because when electron temperature goes higher spin system becomes less localised and this scattering mechanism is no longer valid and hence the anisotropic effect is vanishing.

As a conclusion the interpretation for magnetic anisotropy of resistivity is not certain. The explanation of magnetic field effect to the hotter and cooler carriers in terms of many-valley model is vague. We are in favour of the model of spin-orbit interaction which was originally suggested for ferromagnetics.

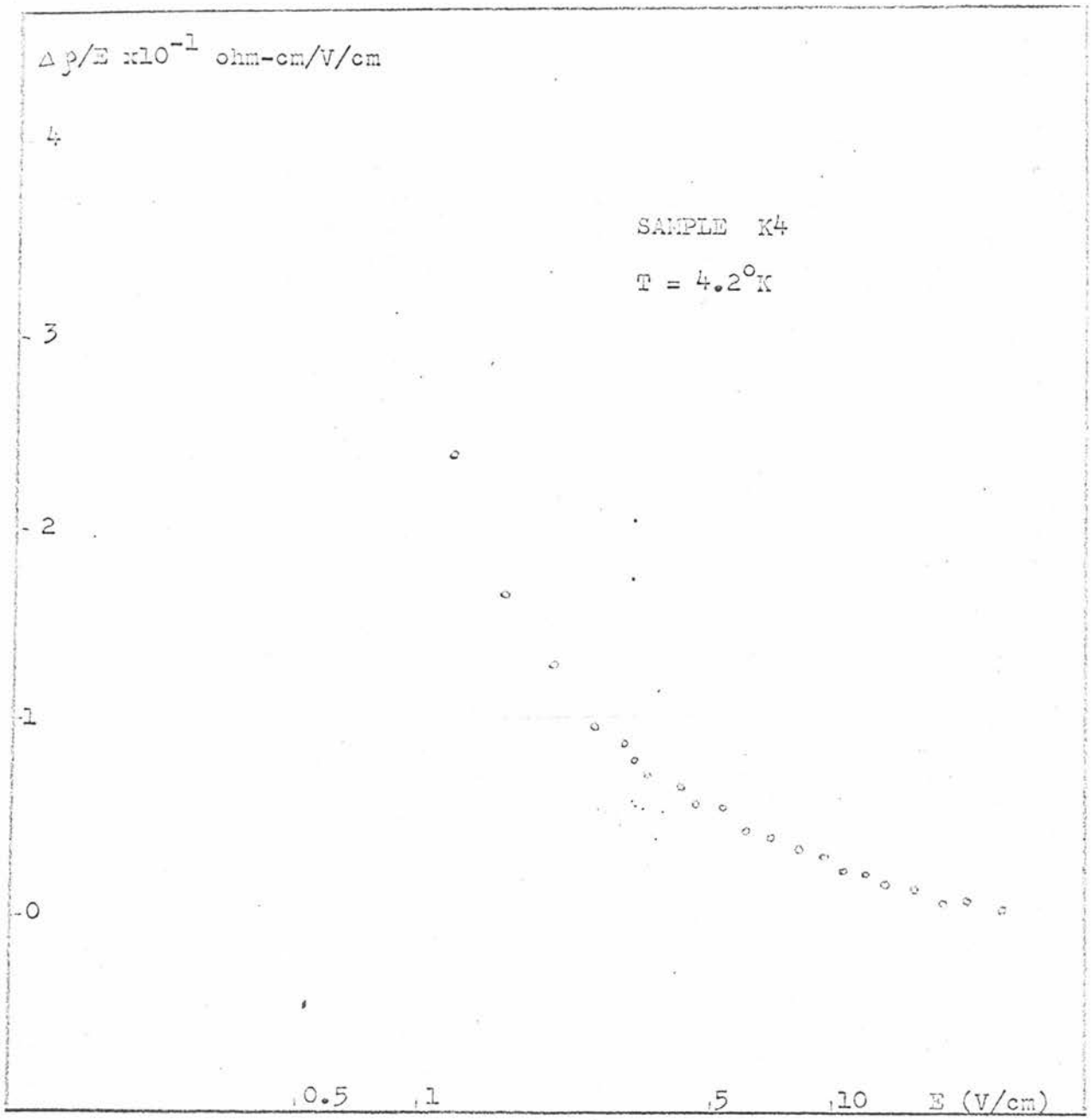

FIGURE 5.22

CONCLUSION

Using fast pulse techniques the resistivity, Hall effect and magnetoresistance of PbS have been measured in electric fields up to 10^3 volt cm^{-1} and in magnetic fields up to 37 K-gauss with a view to determining the main scattering mechanisms at 77° K and in the helium temperature range. At 77°K, apart from a shallow minimum at low fields, the resistivity increases with electric field confirming phonon scattering at this temperature. The comparison of experiment and theory shown in Fig. 4.4 provides strong evidence of a substantial contribution from polar optical phonons. This evidence, produced at a fixed lattice temperature, cannot be explained away in terms of a temperature dependent effective mass which, as mentioned in the introduction, has been used to explain the temperature dependence of mobility without considering optical phonon scattering. It can therefore be claimed beyond any reasonable doubt that optical phonons play a substantial part in scattering electrons at 77°K and thus presumably at higher temperatures.

In contrast to the increase in resistance with electric field at 77°K a decrease is found at low temperatures so it is at once clear that phonon scattering is no longer predominant. Neutral impurity scattering can be ruled out since it is independent of electron energy. Ionised impurity scattering should give a decrease in resistance as the electric field increases but we would expect the effect to increase with the electron

density. In fact the change in resistivity decreases with the increase of electron density, the resistivity becoming virtually constant with electric field for a concentration of 5×10^{17} cm^{-3}. Ionised impurity scattering can therefore also be ruled out, in agreement with evidence from several kinds of measurement.

However going over the same concentration range from about 5×10^{17} to $< 10^{16}$ cm^{-3} it has been found that both the resistance minimum and negative magnetoresistance increase in value. To explain this, scattering by localised spins has been suggested with the especial advantage that a tentative theory by Toyozawa predicts just such a change in effect with impurity concentration. The application of the theory to negative magnetoresistance and resistance minimum is similar to that used by Kondo for dilute alloys. It has been adapted by Tanaka[79] for semiconductors and following his method of calculation we do indeed find a decrease in localised spin concentration as the electron density increases.(table 5.1)

We suggest therefore that, for samples of PbS in the 10^{16}---10^{17} cm^{-3} range, scattering by localised spins is responsible for the observed behaviour at liquid helium temperatures.

At low electric fields the resistance is independent of field as is to be expected since the electrons remain at the lattice temperature. At very high fields the resistance is again approximately independent of field since by then the degeneracy which is essential for Kondo type behaviour has been largely removed. In the intermediate range the experimental results,

when plotted on a ρ--lnE graph, give straight line portions similar to those obtained from ρ--lnT graphs carried out at constant field.

The change in resistivity with electric field is found to increase with magnetic field, rather slowly at first but much more rapidly for fields greater than 10^4 gauss.

The magnetoresistance anisotropy decreases as the electric field increases and effectively vanishes at high electric field.

APPENDIX A

A1. Effect of screening by the electrons on the relaxation time [61][62]

The field generated by polar vibrations can be screened by the electrons which modifies the matrix element of the electron-phonon interaction. The effects are:

(1) renormalization of the effective charge

(2) modification of the frequency of the longitudinal optical phonon.

The effective charge is given as

$$(e^*)^2 = \frac{Ma^3\omega_l^2 (\epsilon_\infty^{-1} - \epsilon_o^{-1})}{2\pi\left[1 + \frac{1}{(qr_s)^2}\right]^2} \qquad \text{.....(A11)}$$

The frequency of the longitudinal optical phonons becomes

$$\omega^2 = \omega_l^2 \left[\frac{1 + \frac{\epsilon_\infty}{\epsilon_o}\frac{1}{(qr_s)^2}}{1 + \frac{1}{(qr_s)^2}}\right] = \omega_l^2\left[\frac{1}{1 + \frac{1}{(qr_s)^2}}\right] \qquad \text{.....(A12)}$$

($\because$, for PbS $\epsilon_o >> \epsilon_\infty$)

where ω_l is the frequency in the absence of screening and the screening radius is defined as

$$\frac{1}{r_s^2} = \frac{2^{5/2} e^2 (m_d^*)^{3/2} (K_o T)^{\frac{1}{2}}}{\pi \hbar^3 \epsilon_\infty} \; L$$

and where m_d^* is the density-of-states effective mass near band edge.

$$L = \int_0^\infty \left(-\frac{df}{dx}\right) \left(x + \frac{k_o T}{\mathcal{E}_g} x^2\right)^{\frac{1}{2}} \left(1 + 2\frac{k_o T}{\mathcal{E}_g} x\right) dx$$

By considering (A11) and (A12), we obtain the following factor in the expression for $1/\tau$

ie. $\frac{1}{\tau} \propto \left(1 - \delta \ln(1 - 1/\delta) \right)$ $\qquad \delta \equiv (2kr_s)^{-2}$

(The symbolic system and etc. throughout this appendix are referred to the preceding chapters and the corresponding references.)

A2. Influence of nonparabolicity of the relaxation time (62) (94) (95)

We consider electron wave function

$$\Psi = u_{\underline{k}^{\pm}}(\underline{r})\, e^{i\underline{k}.\underline{r}} \qquad \text{.....(A21)}$$

The nonparabolicity of the band is related to the $\underline{k}$ dependence of the periodic part $u_{\underline{k}}$ of the Bloch function by the $\underline{k}.\underline{p}$-perturbation theory in which the conduction band is described by s-like functions, u_c and Tu_c and their valence band, by p-like functions u_v and Tu_v (where T is the time reversal operator.)

Then the periodic parts are:

$$u_{\underline{k}^+} = a\left(u_c + \frac{\underline{p}_1^*.\underline{k}}{\mathcal{E}_g+\mathcal{E}} u_v + \frac{\underline{p}_2^*.\underline{k}}{\mathcal{E}_g+\mathcal{E}} Tu_v\right)$$

$$u_{\underline{k}^-} = a\left(Tu_c + \frac{\underline{p}_2.\underline{k}}{\mathcal{E}_g+\mathcal{E}} u_v + \frac{\underline{p}_1.\underline{k}}{\mathcal{E}_g+\mathcal{E}} Tu_v\right)$$

where (1) $a^2 = (\mathcal{E}_g+\mathcal{E})/(\mathcal{E}_g+2\mathcal{E})$

(2) $$\begin{cases} p_1 \equiv \frac{\hbar}{m_o} \int u_c^* \ \hat{\underline{p}} \ u_v \ d^3\underline{r} \\ p_2 \equiv \frac{\hbar}{m_o} \int u_c^* \ \hat{\underline{p}} \ Tu_v \ d^3\underline{r} \end{cases}$$ $\hat{\underline{p}}$ is momentum operator.

(3) the relationship between energy and $\underline{k}$ is governed by the following approximation:

$$\varepsilon + \frac{\varepsilon^2}{\varepsilon_g} = \frac{\hbar^2 k^2}{2m^*}$$

$$\therefore, \quad \varepsilon (\varepsilon_g + \varepsilon) = (\text{a real number})^2 \times k^2$$

If $\varepsilon \doteq \varepsilon'$; $\underline{k} \pm \underline{q} = \underline{k}'$ and $\underline{k} \gg \underline{q}$ we obtain the following factors in the expression of $1/\tau$

$$\frac{1}{\tau} \sim \left[\frac{1 + \frac{2\varepsilon}{\varepsilon_g}}{(1 + \frac{\varepsilon}{\varepsilon_g})^{\frac{1}{2}}} \right] \quad \text{and} \quad \left[1 - \frac{2\varepsilon(\varepsilon_g + \varepsilon)}{(\varepsilon_g + 2\varepsilon)^2} \right]$$

For the first term we know that

$$\varepsilon + \frac{\varepsilon^2}{\varepsilon_g} = \frac{\hbar^2 k^2}{2m^*} \implies k = \sqrt{\frac{2m^*}{\hbar^2} (\varepsilon + \frac{\varepsilon^2}{\varepsilon_g})}$$

and $$v = \frac{1}{\hbar} \nabla_k \varepsilon = \frac{1}{\hbar} \frac{\partial \varepsilon}{\partial k} = 1/\hbar \ (\frac{1}{\frac{\partial k}{\partial \varepsilon}})$$

$$\therefore, \quad \frac{1}{\tau} \sim \frac{1}{v} \sim (1 + \frac{2\varepsilon}{\varepsilon_g}) \ / \ (1 + \frac{\varepsilon}{\varepsilon_g})^{\frac{1}{2}}$$

The second term is a correction which is due to the fact that the electron wave functions in a solid have the form of (A21).

From A1 and A2 we have

$$\frac{1}{\tau} \sim \frac{1}{\tau_o} \left[\frac{1 + \frac{2\varepsilon}{\varepsilon_g}}{(1 + \frac{\varepsilon}{\varepsilon_g})^{\frac{1}{2}}} \right] \left[\left\{ 1 - \delta \ln(1+\frac{1}{\delta}) \right\} - \frac{2\varepsilon(\varepsilon_g+\varepsilon)}{(\varepsilon_g+2\varepsilon)^2} \left\{ 1 - 2\delta + 2\delta^2 \ln(1+\frac{1}{\delta}) \right\} \right]$$

where τ_o is the mean free time without considering the nonparabolicity and the screening effect.

A3. The calculation of the hot electron temperature where the resistivity minimum occurs.

$$\text{Let } y = \left\{ 1 - \delta \ln(1+\frac{1}{\delta}) \right\} - \frac{2\varepsilon(\varepsilon_g+\varepsilon)}{(\varepsilon_g+2\varepsilon)^2} \left\{ 1 - 2\delta + 2\delta^2 \ln(1+\frac{1}{\delta}) \right\}$$

$$\therefore \quad \frac{2\varepsilon(\varepsilon_g+\varepsilon)}{(\varepsilon_g+2\varepsilon)^2} \approx \frac{1}{2} \qquad \text{if } \varepsilon_g \approx \varepsilon$$

This is true because ,for instance, experiment is carried out at nitrogen temperature and electron temperature is about $200^{\circ}K$ and we have

$$\varepsilon \doteq \frac{3}{2} kT_e \doteq \frac{3}{2} \times 1.36 \times 10^{-16} \text{ erg deg}^{-1} \times 200^{\circ}K$$

$$\doteq \frac{3}{2} \times 1.36 \times 2 \times 10^{-14} \text{ erg} = 2.5 \times 10^{-1} \text{ ev}$$

$$\varepsilon_g \doteq 3 \times 10^{-1} \text{ ev}$$

$$\therefore \quad y = \left[1 - \delta \ln(1+\frac{1}{\delta}) \right] - \frac{1}{2} \left[1 - 2\delta + 2\delta^2 \ln(1+\frac{1}{\delta}) \right]$$

$$= \frac{1}{2} - \delta \ln(1+\frac{1}{\delta}) + \delta - \delta^2 \ln(1+\frac{1}{\delta})$$

$$\frac{dy}{d\delta} = -\ln(1+1/\delta) - \frac{\delta}{(1+1/\delta)} \cdot \frac{-1}{\delta^2} + 1 - 2\delta \ln(1+1/\delta) - \delta^2 \frac{1}{(1+1/\delta)} \frac{-1}{\delta^2}$$

$$= -\ln(1+1/\delta) + \frac{1}{(1+1/\delta)\delta} + 1 - 2\delta \ln(1+1/\delta) + \frac{1}{(1+1/\delta)}$$

$$= 1 - \ln(1+1/\delta).(2\delta+1) + \frac{1}{(1+1/\delta)} (1/\delta + 1)$$

$$= 2 - \ln(1+1/\delta)(2\delta+1)$$

If $dy/d\delta = 0$ ie.. $\ln(1+1/\delta) = 2/(2\delta+1)$

$$1/\delta - 1/2(1/\delta^2) + (1/3)(1/\delta^3) - (1/4)(1/\delta^4) \simeq \frac{2}{(2\delta+1)}$$

$$2\delta^2 - 2\delta - 3 = 0$$

$$\delta = \frac{1}{2} + \frac{1}{2}\sqrt{7}$$

and $\because$, $\delta \simeq C_s T_e^2$

$\therefore$, we have $$T_e\Big]_{MIN} = \left[\left(\frac{1}{2} + \frac{1}{2}\sqrt{7} \right) \Big/ C_s \right]^{\frac{1}{2}}.$$

APPENDIX B (S2)

(The symbolic system and etc. are referred to the preceding chapters and the corresponding references.)

B1. The hamiltonian of spin-spin interaction

$$H_{int}(\underline{r},\varsigma) = \phi^*(\underline{r},\varsigma)V(\underline{r})\phi(\underline{r},\varsigma)$$

$$V(\underline{r}) = -\sum_n g\delta(\underline{r}-\underline{R}_n)\,\underline{\sigma}\cdot\underline{S}_n$$

$$\underline{\sigma}\cdot\underline{S}_n = \sigma_x S_{nx}+\sigma_y S_{ny}+\sigma_z S_{nz}$$

Therefore the total hamiltonian

$$H_{int} = \sum_\varsigma \int d^3\underline{r}\, \mathcal{H}_{int} = -\sum_\varsigma \int d^3\underline{r}\, o^*(\underline{r},\varsigma) g \sum_n \delta(\underline{r}-\underline{R}_n)\underline{\sigma}\cdot\underline{S}_n\, \phi(\underline{r},\varsigma)$$

$$\because,\quad \phi(\underline{r}) = \sum_{\underline{k},s} \frac{e^{i\underline{k}\cdot\underline{r}}}{\sqrt{V}}\, a_{\underline{k}\,s}\, \alpha_s(\varsigma)$$

$$H_{int} = -g\sum_\varsigma \sum_n d^3\underline{r} \sum_{\underline{k}'s'} \frac{e^{-i\underline{k}'\underline{r}}}{V}\, a^*_{\underline{k}'s'}\alpha_{s'}(\varsigma)\delta(\underline{r}-\underline{R}_n)\underline{\sigma}\cdot\underline{S}_n \sum_{\underline{k}s} \frac{e^{i\underline{k}\cdot\underline{r}}}{\sqrt{V}}\, a_{\underline{k}s}\alpha_s(\varsigma)$$

$$= -\frac{g}{V}\sum_n \sum_{\substack{\underline{k}',s',\varsigma \\ \underline{k},\,s}} e^{i(\underline{k}-\underline{k}')\underline{R}_n}\, \alpha_{s'}(\varsigma)\underline{\sigma}\cdot\underline{S}_n\alpha_s(\varsigma)a^*_{\underline{k}'\underline{s}'}\, a_{\underline{k}s}$$

Then we introduce

$$\alpha_+(\varsigma) = \alpha_{\frac{1}{2}}(\varsigma) = \alpha(\varsigma)$$

$$\alpha_-(\varsigma) = \alpha_{-\frac{1}{2}}(\varsigma) = \beta(\varsigma)$$

$$a_{\underline{k}^+} = a_{\underline{k}\frac{1}{2}} \qquad a_{\underline{k}^-} = a_{\underline{k}-\frac{1}{2}}$$

$$a^*_{\underline{k}^+} = a^*_{\underline{k}\frac{1}{2}} \qquad a^*_{\underline{k}^-} = a^*_{\underline{k}-\frac{1}{2}}$$

$$\therefore \quad \sum_{s,s',\varsigma} \alpha_{s'}(\varsigma)\,(\rho_x S_{nx}+\rho_y S_{ny}+\rho_z S_{nz})\,\alpha_s(\varsigma)\,a^*_{\underline{k}'s'}a_{\underline{k}s}$$

$$= \sum_{s,s',\varsigma}\Big[(1)+(2)+(3)\Big]$$

$$\sum_{s,s',\varsigma}(1) = \sum_{s,s',\varsigma}\alpha_{s'}\rho_x S_{nx}\alpha_s a^*_{\underline{k}'s'}a_{\underline{k}s} = \sum_{s,s',\varsigma}\alpha_{s'}\rho_x\alpha_s S_{nx}a^*_{\underline{k}'s'}a_{\underline{k}s}$$

$$= \sum_{\varsigma}\Big[\alpha_+(\tfrac{1}{2}\alpha_-)S_{nx}a^*_{\underline{k}'+}a_{\underline{k}+} + \alpha_-(\tfrac{1}{2}\alpha_+)S_{nx}a^*_{\underline{k}'-}a_{\underline{k}-} + \alpha_+(\tfrac{1}{2}\alpha_+)S_{nx}a^*_{\underline{k}'+}a_{\underline{k}-}$$

$$+ \alpha_-(\tfrac{1}{2}\alpha_-)S_{nx}a^*_{\underline{k}'-}a_{\underline{k}+}\Big]$$

$$= \tfrac{1}{2}S_{nx}a^*_{\underline{k}'+}a_{\underline{k}-} + \tfrac{1}{2}S_{nx}a^*_{\underline{k}'-}a_{\underline{k}+}$$

by the orthogonormality of the spin function.

Similarly,

$$\sum_{s,s',\varsigma}(2) = \sum_{s,s',\varsigma}\alpha_{s'}\rho_y\alpha_s S_{ny}a^*_{\underline{k}'s'}a_{\underline{k}s} = -\tfrac{1}{2}S_{ny}a^*_{\underline{k}'+}a_{\underline{k}-} + \tfrac{1}{2}S_{ny}a^*_{\underline{k}'-}a_{\underline{k}+}$$

$$\sum_{s,s',\varsigma}(3) = \tfrac{1}{2}S_{nz}a^*_{\underline{k}'+}a_{\underline{k}+} - \tfrac{1}{2}S_{nz}a^*_{\underline{k}'-}a_{\underline{k}-}$$

$$\therefore \quad \sum_{s,s',\varsigma}\Big[(1)+(2)+(3)\Big] = \tfrac{1}{2}\Big[(a^*_{\underline{k}'+}a_{\underline{k}+}-a^*_{\underline{k}'-}a_{\underline{k}-})S_{nz}+a^*_{\underline{k}'+}a_{\underline{k}-}S_{n-}+a^*_{\underline{k}'-}a_{\underline{k}+}S_{n+}\Big]$$

If we let $J = \tfrac{1}{2}g\,\frac{N}{V}$ so finally,

$$H' = H_{int} = -\left(\frac{J}{N}\right)\sum_{n\underline{k}\underline{k}'} e^{i(\underline{k}-\underline{k}')\underline{R}_n}\Big[(a^*_{\underline{k}'+}a_{\underline{k}+}-a^*_{\underline{k}'-}a_{\underline{k}-})S_{nz}+a^*_{\underline{k}'+}a_{\underline{k}-}S_{n-}+a^*_{\underline{k}'-}a_{\underline{k}+}S_{n+}\Big]$$

$$H' = -\left(\frac{J}{N}\right) \left[(I) + (II) + (III) + (IV) \right]$$

B2. Calculation of matrix elements and transition probability in the first order Born approximation

For the process I (see section 5.4.3).

$|\underline{k}^+, M_n\rangle$ to $|\underline{k}'^+, M_n\rangle$

Matrix elements

$$\sum_n H'_{\underline{k}^+ M_n, \underline{k}'^+ M_n} = -(J/N) \sum_n \left[(I) + (II) + (III) + (IV) \right]$$

$$(I) = \sum e^{i(\underline{k}-\underline{k}')\underline{R}_{\bar{n}}} \left\langle \bar{\underline{k}}^+, jM_n \middle| a^*_{\underline{k}'^+} a_{\underline{k}^+} S_{\bar{n}z} \middle| \bar{\underline{k}}'^+, jM_n \right\rangle$$

$$= \sum_{\underline{k}'} e^{i(\bar{\underline{k}}'-\underline{k}')\underline{R}_n} \left\langle \bar{\underline{k}}^+, jM_n \middle| a^*_{\underline{k}'^+} M_n \middle| 0, jM_n \right\rangle$$

$$= e^{i(\bar{\underline{k}}'-\underline{k})\underline{R}_n} M_n$$

$\because$, $S_{nz} \left| \bar{\underline{k}}'^+, jM_n \right\rangle = M_n \left| \bar{\underline{k}}'^+, jM_n \right\rangle$ for $n=n$

$= 0$ for $n \neq n$

$$a_{\underline{k}^+} M_n \left| \bar{\underline{k}}'^+, jM_n \right\rangle = M_n \left| 0, jM_n \right\rangle \quad \text{for } \bar{\underline{k}}' = \underline{k}$$

$= 0$ for $\bar{\underline{k}}' \neq \underline{k}$

$$a^*_{\underline{k}'^+} M_n \left| 0, jM_n \right\rangle = M_n \left| \underline{k}'^+, jM_n \right\rangle$$

and by the orthonormal property of eigenfunction ie.,

$$\left\langle \bar{\underline{k}}^+, jM_n \middle| \underline{k}'^+, jM_n \right\rangle = 1 \quad \text{for } \bar{\underline{k}} = \underline{k}'$$

$= 0$ for $\bar{\underline{k}} \neq \underline{k}'$

$$(II) = -\sum_{\underline{k}\underline{k}'\bar{n}} e^{i(\underline{k}-\underline{k}')\underline{R}_{\bar{n}}} \left\langle \bar{\underline{k}}^{+},\ jM_n \middle| a^{*}_{\underline{k}'} - a_{\underline{k}} - S_{nz} \middle| \bar{\underline{k}}'^{+},\ jM_n \right\rangle = 0$$

$$(III) = \sum_{\underline{k}\underline{k}'\bar{n}} e^{i(\underline{k}-\underline{k}')\underline{R}_{\bar{n}}} \left\langle \bar{\underline{k}}^{+},\ jM_n \middle| a^{*}_{\underline{k}'} a_{\underline{k}} - S_{n-} \middle| \bar{\underline{k}}'^{+},\ jM_n \right\rangle = 0$$

$$(IV) = \sum_{\underline{k}\underline{k}'\bar{n}} e^{i(\underline{k}-\underline{k}')\underline{R}_{\bar{n}}} \left\langle \bar{\underline{k}}^{+},\ jM_n \middle| a^{*}_{\underline{k}'} - a_{\underline{k}^{+}} S_{n+} \middle| \bar{\underline{k}}'^{+},\ jM_n \right\rangle$$

$$= \sum_{\underline{k}'} e^{i(\bar{\underline{k}}'-\underline{k}')\underline{R}_n} \sqrt{(j-M_n)(j+M_n+1)} \left\langle \bar{\underline{k}}^{+},\ jM_n \middle| a^{*}_{\underline{k}'} - \middle| 0,\ jM_n \right\rangle = 0$$

$$\therefore \quad S_{\bar{n}+} \left| \bar{\underline{k}}'^{+},\ jM_n \right\rangle = \sqrt{(j-M_n)(j+M_n+1)} \left| \bar{\underline{k}}'^{+},\ j(M_n+1) \right\rangle$$

So $H'_{\bar{\underline{k}}^{+},\ \bar{\underline{k}}'^{+}} = -(J/N) \sum_{n} e^{i(\bar{\underline{k}}'-\bar{\underline{k}})\underline{R}_n} M_n$

Similarly, $H'_{\bar{\underline{k}}'^{+},\ \bar{\underline{k}}^{+}} = -(J/N) \sum_{n'} e^{i(\bar{\underline{k}}-\bar{\underline{k}}')\underline{R}_{n'}} M_{n'}$

Hence, $H'_{\underline{k}^{+},\underline{k}'^{+}} H'_{\underline{k}'^{+},\underline{k}^{+}} =$

$$= (J/N)^2 \sum_{n=n'} M_n^2 + \sum'_{n\neq n'} (J/N)^2 e^{i(\bar{\underline{k}}-\bar{\underline{k}}')(\underline{R}_n-\underline{R}_{n'})} M_n M_{n'}$$

$$= (J/N)^2 \tfrac{1}{3} j(j+1)CN$$

$\therefore$ the 2nd term is very small and $\sum_n M_n^2 = \tfrac{1}{3} j(j+1)CN$

$\therefore$ localized spins are randomly oriented.

Transition probability $= w(\underline{k}\to\underline{k}') = 2\pi/\hbar\ \delta(\varepsilon_{\underline{k}}-\varepsilon_{\underline{k}'}) \left[H'_{\underline{k}\underline{k}'} H'_{\underline{k}'\underline{k}} + \sum_{q=\underline{k}} \left(H'_{\underline{k}q} H'_{q\underline{k}'} H'_{\underline{k}\underline{k}} + \text{c.c.} \right) / (\varepsilon_{\underline{k}}-\varepsilon_{q}) \right]$

$= 2\pi/\hbar\ (J/N)^2 \tfrac{1}{3} j(j+1)CN\,\delta(\varepsilon_{\underline{k}}-\varepsilon_{\underline{k}'})$

$$= \frac{2\,J^2 j(j+1)C}{3hN}\,\delta(\varepsilon_{\underline{k}}-\varepsilon_{\underline{k}'})$$

Calculations for all the others in the first Born approximation can be obtained similarly.

B3. Calculation of Matrix elements and transition probability due to the second order Born approximation

For example, we consider process 1 group c in section 5.4.3

ie., $|\underline{k}^+\rangle \longrightarrow |\underline{q}^-\rangle \longrightarrow |\underline{k}'^+\rangle$

$|j,M_n\rangle \quad |j,(M_n+1)\rangle \quad |j,M_n\rangle$

The matrix element:

$$H'_{\underline{k}^+,M_n;\underline{q}^-(M_n+1)}\; H'_{\underline{q}^-(M_n+1);\underline{k}'^+M_n}\; H'_{\underline{k}'^+M_n;\underline{k}^+M_n}$$

$$= -(J/N)^3 e^{i\left[(\underline{q}-\underline{k})\underline{R}_n+(\underline{k}'-\underline{q})\underline{R}_{n'}+(\underline{k}-\underline{k}')\underline{R}_{n''}\right]} M_n(j+M_n+1)(j-M_n)$$

$$= -(J/N)^3\, M_n(j-M_n)(j+M_n+1)$$

$$\therefore\quad H'_{\underline{k}^+M_n;\underline{q}^-(M_n+1)} = -(J/N)e^{i(\underline{q}-\underline{k})\underline{R}_n}\,(j+M_n+1)(j-M_n)$$

$$H'_{\underline{q}^-(M_n+1);\underline{k}'^+M_n} = -(J/N)\, e^{i(\underline{k}'-\underline{q})\underline{R}_{n'}}\,(j+M_n+1)(j-M_n)$$

$$H'_{\underline{k}'^+M_n;\underline{k}^+M_n} = -(J/N)\, e^{i(\underline{k}-\underline{k}')\underline{R}_{n''}}\, M_n$$

Transition probability:

Transition probability:

$$2\pi/\hbar\ \delta(\varepsilon_{\underline{k}}-\varepsilon_{\underline{k}'})\sum_{\underline{q}n}\left[H'_{\underline{k}^+M_n,\underline{q}^-(M_n+1)}H'_{\underline{q}^-(M_n+1),\underline{k}'^+M_n}H'_{\underline{k}'^+M_n,\underline{k}^+M_n}+c.c\right](1-f^o_{\varepsilon})\Big/(\varepsilon_{\underline{k}}-\varepsilon_{\underline{q}}$$

$$=2(2\pi/\hbar)\ \delta(\varepsilon_{\underline{k}}-\varepsilon_{\underline{k}'})(-J/N)^3\sum_n M_n(j-M_n)(j+M_n+1)\sum_{\underline{q}}(1-f^o_{\underline{q}})\Big/(\varepsilon_{\underline{k}}-\varepsilon_{\underline{q}})$$

the factor 2 comes from the c.c. terms.

All the other 2nd order approximation terms will follow the similar calculations.

B4. Calculation for the temperature dependence of resistivity

Relaxation time of the scattering is given by

$$\frac{1}{\tau_k}=\sum_{\underline{k}'}w(\underline{k}^{\pm}\longrightarrow\underline{k}'^{\pm})+w(\underline{k}^{\pm}\longrightarrow\underline{k}'^{\mp})$$

$$=6\pi J^2s(s+1)C/3hN\left[1+4Jg(\varepsilon_{\underline{k}})\right]\sum_{\underline{k}'}\delta(\varepsilon_{\underline{k}}-\varepsilon_{\underline{k}'})$$

$$=6\pi J^2s(s+1)C/3hN_o\left[1+4Jg(\varepsilon_{\underline{k}})\right]\frac{1}{V}\sum_{\underline{k}'}\delta(\varepsilon_{\underline{k}}-\varepsilon_{\underline{k}'})$$

$$=4\pi/(2\pi)^3\int_0^{\infty}\delta\left[\frac{\hbar^2}{2m}(k^2-k'^2)\right]k'^2dk'$$

$$\left(\because\ \frac{1}{V}\sum_{\underline{k}'}\delta(\varepsilon_{\underline{k}}-\varepsilon_{\underline{k}'})=\frac{1}{(2\pi)^2}\int_0^{\infty}\delta(\varepsilon_{\underline{k}}-\varepsilon_{\underline{k}'})d^3\underline{k}'=\right.$$

$$=\frac{1}{2\pi^2}\frac{2m}{h^2}\int_o^{\infty}\delta(k^2-k'^2)k'^2dk'\qquad\left(\because,\ \delta(\lambda x)=1/\lambda\,\delta(x)\quad\text{for}\lambda>0\right)$$

$$=m/\pi^2h^2 2k\int_o^{\infty}\left[\delta(k-k')+\delta(k+k')\right]k'^2dk'$$

$$=mk^2/2\pi^2h^2k=mk/2\pi^2h^2$$

$(\because\ \delta(a^2-x^2) = \frac{1}{2a}\left[\delta(a-x)+\delta(a+x)\right]$ for $a > 0$)

and $\therefore\ \int_0^\infty k'^2\,\delta(k-k')dk' = k^2$.

$$\int_0^\infty k'^2\,\delta(k+k')\,dk' = \int_0^\infty k'^2\,\delta\,k'-(-k)\,dk' = 0 \qquad \text{as } k'=-k\ )$$

Then

$$\frac{1}{\tau_K} = \frac{J^2 s(s+1)C}{\hbar}\,\frac{mk}{N_o \pi^2 \hbar^2}\left[1+4Jg(\varepsilon_k)\right]$$

$$= \frac{3\pi z J^2 s(s+1)C}{2\varepsilon_F \hbar}\left[1+4Jg(\varepsilon_{\underline{k}})\right]$$

$(\because\ z=n/N_o\ ;\quad n=(2m)^{3/2}\,\varepsilon_F^{3/2} \Big/ 3\pi^2\hbar^3 = \tfrac{2}{3}\,k_o^3/2\pi^2$

$mk/N_o\pi^2\hbar^2 = (2m/N_o k_o^2\hbar^2)(k_o^2/2\pi^2) = 3n/2N_o\varepsilon_F = 3z/2\varepsilon_F$)

Resistivity

$$\rho = \frac{1}{\sigma} = \frac{12\pi^3}{e^2}\,\frac{1}{\int \tau_{\underline{k}} v_{\underline{k}}^2\,\frac{df_{\underline{k}}}{d\varepsilon_{\underline{k}}}\,d^3k}$$

$$= \frac{C\rho_M 12\pi^3 n}{m}\,\frac{1}{\int\left[1-4Jg(\varepsilon_{\underline{k}})\right] v_{\underline{k}}^2\,\frac{df_{\underline{k}}}{d\varepsilon_{\underline{k}}}\,d^3k}$$

$(\because\ \tau_k = \left[\frac{3\pi z J^2 s(s+1)C}{2\varepsilon_F\hbar}\right]^{-1}(1+4Jg(\varepsilon_{\underline{k}}))^{-1} \simeq \left[C\rho_M \frac{e^2 zN}{mV}\right]^{-1}(1-4Jg(\varepsilon_{\underline{k}}))$

$$= \left[C\rho_M\ \frac{e^2 n}{m}\right]^{-1}(\,1-4Jg(\varepsilon_{\underline{k}}))$$

$$\rho_M = \frac{3\pi m J^2 s(s+1)\ V}{2e^2\hbar\varepsilon_F\ N}\ )$$

$$\therefore, \quad \rho = -\rho_M \frac{12\pi^3 n}{m} \frac{1}{A} \left[\frac{1}{1 - \frac{4J}{A} \int v_{\underline{k}}^2 \, g(\varepsilon_k) \, \frac{df_{\underline{k}}}{d\varepsilon_{\underline{k}}} \, d^3k} \right]$$

$$\doteq -\rho_M \frac{12\pi^3 n}{m} \frac{1}{A} \left[1 + \left(\frac{4J}{A}\right) \int v_{\underline{k}}^2 \, g(\varepsilon_{\underline{k}}) \frac{df_{\underline{k}}}{d\varepsilon_{\underline{k}}} \, d^3k \right]$$

$$\left(\because, \quad d^3k = 4\pi k^2 dk = 4\pi k^2 \frac{m}{\hbar^2 k} d\varepsilon = \frac{4\pi\sqrt{2m}\, m}{\hbar^3} \varepsilon^{\frac{1}{2}} d\varepsilon \right.$$

$$A = \int_0^\infty v_{\underline{k}}^2 \frac{df_{\underline{k}}}{d\varepsilon_{\underline{k}}} \, d^3k = \frac{8\pi\sqrt{2m}}{\hbar^3} \int_0^\infty \varepsilon^{3/2} \frac{df}{d\varepsilon} \, d\varepsilon$$

$$\doteq -\frac{8\pi\sqrt{2m}}{\hbar^3} \varepsilon_F^{3/2} = -\frac{12\pi^3 n}{m} \qquad \because, \quad \frac{df}{d\varepsilon} \sim -\delta(\varepsilon - \varepsilon_F) \qquad \left. \right)$$

$$\rho = \rho_M \left[1 - \frac{4Jm}{12\pi^3 n} v_{\varepsilon_F}^2 \int g(\varepsilon_{\underline{k}}) \frac{df_{\underline{k}}}{d\varepsilon_{\underline{k}}} \, d^3\underline{k} \right]$$

$$= \rho_M \left[1 - \frac{4Jm}{12\pi^3} \frac{3 \, 2\hbar^3}{(2m)^{3/2} \varepsilon_F^{3/2}} \frac{2\varepsilon_F}{m} \int g(\varepsilon_{\underline{k}}) \frac{df_{\underline{k}}}{d\varepsilon_{\underline{k}}} \, d^3k \right]$$

$$= \rho_M \left[1 - (\hbar^2 J / \pi m k_o) \int g(\varepsilon_{\underline{k}}) \frac{df_{\underline{k}}}{d\varepsilon_{\underline{k}}} \, d^3k \right]$$

$$\left(\because, \quad \int g(\varepsilon_{\underline{k}}) \frac{df_{\underline{k}}}{d\varepsilon_{\underline{k}}} \, d^3k = \int \sum_{\underline{k}'} \frac{1}{N} \frac{f^o_{\underline{k}'}}{\varepsilon_{\underline{k}'} - \varepsilon_{\underline{k}}} \frac{df^o_{\underline{k}}}{d\varepsilon_{\underline{k}}} \, d^3k \right.$$

$$= \frac{V}{(2\pi)^3 N} \iint \frac{f^o_{\underline{k}}}{\varepsilon_{\underline{k}'} - \varepsilon_{\underline{k}}} \frac{df^o_{\underline{k}}}{d\varepsilon_{\underline{k}}} \, d^3k \, d^3k'$$

$$= -\frac{4\pi^3 V}{\pi N \hbar^6} \iint \frac{(\varepsilon_{\underline{k}} \, \varepsilon_{\underline{k}'})^{\frac{1}{2}}}{\varepsilon_{\underline{k}'} - \varepsilon_{\underline{k}}} f^o_{\underline{k}} \frac{df^o_{\underline{k}'}}{d\varepsilon_{\underline{k}'}} \, d\varepsilon_{\underline{k}} \, d\varepsilon_{\underline{k}'}$$

$$= -\frac{8m^3V\varepsilon_F}{Nh^6\pi} - \frac{4m^3V\varepsilon_F}{Nh^6\pi}\iint \ln\left|\frac{\sqrt{\varepsilon_k}-\sqrt{\varepsilon_{k'}}}{\sqrt{\varepsilon_k}+\sqrt{\varepsilon_{k'}}}\right| \frac{df^o}{d\varepsilon_k}\frac{df^o}{d\varepsilon_{k'}}\, d\varepsilon_k\, d\varepsilon_{k'}$$

and $\therefore$ the integral

$$= \iint \ln\left|\frac{\varepsilon_k-\varepsilon_{k'}}{\varepsilon_k+\varepsilon_{k'}+2\sqrt{\varepsilon_k\varepsilon_{k'}}}\right| \frac{df^o}{d\varepsilon_k}\frac{df^o}{d\varepsilon_{k'}}\, d\varepsilon_k\, d\varepsilon_{k'}$$

$$= \iint \ln\left|\frac{\varepsilon_k-\varepsilon_{k'}}{4\varepsilon_F}\right| \frac{df^o}{d\varepsilon_k}\frac{df^o}{d\varepsilon_{k'}}\, d\varepsilon_k\, d\varepsilon_{k'}$$

$$= \iint \ln|\varepsilon_k-\varepsilon_{k'}| \frac{df^o}{d\varepsilon_k}\frac{df^o}{d\varepsilon_{k'}}\, d\varepsilon_k\, d\varepsilon_{k'} - \iint \ln 4|\varepsilon_F| \frac{df^o}{d\varepsilon_k}\frac{df^o}{d\varepsilon_{k'}}\, d\varepsilon_k\, d\varepsilon_{k'} = \alpha - \beta$$

and $\therefore$, $f = \dfrac{1}{e^{\frac{\varepsilon-\varepsilon_F}{KT_e}}+1}$; let $x=\dfrac{\varepsilon-\varepsilon_F}{KT_e}$; $KT_e dx = d\varepsilon$; $F(x)=\dfrac{1}{e^x+1}$

$\therefore$, $\alpha = \displaystyle\int_{-\frac{\varepsilon_F}{KT_e}}^{\infty}\int \ln|(x-x')KT_e| \frac{dF(x)}{dx}\frac{dF(x')}{dx'}\, dx\, dx'$

$$= \left[\int_{-\frac{\varepsilon_F}{KT_e}}^{\infty}\int \ln|x-x'| \frac{dF(x)}{dx}\frac{dF(x')}{dx'}\, dx\, dx'\right] + \left[\ln KT_e \int_{-\frac{\varepsilon_F}{KT_e}}^{\infty}\int \frac{dF(x)}{dx}\frac{dF(x')}{dx'} dx dx'\right]$$

If $\varepsilon_F >> KT_e$

$$\alpha = \left[\int_{-\infty}^{\infty}\int \ln|x-x'| \frac{dF(x)}{dx}\frac{dF(x')}{dx'} dx\, dx'\right] + \left[(\ln T_e + \ln K)\int_{-\infty}^{\infty}\int \frac{dF(x)}{dx}\frac{dF(x')}{dx'} dx\, dx'\right]$$

$$= \left[\text{temperature independent term}\right] + \left[\ln T_e + \ln K\right]$$

and

$$\beta = \ln 4|\varepsilon_F| \iint_{-\infty}^{+\infty} \frac{dF(x)}{dx} \frac{dF(x')}{dx'} \, dx \, dx' = \ln 4|\varepsilon_F|$$

Then

$$\rho = C\rho_M \left\{ 1 - \frac{\hbar^2 J}{k_o m \pi} \left[- \frac{8m^3 v \varepsilon_F}{\pi N \hbar^6} - \left(\frac{4m^3 v \varepsilon_F}{N \pi \hbar^6} \right) (\text{const} - \ln T_e) \right] \right\}$$

$$= C\rho_M \left(1 + \frac{3zJ}{E_F} \ln T_e \right)$$

$$\left(\because \quad \frac{\hbar^2 J}{m \pi k_o} \frac{8m^3 v \varepsilon_F}{N \pi \hbar^6} = \frac{8m^2 v \varepsilon_F J \hbar}{\pi^2 \hbar^4 N (2m)^{\frac{1}{2}} \varepsilon_F^{\frac{1}{2}}} \right.$$

$$= \cdot 6 \frac{JnV}{\varepsilon_F N}$$

$$= 6zJ/\varepsilon_F$$

and $\because$

$$\frac{h^2 J}{m k_o \pi} \left(\frac{4m^3 v \varepsilon_F}{N \pi \hbar^6} \right) = 3Jz/E_F$$

REFERENCES

1. Ryder, E.J. and Shockley, W. Phys. Rev. 81, 139 (1951).
2. Gunn, J.B. J. Electronics 2,87 (1956).
3. Seeger, K. Phys. Rev. 114, 476 (1959).
4. Prior, A.C. J. Phys. Chem. Solid 12, 175 (1960).
5. Zucker, J. J.Phys. Chem. Solid 12, 350 (1960).
6. Yu.Pozhela and Vebra, A. Tr. AN. Lit SSR. B2 (25), 99 (1961).
7. Banis, T. Ya. and Pozhela, Yu K. Lit. fiz. sb. 4, 479 (1964).
8. Sasaki, W. and Shibuya, M. J. Phys. Soc. Jap. 11, 1202 (1956).
9. Nathan, I.N. Bull. Am. Phys. Soc. Ser. 2,5, 194 (1960).
10. Koenig, S.H. Proc. Phys. Soc. (Lon) 73, 959 (1959).
11. Jørgensen, M.H. Mayer, N.Y. and Schmit-Tiedemann, K.J. Solid state Comm. 1,226, (1963).
12. Sarbei, O.G. and Boicheuko, B.L. UFZh, 9, 344 (1964).
13. Gibbi, W.E.K. J. Phys. Chem. Solid 25, 247 (1964).
14. Kogan,Sh.M. and Sandomirskii, V.B. Fiz. Tverd. Tela. 2, 2570, (1960).
15. Pozhela, Yu. K. and Shilal'nikas, V.I. Sov. Phys. --Solid State 5,532 (1963).
16. see Ref. 2.
17. Plasma Effects in Solids, Dunod, Paris (1964).
18. Sandaevskii, V.P. Karakushan, E.I. and Stafeev, V.I. Phys. Status Solidi 14, 241 (1966).
19. Bouch-Bruevich, V.L. and Kalashvikov, S.G. S P S S,7, 599 (1965).
20. Kalashuikov, S.G., Kagan, M.S. and Vdovenkov V.A. Fiz. Tekh. Poluprov. 1, 116 (1967).
21. Fröhlich, H. Proc. Royal Soc. A188, 532 (1947).
22. Fröhlich, H. and Paranjape, B.V. Proc. Royal Soc. B69, 21 (1956).
23. Stratton, R. Proc. Royal Soc. A242, 355 (1957) and A246, 406 (1958).

24. Matz, D. and Garcia-Molinor, F. J. Phys. Chem. Solids 26, 551 (1965).

25. Yamashita, J. and Watanabe, M. Progr. Theor. Phys. (Kyoto) 12, 443 (1954).

26. Adawi, I. Phys Rev. 112, 1567 (1958).

27. Yamashita, J. and Inone, K. J. Phys. Chem. Solids 12, 1 (1959).

28. Davydov, B.I. Zh. Eksp. Teor. Fiz. 6, 463 (1936).

29. Levinson, I.B. S P S S 6, 1665 (1965).

30. Kurosawa, T. Proc. Intern. Conf. Phys. Semicond., Kyoto (1966).

31. Budd, H.F. Proc. Intern. Conf. Semicond. (Kyoto) 420 (1966).

32. Rees, D.H. and Fawcett, W. 8th IPPS Solid State Conf. (Manchester) (1971).

33. Reik, H.G. and Risken, H. Phys. Rev. 124, 777 (1961).

34. Reik, H.G. and Risken, H. Phys. Rev. 126, 1737 (1962).

35. Moizhes, B.Ya. and Ravich, Yu.I. Sov. Phys--Semicond. 1, 149 (1967).

36. Tamarcheuko, V.I.,Ravich, Yu.I., Morgovskii, L.Ya. and Dubrovskaya, I.N. S P S S 11, 2599 (1970).

37. Ravich, Yu.I. and Morgovskii, L.Ya. Sov. Phys.--Semicond. 3, 1278 (1970).

38. Ravich, Yu.I., Curieva, E.A., Dubrovskaya, I.N., Efimova, B.A., Prokofeva, L.V. and Tamarcheuko Sov. Phys.--Solid State 3, 711 (1970).

39. Lovell, D.J. Am. J. Phys. 37, 5, 467 (1969).

40. Putley, E.H. Materials used in Semiconductor devices, 109, (1965).

41. Teichmann, H. Semiconductor (Lon.) 74, (1964).

42. Lim, P.S. and Kleinman, L. Phys. Rev. 142, 478 (1966).

43. Cuff, K.F., Ellet, M.R., and Kuglin, C.D. Proc. Intern. Conf. Semicond. 316,(62)

44. Yau, K.L. and Finlayson, D.M. '77° experimantal space in a superconducting magnet.' submitted (1971).

45. Nanney, G.A. Phys. Lett. 26A, 66 (1967).

46. St.--Onge, H., Walpole, J.N. and Rediber, R.H. Conf. WAa-5. 131 (1970).

47. Stratton, R. Proc. Roy. Soc. A242, 355 (1957).

48. Hasegawa, A. and Tamashita, J. Phys. Soc. Jap. 17, 1751 (1962).

49. Koenig, S.H. see Ref. 10.

50. Conwell, E.M. Solid State Phys. Supplement 9, 14(1967).

51. Stratton, R. see Ref. 23.

52. Conwell, E.M. see Ref. 50, P.107 (1967).

53. Conwell, E.M. see Ref. 50, P.111 (1967).

54. Conwell, E.M. see Ref. 50, P.152 (1967).

55. Conwell, E.M. see Ref. 50, P. 157 (1967).

56. Kinch, M.A. Brit. J. Appl. Phys. 17, 1257 (1966).

57. Finlayson, D.M. and Stewart, A.D. Brit. J. Appl. Phys. 17, 737 (1966).

58. Kaidanov, V.I., Vinogradova, M.I. and Kolomoeta, N.V.
Sov. Phys.---Semicond. 2,645 (1968).

59. Ravich, Yu.I., Gurieva, E.A.,Dubrovskaya, I.N., et al. see Ref. 38 (1970).

60. Stokoe, T.Y. and Cornwell, J.F. 'High Field Transport In Semiconductors'
in press. (1971).

61. Tamarchanko et al. see Ref.36. (1970).

62. Ravich, Ya.I. and Morgovskii, L.Ya. Sov. Phys.--Semicond. 3, 1278 (1970).

63. Howarth, D.J. and Soudheimer, E.H. Proc. Roy. Soc. A219, 53 (1953).

64. Licea, I. Phys. Stat. Sol. 25, 461 (1968).

65. Conwell, E.M. see Ref. 50, P.24. (1967).

66. Gunn, J.B., Inuishi, Y. and Harnaguchi, C. J. Phys. Soc. Jap. 17, 1813(1962).

67. Brown, M.A.C.S. Phys. Chem. Solids 19, 218 (1961).

68. Adawi, I. Phys. Rev. 120, 118 (1960).

69. Yamashita, J. Prog. Theoret. Phys.(Kyoto) 24, 357,(1960).

70. Finlayson, D.M. and Mathewson, A.G. J. Phys. Chem. Solids 28, 1501 (1967).

71. Ziman, J.M. Principles of the Theory of Solids P.188 (1964).

72. Denilychev, B.A. J E T P. Letters 2, 300 (1965).

73. Miyazawa, H. and Ikoma, H. J. Phys. Soc. Jap. 23, 290 (1967).

74. Sandercock, J.R. Ph.D. thesis, Univ. of Oxford (1968).

75. Erginsoy, C. Phys. Rev. 79, 1013 (1950).

76. Toyozawa, Y. J. Phys. Soc. Jap. 17, 986 (1962).

77. Kondo, J. Progr. Theo. Phys. 32, 37 (1964).

78. Kasuya, T. Progr. Theo. Phys. (Kyoto) 16, 45 (1956).

79. Katayama, Y. and Tanaka, S. Phys. Rev. 153, 873 (1967).

80. Finlayson, D.M. and Mathewson, A.G. see Ref. 70 (1967).

81. Chan, Y.C., Finlayson, D.M. and Johnson, I.A.
Proc. 12th Intern. Conf. on LT. Phys. (Kyoto) (1970).

82. Chan, Y.C. Ph.D. thesis, University of St. Andrews (1970).

83. Nakamura, A. and Kinoshita, M. J. Phys. Soc. Jap. 27, 382 (1969).

84. Beal-Monod, M.T. and Weiner, R.A. Phys. Rev. 170, 552 (1968).

85. Gueron, M. Proc. Intern. Conf. Semicond.Phys. (Paris) P.433 (1964).

86. Isaacson, R.A. and Bridges, F. Solid State Commun. 4, 633 (1966).

87. Beal-Monod et al. see Ref. 84. (1968).

88. Vn Dinh Ky J E T P. 24, 995 (1967).

89. Vonsovskii, S. and Rodionov, K. Dokl. Akad. Nauk. SSSR 75, 643 (1950).

90. Rodionov, K. and Shavsov, V. Fiz. Metallov. Metall. 4, 385 (1957).

91. Smith, J. Physica 17, 612 (1951).

92. Mansocci V. Phys. Rev. 137A, 1842 (1965).

93. Berger, L., Physica 30, 1141 (1961).

94. Kane, E.O. J. Phys. Chem. Solids 1, 247 (1956).

95. Korenblit, L.L. and Sherstobitov, V.E. Sov. Phys.--Semicond. 2,564(1968).

96. Smith, R.A. Advances in Physics, 2,321 (1953).

97. Petritz, R.L. and Scanlon, W.W. Phys. Rev. 97,1620,

98. Finlayson, D.M. and Greig, D. Pro.Phys. Soc. 69, 796,

99. Finlayson, D.M. and Greig, D. Pro. Phys. Soc. 73, 49

100. Smirnov, et. al. Sov. Phys. Sol. State 2, 1793, (1960).

101. Muzhdaba, V.M. and Shalyt, S.S. S.P.S.S. 8, 2997,(1967).

102. Kaidanov,V.I. et.al. S.P.S.S.8,246,(1966);S.P.Semc.2,645,(1968).